MYD88: CENTRAL RELAY STATION OF INTERLEUKIN 1 SIGNALING PATHWAY

By

Chunsheng Li

Dissertation

Submitted to the Faculty of the

Graduate School of Vanderbilt University

in partial fulfillment of the requirements

for the degree of

DOCTOR OF PHILOSOPHY

in

Microbiology and Immunology

December, 2005

Nashville, Tennessee

Approved:

Professor Derya Unutmaz

Professor Jack J. Hawiger

Professor Luc Van Kaer

Professor Dean W. Ballard

Professor Brian E. Wadzinski

To my wife

Yi

whom I love deeply

ACKNOWLEDGEMENTS

I wish to wholeheartedly thank my mentor Dr. Jacek Hawiger for allowing me to spend the past several years in his laboratory. Jacek not only provided me with his great guidance and support during my training, but he also served as a role model for how to be an excellent, successful scientist and an exceptional person. I am also grateful to the members of my dissertation committee (Dr. Derya Unutmaz, Dr. Dean Ballard, Dr. Luc Van Kaer, and Dr. Brian Wadzinski). Each of them provided me with guidance as well as with constant support and constructive criticism. I also want to thank the Department of Microbiology and Immunology for providing an environment where I could obtain an outstanding training and education, as well as good times outside of the laboratory.

The research reported herein could not have been performed without the support of all of the lab members past and present. Dr. Danya Liu and Dr. Yan Liu are collaborators, friends, and family members that have always been helpful and supportive during this journey. I am indebted to Dr. Jozef Zienkiewicz, with whom I have the privilege to work on development of the computational models. I thank Dr Daniel Moore for critical reading of my thesis. I also want to thank the rest of the people in Hawiger`s laboratory (Daewoong, Jennifer, Ruth Ann, Ty and Chad) for their constant support and friendship.

My parents have been the inspiration, the essential models for my life. My wife, Yi, has always been the best friend, best companion, and my one-woman cheer leader in the graduate school.

The author's work was supported by NIH Grants HL69542, HL62356, and HL68744.

TABLE OF CONTENTS

LIST OF TABLES

LIST OF FIGURES

LIST OF ABBREVIATIONS

AP-1	activation protein –1
Caspase	apoptosis-related cysteine protease
CBA	cytometric bead array
DD	death domain
DMEM	Dulbecco's Modified Eagle's Medium
DN	dominant negative
EDTA	ethylenediaminetetraacetic acid
HEK	human embryonic kidney
Ig	immunoglobulin
IKK	I kappa B kinase
IL	interleukin
IL1RAcP	interleukin 1 receptor accessory protein
IL1RI	interleukin 1 receptor I
IRAK	interleukin 1 receptor–associated kinase
JNK	c-Jun N-terminal kinase
kDa	kilo Dalton
LPS	lipopolysaccharide
MAL	MyD88 adaptor-like protein
MAP3K	mitogen–activated protein kinase kinase kinase
Min	minutes

MKK	MAP kinase kinase
MyD88	myeloid differentiation primary response gene 88
NFκB	nuclear factor kappa B
NP-40	Nonidet P-40
PAMP	pathogen–associated molecular patterns
PBS	phosphate-buffered saline
PCR	polymerase chain reaction
PMSF	phenylmethylsulphonylfluoride
PVDF	polyvinylidene fluoride
RT	reverse transcription
SARM	sterile alpha and TIR motif containing
SDS	sodium dodecyl sulfate
SDS-PAGE	sodium dodecyl sulfate polyacrylamide gel electrophoresis
SEB	staphylococcal enterotoxin B
TAK	transforming growth factor(TGF) beta-activated kinase
TICAM1	Toll-like receptor adaptor molecule 1
TIR	Toll/interleukin 1 receptor
TLR	Toll-like receptor
TNF	tumor necrosis factor
TRAF	TNF receptor-associated factor
TRAM	TRIF-related adapter molecule
TRIF	TIR domain containing adaptor inducing interferon-beta

CHAPTER I

BACKGROUND AND LITERATURE REVIEW

Cytokine-driven inflammation and diseases

Inflammation and inflammation-mediated diseases

In antiquity, the clinical features of inflammation were defined as *rubor* (redness), *calor* (warmth), *tumor* (swelling) and *dolor* (pain). These hallmarks of inflammation were first described about two thousand years ago by Celsus - Aulus (Aurelius) Cornelius, a Roman physician and medical writer. Now, inflammation is defined as a complex reaction of the innate immune system in vascularized tissues that involves the accumulation and activation of leukocytes and plasma proteins at the site of injury caused by infectious gents, chemical toxins, or trauma. Inflammation is initiated by changes in blood vessels that induce leukocyte recruitment. Local adaptive immune responses can promote inflammation as well. Although inflammation serves a protective function in controlling infections and promoting tissue repair, it can also cause "collateral" tissue damage and disease.

Inflammation is the major mechanism of cardiac, pulmonary and vascular diseases mediated by leukocytes and plasma proteins. The inflammatory response underlies a variety of human diseases including atherosclerosis,

coronary and peripheral arterial disorders exemplified by Kawasaki disease and systemic lupus, acute and chronic lung diseases such as asthma, acute respiratory distress syndromes, and interstitial lung disease. Inflammation is also related to a variety of autoimmune diseases including type 1 diabetes, multiple sclerosis, and rheumatoid arthritis (Baugh and Bucala, 2001; Dinarello, 2002). Thus, understanding the mechanism underlying inflammation will help in development of effective therapies for these diseases.

Inflammation is mediated by proinflammatory cytokines

Cytokines mediate major pathological processes including inflammation, angiogenesis, tissue remodeling, and fibrosis (Andreakos et al., 2004). The key cytokines involved in these processes are interleukin-1 (IL-1) and tumor necrosis factor-alpha (TNF-α) (Baugh and Bucala, 2001; Dinarello, 1996; Dinarello, 2000; Dinarello, 2002). Both of these cytokines are mediators for local inflammation by acting on vascular endothelium at the site of infection to induce the expression of adhesion molecules that promote migration of inflammatory and immunocompetent cells into the extravascular tissue compartment. In addition, large quantities of IL-1 and TNF-α in circulation are responsible for the systemic manifestations of infection by causing fever, producing hepatic acute phase plasma proteins, and initiating metabolic wasting (cachexia) (Roubenoff et al., 1994). A striking example of cytokine-induced systemic inflammation is septic shock, which is the most severe pathologic consequence of infection by gram-

negative and some gram-positive bacteria, characterized by circulatory collapse and disseminated intravascular coagulation (Hawiger, 1976). Thus, anti-cytokine therapy is a potential effective strategy for treatment of these diseases.

To counteract the detrimental effect of these cytokines in inflammatory responses, therapeutic application of TNF-α neutralization with specific antibody and IL-1 blockade with a receptor antagonist have been developed. The latter, Anakinra, is the recombinant form of the naturally occurring IL-1 receptor antagonist (IL-1Ra) (Dinarello, 2004). Anakinra is successfully applied for treatment of autoinflammatory diseases due to excessive production of IL-1β (Hawkins et al., 2004; Hawkins et al., 2003; Hoffman et al., 2004; Lovell et al., 2005). Alternatively, specific blockade of the downstream signaling pathways of these cytokines can directly target the pathological processes without wide-spread impairment of host defense mechanisms caused by using receptor antagonist or neutralizing antibody. To obtain more mechanistic insight assisting the development of specific therapeutic agents for IL-1-driven inflammation-related diseases, my thesis studies focused on the molecular mechanism of an essential step in IL-1 mediated signaling, the interaction between the IL-1 receptor and its downstream adaptor, myeloid differentiation primary response gene 88 (MyD88).

IL-1β: a key cytokine in inflammatory response

IL-1β is a potent proinflammatory cytokine

As one of the most potent proinflammatory cytokines, IL-1 plays an important role in inflammatory and immune responses. Its actions include the induction of fever, stimulation of the synthesis of hepatic acute phase reactants, upregulation of endothelial cell adhesion molecules, and stimulation of chemokine production by endothelial cells and macrophages (Auron et al., 1984; Dinarello, 1996). IL-1 was originally identified under a number of names corresponding to its different biological activities (endogenous pyrogen, lymphocyte activating factor, thymocyte proliferation factor, and catabolin, amongst others).

The role of the pleiotropic cytokine IL-1 in innate immune response to microbial pathogens is well established (Murphy et al., 2000). IL-1 is produced mainly by mononuclear phagocytes upon stimulation by pathogen - associated molecular patterns (PAMP), such as lipopolysaccharide (LPS), and by other cytokines, such as TNF-α (Liu et al., 2004a). IL-1 is also produced by many cell types other than activated macrophages such as peripheral neutrophilic granulocytes, endothelial cells, fibroblasts, Langerhans cells of the skin, microglia cells and many other cell types. Functional IL-1 agonist exists in two forms: IL-1α and IL-1β (Dinarello and Wolff, 1993)**.** Each of these two forms is encoded by a separate gene as a 31 kDa precursor protein termed proIL-1α and proIL-1β,

which are proteolytically cleaved by calpain and caspase-1 (also named IL-1β converting enzyme, ICE), respectively (Kobayashi et al., 1990). IL-1α is localized either on the cell surface as well as in the cytoplasm, indicating IL-1α exerts its biological function in an autocrine manner. In sharp contrast, IL-1β is released from activated macrophages and transduces signal to other cells. Both agonists, IL-1α and IL-1β, bind to the same receptor complex and have identical biologic effects, although the majority of the circulating ligand for IL-1 receptor complex is IL-1β. IL-1Ra is another member of IL-1 family, produced by most cell types expressing IL-1 and binds to the same IL-1 receptor complex as a competitive antagonist (Arend et al., 1998). Competition between IL-1β and IL-1Ra determines lymphocyte response to stimuli like phytohaemagglutin (Dabrowski et al., 2001).

IL-1β production is regulated by the "inflammasome"

As depicted in figure 1, upon activation by PAMP, macrophages are programmed to express IL-1β in a NFκB-dependent manner which will be described later in this chapter. IL-1β is synthesized as an inactive proIL-1β precursor, of which the proteolytic maturation is controlled by the cysteine protease caspase-1 (Thornberry et al., 1992). The latter itself is present in the cytosol as a 45 kDa precursor, which can be induced to undergo a series of processing events necessary for its activation. Although the mechanism of caspase-1 activation is still unclear, a multiprotein complex (termed the

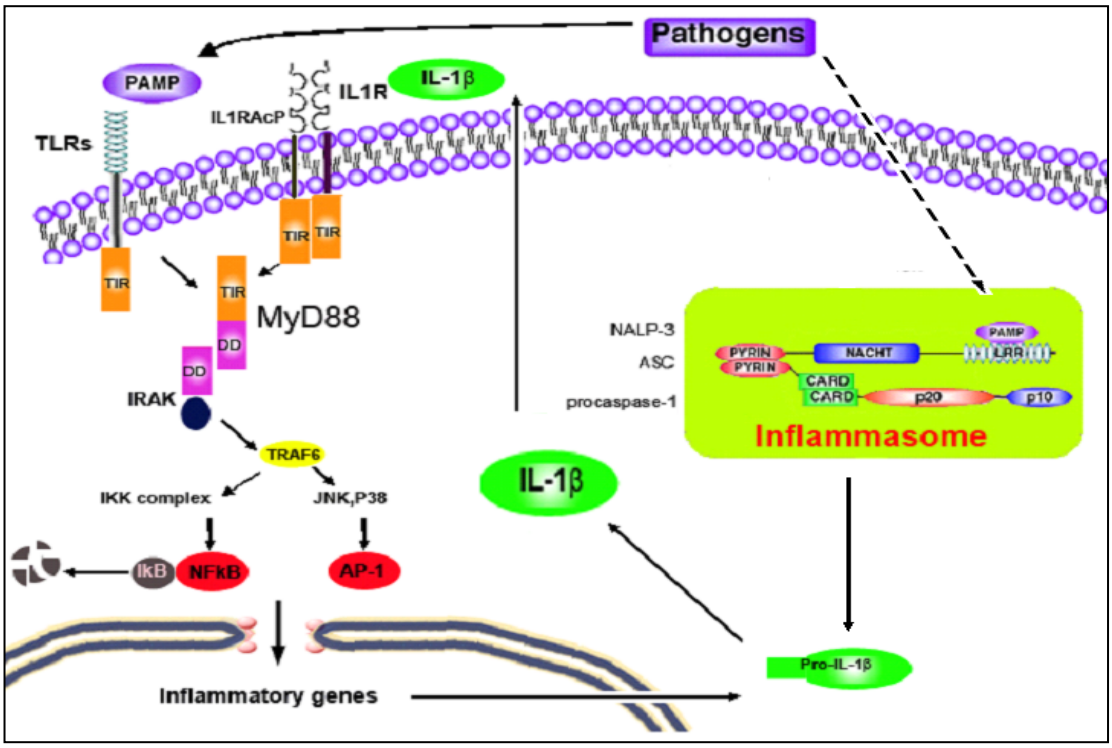

Figure 1. IL-1β signaling, expression and cleavage
IL-1β expression in macrophages is induced in a NFκB-mediated, MyD88-dependent fashion. Initially synthesized as an inactive precursor, IL-1β is proteolytically processed into mature form by the cysteine protease, caspase-1, which originally exists as a 45kDa precursor in the cytosol and undergos a series of processing events for its activation. The activation of procaspase-1 is mediated by a multiprotein complex ("inflammasome"), which also consists of NALP-3 (NACHT/LRR/pyrin domain-containing protein) and Asc (apoptosis-associated speck-like protein containing a CARD) (Martinon et al., 2002). NALP-3 belongs to the nucleotide-binding oligomerization domain protein family, which has been implicated recently in innate recognition of bacteria and the induction of inflammatory response. Asc is a caspase-recruitment domain (CARD) and pyrin domain containing protein, mediating the procaspase-1 oligomerization via binding to procaspase-1 by CARD-CARD interaction and to NALP-3 by pyrin-pyrin domain interaction (Srinivasula et al., 2002).

"inflammasome") that is involved in the activation of procaspase-1 upon LPS stimulation was identified recently (Martinon et al., 2002). The inflammasome consists of caspase-recruitment domain (CARD) and pyrin domain-containing proteins including Asc (apoptosis-associated speck-like protein containing a CARD), which mediate the oligomerization of procaspase-1 to facilitate its activation process (Srinivasula et al., 2002). The CARD of Asc binds the CARD of procaspase-1, whereas the pyrin domain of Asc can interact with the pyrin domain of NALP-3 (NACHT/LRR/pyrin domain-containing protein 3), a protein belonging to the nucleotide-binding oligomerization domain protein family, which has been implicated recently in innate recognition of bacteria and the induction of inflammatory responses (Mariathasan et al., 2004; Yu et al., 2005).

IL-1 is an important mediator in pathogenesis of multiple diseases

Production of functional IL-1β is process that is a tightly controlled by both its NFκB-mediated transcriptional activation and inflammasome-mediated proteolytic maturation. Apart from its role in orchestrating acute phase responses, IL-1β is an important mediator in the pathogenesis of many inflammatory and immunological mediated diseases. Unrestrained processing, release, and stimulation by IL-1β can be detrimental to the host. Abnormal IL-1β is related to many inflammatory diseases (Aksentijevich et al., 2002; Hawkins et al., 2004). A spectrum of diseases is related to abnormal inflammasome function. It ranges from Neonatal-Onset Multisystem Inflammatory Disease (NOMID, also known as

chronic infantile neurologic, cutaneous, articular [CINCA] syndrome) to Muckle-Wells syndrome to familial cold autoinflammatory syndrome (Aksentijevich et al., 2002; Hawkins et al., 2004; Hoffman et al., 2001). NOMID and Muckle-Wells Syndrome are closely associated with germline mutations in NALP-3 (Aksentijevich et al., 2002). As exemplified by NOMID, these autoinflammatory diseases are characterized by fever, chronic meningitis, uveitis, sensorineural hearing loss, urticaria, and a characteristic deforming arthropathy (figure 2). Recently, antagonist therapy with the recombinant form of IL-1Ra (Anakinra) has been shown to be effective to alleviate these symptoms (Dinarello, 2004).

The overproduction of IL-1β, orchestrated by TNF-α, drives pathophysiological processes that lead to the clinical symptoms of rheumatoid arthritis (RA) (Schiff, 2000). IL-1β has been implicated in a number of other chronic inflammatory or autoimmune diseases including diabetes, graft-versus-host disease, inflammatory bowel disease, various allergic skin diseases, and asthma (Rosenwasser, 1998). IL-1β also mediates systemic host defense responses to pathogens and to injury within the central nervous system (CNS) (Basu et al., 2004; Basu et al., 2005) . Polymorphisms in the IL-1β locus in patients have been associated with increased IL-1β levels in the brain and are considered one of the indicators for higher risk of Alzheimer disease (Mrak and Griffin, 2001). IL-1 has trophic effects on hematopoietic lineages and has been implicated in both the promotion and suppression of hematopoietic malignancies as well as some solid malignancies. In addition, *in vivo* angiogenesis and

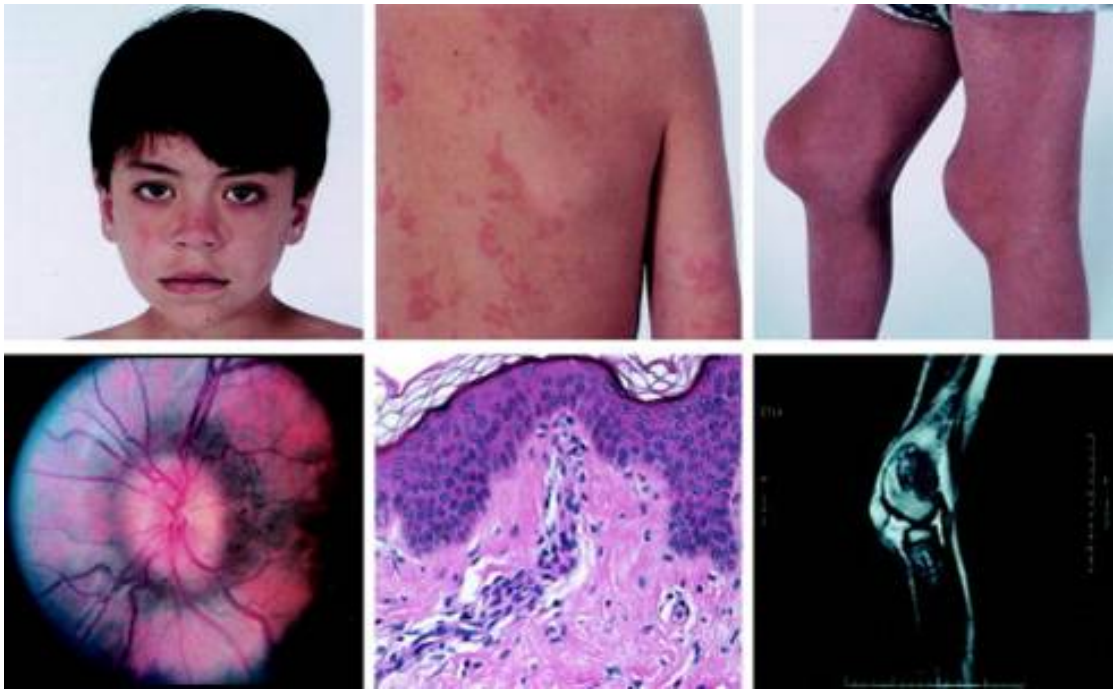

Arthritis & Rheumatism Vol.46, 12: 3340-3348

Figure 2. Neonatal-Onset Multisystem Inflammatory Disease (NOMID)
Clinical features of neonatal-onset multisystem inflammatory disease/chronic infantile neurologic, cutaneous, and articular (NOMID/CINCA) syndrome. Top left, facial features. Top middle, urticarial rash, which persisted throughout a week-long hospital visit. Top right, contractures of the knees. Bottom left, funduscopic image, demonstrating papilledema in the left eye (present bilaterally). Bottom middle, skin biopsy sample, showing a mild perivascular leukocytic infiltrate, with some eosinophils but no epidermal changes. Bottom right, magnetic resonance image of the right knee, demonstrating the absence of significant synovial enhancement and the presence of epiphyseal and patellar bony overgrowth.

invasiveness of different tumor cells require the production of IL-1 (Voronov et al., 2003). Therefore, better understanding of IL-1 signaling may reveal possible therapeutic targets in cancer, Alzheimer's disease, in addition to autoinflammatory and chronic autoimmune disease such as rheumatoid arthritis.

IL-1β binds to IL-1R/IL-1RAcP complex to induce downstream signaling pathway

Two different membrane receptors for IL-1β have been characterized, namely IL-1RI and IL-1RII. They are transmembrane proteins with three extracellular immunoglobulin-like domains. Although both the IL-1RI and IL-1RII are immunoglobulin superfamily members, their biological function and expression pattern are quite different. Unlike IL-1RII, which is only expressed on B lymphocytes and exerts its function as a decoy to competitively inhibit IL-1 signaling, IL-1RI is expressed on the cell surface of most cell types and is the functional receptor for IL-1 signaling.

The crystal structure of IL-1R/IL-1β complex suggested that IL-1β is wrapped in three immunoglobulin domains of IL-1R (Vigers et al., 1997). The interaction between IL-1 and its receptor is enhanced by involvement of other immunoglobulin superfamily members. IL-1β exerts its function by binding to its cognate receptor complex, formed by two extracellular-immunoglobulin containing proteins, IL-1RI and IL-1 receptor accessory protein (IL1RAcP). IL1RAcP was identified as an essential component in the receptor complex (Greenfeder et al., 1995; Wesche et al., 1997b). As shown in figure 3, via

Figure 3. Toll signaling pathway in Drosophila as the prototype of mammalian IL1R/TLR signaling pathway.

A, Comparison of the Toll signaling pathway in Drosophila and mammalian IL1R/TLR signaling pathway. In Drosophila, activation of the cell surface receptor Toll by the extracellular ligand Spaetzle lead to formation of trimeric complex of dMyD88, Tube and Pelle. Activated kinase Pelle exerts its function by phosphorylation and degradation of IκB-like inhibitor molecule Cactus, in turn activates the nuclear translocation of NFκB-like molecule Dorsal, which regulates transcriptional activation of multiple gene including Drosomysin. Three intermediate signal transducers are required for Dorsal activation via Toll: IRAK-related Pelle, drosophila MyD88, and MAL/TIRAP homolog Tube. The essential receptors and transducers of this pathway are conserved in mammals. See the text for details.

B, The IL-1 signaling pathway in mammals. P: phosphorylation; Ub: Lys63-mediated polyubiquitination. See the text for details and references.

A

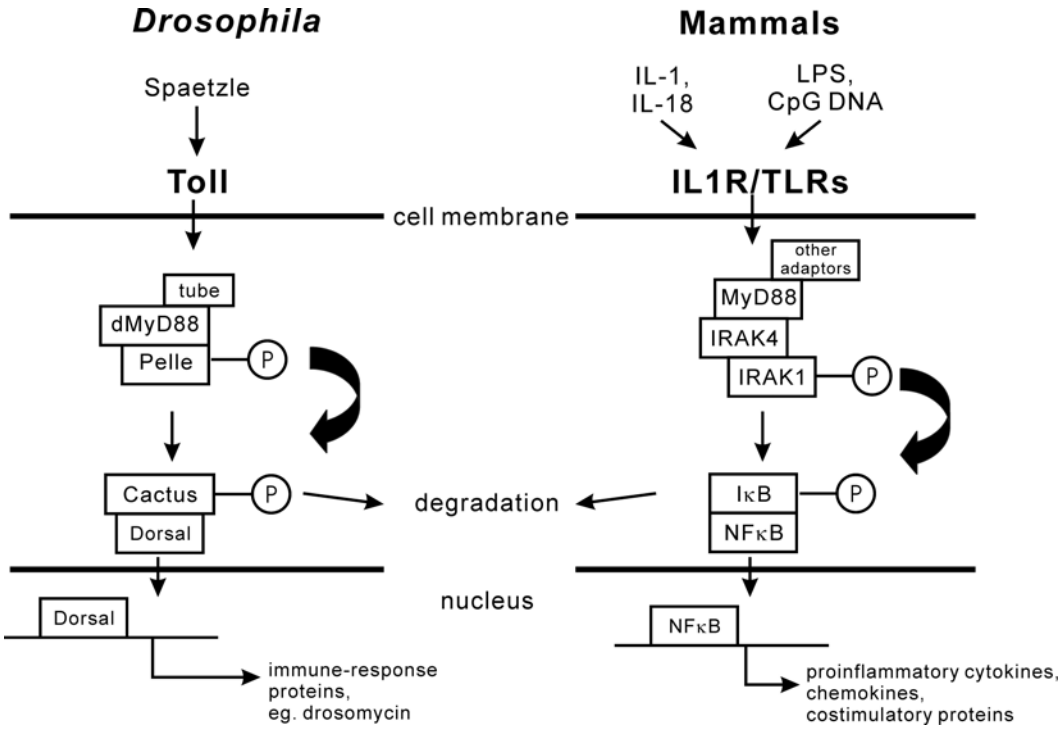
Drosophila
Mammals
Spaetzle
IL-1,
IL-18
LPS,
CpG DNA
Toll
IL1R/TLRs
cell membrane
tube
dMyD88
Pelle
P
other
adaptors
MyD88
IRAK4
IRAK1
P
Cactus
P
degradation
IκB
P
Dorsal
NFκB
nucleus
Dorsal
NFκB
immune-response
proteins,
eg. drosomycin
proinflammatory cytokines,
chemokines,
costimulatory proteins

B

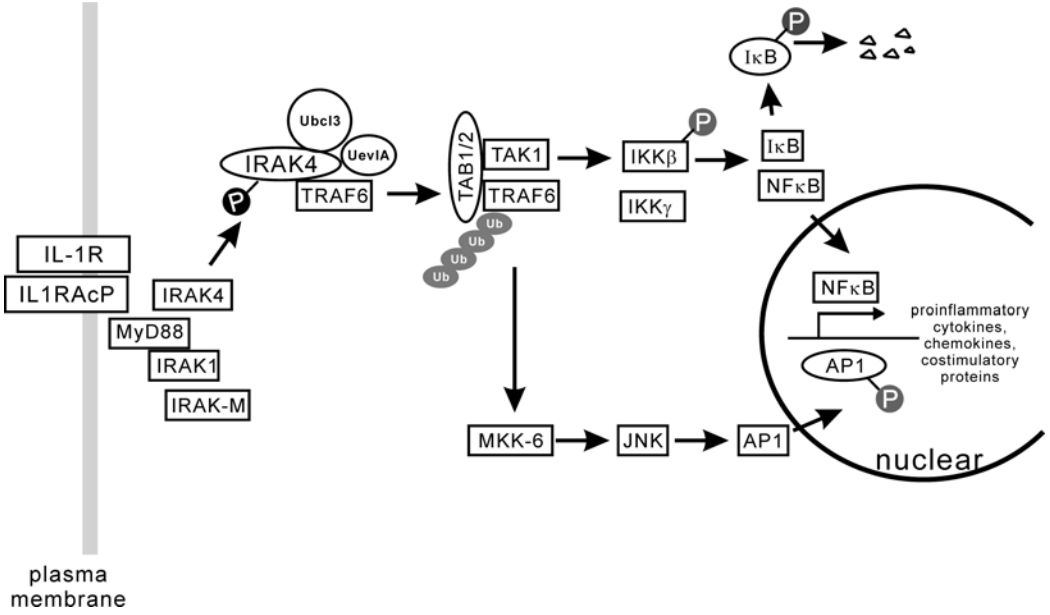
IκB
P
Ubc13
UevIA
IRAK4
TRAF6
TAB1/2
TAK1
TRAF6
IKKβ
IKKγ
IκB
NFκB
Ub
IL-1R
IL1RAcP
IRAK4
MyD88
IRAK1
IRAK-M
NFκB
proinflammatory
cytokines,
chemokines,
costimulatory
proteins
AP1
MKK-6
JNK
AP1
nuclear
plasma
membrane

binding to its cognate receptor complex IL-1β activates specific protein kinases, including the NFκB inducing kinase (NIK) and three distinct mitogen-activated protein (MAP) kinase cascades (Dinarello, 1996). These signal transducers mobilize transcription factors, including nuclear factor kappa-B (NFκB), activator protein – 1 (AP-1) and cyclic AMP (cAMP) element binding protein (CREB). In turn, these transcription factors initiate the synthesis of a plethora of immediate early genes essential to the inflammatory response (Dinarello, 1996). Importantly, IL-1β induces genes that encode other mediators of inflammation such as inflammatory cytokine IL-6, TNF, interferons and chemokine macrophage inflammatory protein-1 (MIP1). IL-1 also activate cyclooxygenase type 2 (COX-2), type 2 phospholipase A and inducible nitric oxide synthase (iNOS), which account for the large amount of prostaglandin-E2 (PGE2), platelet activating factor and nitric oxide (NO) produced by stimulation both *in vitro* and *in vivo*. Additionally, IL-1 increases the expression of cell adhesion molecules such as intercellular adhesion molecule-1 (ICAM-1) on mesenchymal cells and vascular-cell adhesion molecule-1 (VCAM-1) on endothelial cells to promote the infiltration of inflammatory and immunocompetent cells into the extravascular space. IL-1 is also act as an angiogenic factor by increasing the expression of vascular endothelial growth factor (Akira and Sato, 2003; Dinarello, 1996; Dinarello, 2002; Vannier and Dinarello, 1994; Yamamoto et al., 2004).

Expanding IL-1 family members

New molecules similar to IL-1 were identified recently based on both sequence homology and the presence of key structural motifs. For example, IL-18 is classified as an IL-1 family member (i.e., IL-1γ), which is predicted to fold as a β-rich trefoil, the typical structure for IL-1 ligands. Moreover, IL-18 has similar characteristics of processing, receptor usage, and signaling. (Bazan et al., 1996; Ghayur et al., 1997; Gu et al., 1997; Kojima et al., 1998; Tsuji-Takayama et al., 1999) . In addition, novel IL-1 ligands with high level of structural similarities to IL-1Ra have been identified (Barton et al., 2000; Busfield et al., 2000; Kumar et al., 2000; Mulero et al., 1999; Pan et al., 2001; Smith et al., 2000). IL-1δ, for example, specifically inhibits IL-1ε induced activation of NFκB through the orphan IL-1R-related protein 2 (IL-1Rrp2) (Debets et al., 2001). Interestingly, the majority of the IL-1 like proteins (i.e., IL-1Ra and other IL-1Ra-like ligands) are clustered on long arm of human chromosome 2, just like IL-1β and IL-1α (Webb et al., 1986), suggesting a potential functional relevance of the encoded products within this gene cluster.

Receptors for IL-1β (IL-1R and IL1RAcP) are members of IL-1 receptor/TLR superfamily

IL-1R and IL1RAcP contain Toll/interleukin 1 receptor (TIR) domain

The signals generated by IL-1β binding to its cognate receptor complex, formed by two type-I transmembrane proteins, IL-1 receptor I (IL-1RI) and IL-

1R accessory protein (IL1RAcP), are transduced by their cytoplasmic segments denoted as Toll/interleukin 1 receptor (TIR) domain. The TIR domain is about 150-180 amino acids in length and essential for signal transduction via protein-protein interactions. The TIR domain is conserved in *Drosophila* Toll, mammalian Toll-like receptors (TLRs), and cytoplasmic adaptors, which are exemplified by a protein named MyD88. These molecules belong to the IL-1 receptor/TLR superfamily (McGettrick and O'Neill, 2004). All members of this superfamily mediate inflammation-related signaling in a similar pattern since they all contain the TIR domains, through which the stress-activated protein kinases, IKK, JNK, and P38, and the transcription factor, NFκB, are eventually activated (figure 4).

Toll signaling pathway as the prototype of IL-1R/TLR signaling

The Toll signaling pathway in *Drosophila melanogaster* is the prototypical example of signaling by the members of the Toll/IL-1 receptor superfamily. The Toll-mediated pathway is required for activation of Drosomycin, an antifungal peptide in response to microbial challenge (Lemaitre et al., 1996). As shown in figure 3*A*, activation of the cell surface receptor Toll by the extracellular ligand Spaetzle leads to phosphorylation and degradation of an IκB-like inhibitor molecule, Cactus. The removal of Cactus allows the nuclear translocation of NFκB-like molecule Dorsal, which regulates transcriptional activation of multiple genes including Drosomysin. Three intermediate signal transducers are required for Dorsal activation via Pelle (related to Toll/IL-1R-associated kinase, IRAK),

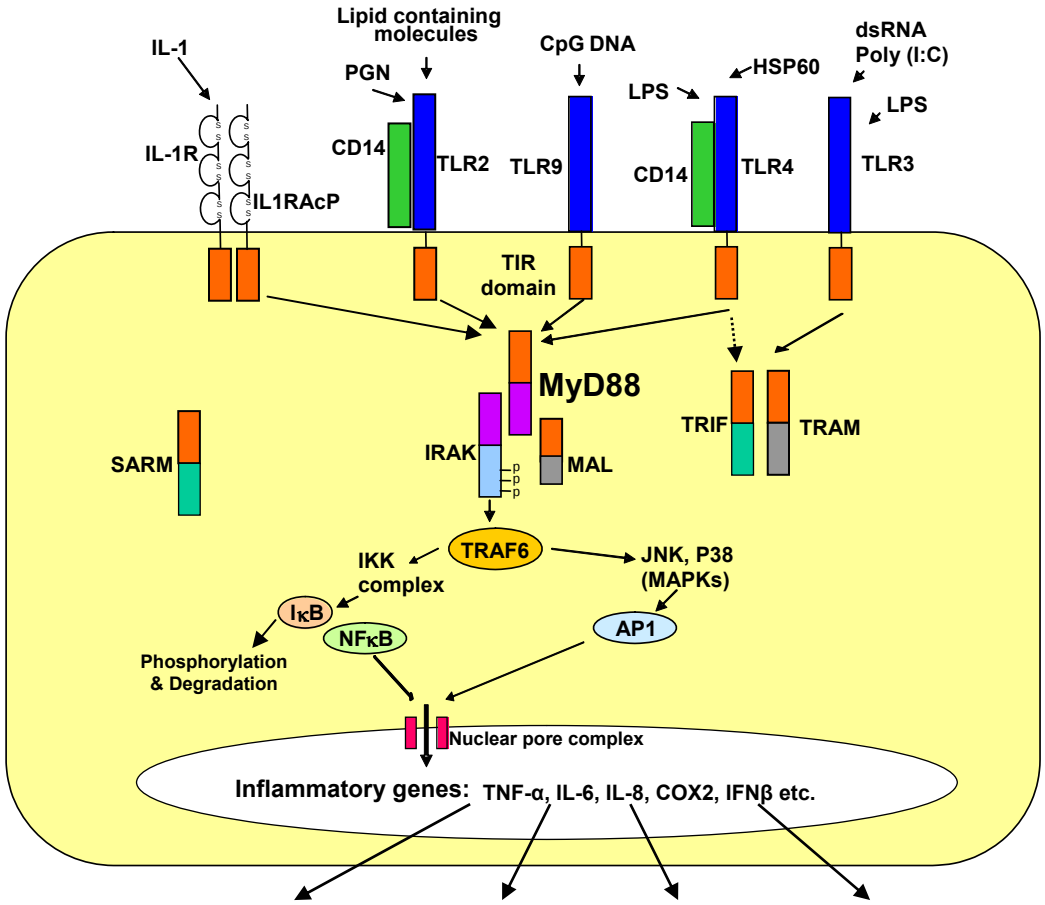

Figure 4. MyD88 as the central relay station for multiple IL1R/TLR signaling pathways. MyD88 integrates signals flowing from IL1R/IL1RAcP complex and from an array of other TLRs except TLR-3. Upon activation of IL1R/TLRs by its ligand, MyD88 recruits IRAK and in turn TRAF6 that ultimately leads to activation of NFκB, P38 and JNK. The TLR-3 signaling pathway uses MyD88-indepednet pathway, in which adaptor proteins TRIF and TRAM are recruited to TLR-3 to activate IRF3 and lead to activation of interferon production. TRIF also activates TRAF6 and leads to NFκB activation. Function of SARM is not identified yet.

drosophila MyD88, and Tube (Lemaitre et al., 1996; Tauszig-Delamasure et al., 2002). Drosophila MyD88 is required for the response to fungal and Gram-positive bacterial infections (Tauszig-Delamasure et al., 2002).

Similar to this ancestral signaling pathway, mammalian cells use these highly conserved intermediate components during IL-1 mediated signaling. MyD88 is the main adaptor protein which integrates signals flowing from multiple TIR domain containing receptors, including IL-1 receptor/IL1RAcP and most Toll-like receptors with the notable exception of TLR-3 (Akira, 2003; McGettrick and O'Neill, 2004). As depicted in figure 3*B*, a family of related kinases, the IRAKs, plays a critical role downstream of MyD88. The first member of this family, IRAK-1, is recruited to the receptor independently of MyD88. By contrast, IRAK-4 is recruited to the receptor through binding of MyD88. Once bound to the receptor complex, IRAK-1 becomes phosphorylated by IRAK-4 and subsequently autophosphorylated (Imler and Zheng, 2004). As a result, the kinases dissociate from the receptor complex and interact with the downstream component TNF receptor-associated factor 6 (TRAF6). Genetic evidence indicates that IRAK-4 plays an essential role in the activation of this pathway, as responses to IL-1 are abolished in IRAK-4 knockout mice (Suzuki et al., 2002). By contrast, other kinases, possibly IRAK-2, can substitute for IRAK-1 since activation of TRAF6 is only attenuated in IRAK-1 deficient cells (Swantek et al., 2000). Another member of the family, IRAK-M, is a negative regulator of the pathway since IRAK-M mutant cells show exacerbated responses to TLR agonists (Kobayashi et al.,

2002). Significantly, TRAF6 activates a heterodimer composed of two ubiquitination proteins called Uev1A and Ubc13 (Deng et al., 2000). Unlike the classical ubiquitination in which ubiquitin chains extending on Lysine 48 and leading to degradation of the modified protein by the proteasome, upon activation of TRAF6, noncanonical ubiquitin chains are extended on Lysine 63 , which trigger association with the MAP3 kinase TAK1 (transforming growth factor-β-activated kinase 1) (Silverman and Maniatis, 2001). Activated TAK1 directly phosphorylates and activates the kinases IKKß (Inhibitor of kappa light polypeptide gene enhancer in B-cells kinase β) and MKK6 (MAP kinase kinase 6).

IKKß is part of a large protein complex named signalsome (Mercurio et al., 1997). This signaling complex also contains the regulatory component IKKγ/NEMO. IKKß phosphorylates the NFκB cytoplasmic inhibitor IκB. After IκB polyubiquitination and degradation by 26S proteosomes, NFκB is released and translocated to the nucleus where it activates transcription of multiple target genes that contain the kappa B element in their promoter regions. MKK6 phosphorylates the c-Jun amino-terminal kinase (JNK) and leads to activation of another stress-responsive transcription factor, activator protein-1 (AP-1) (Silverman and Maniatis, 2001). AP-1 and NFκB activate transcription of genes that encode mediators and suppressors of inflammation (cytokines, chemokines, iNOS, adhesion molecules, etc), as well as costimulatory molecules such as CD40, CD80 and CD86 involved in adaptive immune response.

IL-1R/TLR superfamily members can be divided into three families

The IL-1 receptor/TLR superfamily can be divided into three families (Dunne and O'Neill, 2003). Members of the first family contain one or three extracellular immunoglobulin (Ig) domains exampled by IL-1RI (figure 5). The second family is characterized by extracellular leucine-rich repeats (LRR) instead of immunoglobulin domains and comprises the Toll-like receptors (TLRs) family. TLRs are the mainstay of innate immunity and at least 10 members of the TLR family have been identified. TLRs recognize PAMPs on the surface of multiple pathogenic microorganisms. They also interact with CpG DNA and viral double stranded RNA. Upon ligand binding, TLRs induce production of inflammatory cytokines, chemokines, anti-microbial compounds, and costimulatory molecules, which subsequently participate in the adaptive immune response. Their expression depends on signaling to the nucleus mediated by NFκB, AP-1 and other stress-responsive transcription factors (SRTFs) (Hawiger, 2001). The third family consists of adaptor proteins, including MyD88, MyD88 adaptor-like (MAL/TIRAP), TIR domain−containing adaptor inducing interferon-β (TRIF/TICAM-1), TRIF-related adaptor molecule (TRAM) and sterile alpha and HEAT/Armadillo motifs (SARM) (O'Neill et al., 2003). These TIR-containing adaptors are recruited to the TIR domains of the receptors and initiate signal transduction by activating IRAKs and the adaptor molecule TRAF6, consequently leading to the activation of signal transducers which mobilize SRTFs for nuclear translocation. Different signaling pathways may use different adaptors

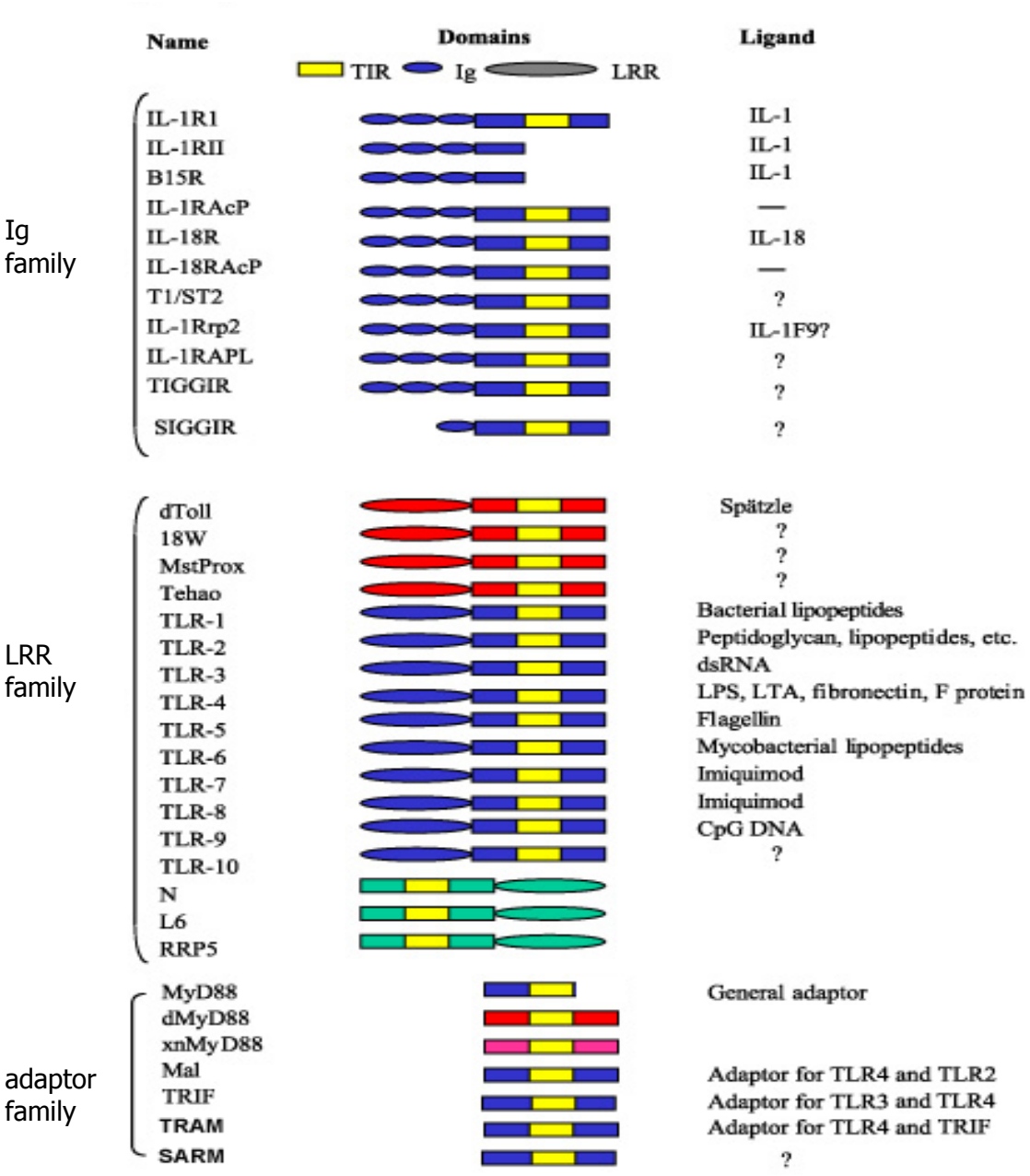

Figure 5. The members of the IL1R/TLR superfamily. Mammalian, *Drosophila*, plant, and *Xenopus* proteins are shown in blue, red, green, and magenta, respectively. The superfamily can be divided into three families. Family 1, the Ig family, all contain extracellular Ig domains and include receptors and accessory proteins for IL-1 and IL-18. Family 2, the LRR family, includes the signaling receptors for LPS (TLR-4) and molecules from Gram-positive bacteria such as peptidoglycan and lipoproteins (TLR-2). The adaptor family contains MyD88, MAL, TRIF, TRAM and SARM. Three superfamily members in *Caenorhabditis elegans* are not shown.

determining some specificity of signaling outcome from different receptors. While almost all the receptors recruit adaptor protein MyD88, some receptors can recruit other adaptors. A good example is the usage of TRIF by TLR-3 and TLR-4 only, which leads to the activation of IFN-regulatory factor 3 (IRF3) and the induction of IFN-β (Hoebe et al., 2003; Yamamoto et al., 2003a).

Whereas much progress has been made in the understanding of the TLR and adaptor families, other molecules in the Ig family have been mostly neglected. These orphan receptors include T1/ST2 (IL-1R4) (Brint et al., 2002; Klemenz et al., 1989; Mitcham et al., 1996), IL-1R-related proteins 1 (IL-1R5) (Parnet et al., 1996) and 2 (IL-1R6) (Lovenberg et al., 1996), IL-1R accessory protein ligand (IL-1R7)(Born et al., 1998), single immunoglobulin domain IL-1R-related protein (SIGIRR, IL-1R8) (Mulero et al., 1999), IL-1R accessory protein-like (IL-1R9)(Carrie et al., 1999), and IL-1R10 (Sana et al., 2000), which all contain extracellular immunoglobulin domains and an intracellular TIR domain. Interestingly, like most of the IL-1 ligands, the majority of these IL-1Rs (IL-1R1, IL-1R2, IL-1R4, IL-1R5, IL-1R6, and IL-1R7) localize on chromosome 2 (Dale and Nicklin, 1999; Lafage et al., 1989; Patterson et al., 1993; Sims et al., 1995). However, the functional significance of this clustering is unclear. Recent discovery of IL-1Rrp2 as a receptor for IL-1F9, suggests that those orphan receptors may bind to other IL-1-like ligands (Debets et al., 2001). Among these orphan receptors, SIGIRR is a negative regulator of Toll-like receptor-interleukin 1 receptor signaling, which is the first member of IL-1R/TLR superfamily to exert

a negative modulating function on the signaling of other members of the superfamily (Wald et al., 2003).

IL1RAcP forms complex with IL-1R and recruits MyD88 via its TIR domain

The best characterized Ig family members include IL-1R and its accessory protein (IL1RAcP). The IL-1RI complex consists of two type I integral membrane proteins: IL-1RI and IL1RAcP (Greenfeder et al., 1995; Sims et al., 1988). Co-expression of IL1RAcP is essential for complete IL-1 responsiveness (Hofmeister et al., 1997; Huang et al., 1997; Korherr et al., 1997; Wesche et al., 1997b). As the second molecule of the IL-1RI complex containing three Ig domains, IL1RAcP does not bind IL-1β by itself (Greenfeder et al., 1995; Wesche et al., 1997b). Instead, IL1RAcP significantly increases, up to five fold, the affinity of IL-1RI for IL-1β. Similar to IL-1RI, IL1RAcP is widely expressed and always shows colocalization with IL-1RI except in rat brain (Radons et al., 2002). The Ig domains of IL-1AcP are involved in the assembly of IL-1RI and IL1RAcP into a heterodimer. It is still unknown whether IL-1RI and IL1RAcP form complexes in resting cells before ligand binding. IL-1β may change the conformation of IL-1RI which in turn recruits IL1RAcP. Alternatively, the binding of IL-1β may increase the affinity of IL-1RI-IL1RAcP interaction. Their heterodimerization depends on the Ig domains as well as the synergy of IL1RAcP box 3 and IL-1R1 boxes 1/2 from TIR domain (Burns et al., 2000).

Specific sites in the cytoplasmic tail (TIR domain) are required for IL-1 signaling, supported by reconstitution assays in IL1RAcP-lacking cells (Radons et al., 2002). Upon activation of the IL-1R complex, IL1RAcP recruits MyD88 via adaptor protein Tollip (Burns et al., 2000). Mapping studies of the TIR domain of IL1RAcP indicated that its EE loop as well as highly conserved box 3 are required for MyD88 adaptor binding. The box 3 of the TIR domain of IL1RAcP (amino acids 538 to 542) is also essential for NFκB activation and IL-2 production (Radons et al., 2002). Adaptor protein Tollip may bind to amino acids 527 to 534 of IL1RAcP. This signaling results in stabilization of IL-2 mRNA through c-Jun NH_2-terminal kinase (JNK) and induction of optimal IL-2 promoter activity(Burns et al., 2000).

MyD88 is the central relay station for IL-1R/TLR signaling pathway

MyD88 is the common adaptor protein in multiple IL-1R/TLRs signaling pathways

MyD88 was originally described as a protein activated by IL-6 and expressed during myeloid differentiation (Lord et al., 1990). Human MyD88 was localized to chromosome 3 (Hardiman et al., 1997). Recent studies indicated that MyD88, as an essential adaptor protein, integrates signals flowing from IL-1R/IL1RAcP complex as well as from an array of other TLRs such as IL-18R, TLR-2, TLR-4, and TLR9 (Akira, 2003). As shown in figure 4, upon activation of IL-1R complex by IL-1, a complex containing MyD88 and IRAK is formed, ultimately

leading to activation of NFκB (Cao et al., 1996; Wesche et al., 1997a). This initial IL-1RI/IL1RAcP – MyD88 adaptor interaction evoked by IL-1β is a critical step in its signaling to the nucleus and, therefore, represents an essential step in innate immunity, as well as a potential target for new anti-inflammatory agents (Bartfai et al., 2003; Li et al., 2005).

TIR-TIR interaction of MyD88 is an essential step in IL-1R/TLR signaling

MyD88 has a bi-domainal structure comprised of an amino terminal death domain(DD), similar to the intracellular segments of TNF receptor 1 (TNFR1) and FAS, and a carboxyl terminal TIR domain with a short intermediate segment in between (figure 6) (McGettrick and O'Neill, 2004; Wesche et al., 1997a). The 3-dimensional structure of the TIR domain has an overall fold with a central five-stranded parallel β-sheets surrounded by five α helices, which are similar to the bacterial chemotaxis protein CheY (Rock et al., 1998). A splice variant of MyD88 (MyD88s) lacking the intermediate segment fails to recruit IRAK4 which is required for phosphorylation of IRAK1, thus it functions as a negative regulator of IL-1R/TLR/MyD88-triggered signals (Burns et al., 2003). Until recently, our understanding of structural characteristics of IL-1R complex-MyD88 adaptor interaction was limited.

MyD88 protein interacts with other TIR-domain containing proteins via the TIR domain mediated heterotypic dimerization (Burns et al., 1998). MyD88 protein can also form homotypic dimers via both the TIR and death domains

A

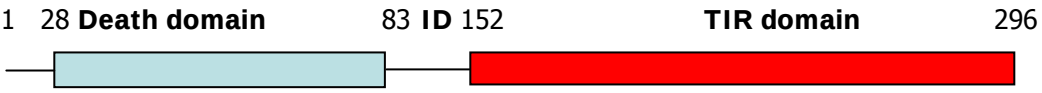

B

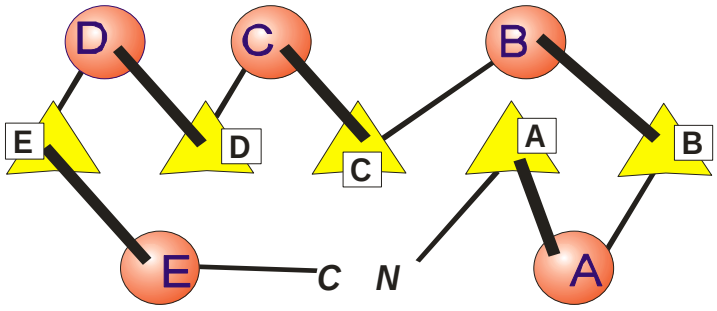

Figure 6. MyD88 contains TIR domain and death domain.
A, MyD88 is comprised of an amino terminal death domain (DD) similar to the intracellular segments of TNF receptor 1 (TNFR1) and FAS, as well as a carboxyl terminal TIR domain with a short intermediate segment in between. There is a short intermediate domain (ID). A splice variant without the ID domain, MyD88s, failed to recruit IRAK4 which is required for phosphorylation of IRAK1. MyD88s may function as a negative regulator of IL-1R/TLR/MyD88-triggered signals.
B, topology diagram of the TIR Domain. Parallel beta-sheets (with β-strands A-E as yellow triangles) are seen at their C-terminal ends; α-helices (red circles labeled A-E) link the β-strands; chain connections are to the front (visible) or back (hidden). Two connecting chains BB loop (between α-B helix and β-B strand) and EE loop (between α-E helix and β-E strand) will be off particular interest to this study of MyD88. Highly conserved sequences denoted Box 1, 2 and 3 are not depicted in this topology diagram (see Figure 8 and 9).

(Burns et al., 1998). As the key relay station in multiple IL-1R/TLR signaling pathways, the structure-function relationship of MyD88 is of special significance. Dominant-negative constructs of MyD88, lacking the death domain, block NFκB activation by multiple ligands in HEK293 cells when co-transfected together with the multiple receptors such as IL-1R, TLR-2, TLR-4, or TLR-9 (Bauer et al., 2001; Muzio et al., 2000). Upon activation of IL-1R complex by IL-1, MyD88 forms a complex containing MyD88, IRAKs and Tollip which leads ultimately to activation of NFκB (Cao et al., 1996; Wesche et al., 1997a). The association of MyD88 with the activated IL-1R complex is evidenced by coimmunoprecipitation experiments (Wesche et al., 1997a).

The significance of MyD88 in multiple IL-1R/TLR signaling is further demonstrated by recent studies in MyD88 deficient mice, which do not respond to ligands such as IL-1, IL-18, peptidoglycan, and CpG-DNA (Adachi et al., 1998; Kawai et al., 1999). However, in response to LPS and polyI:C, NFκB and MAPK activation still occurred albeit with slower kinetics despite the fact that cytokine production in macrophages and dendritic cells of these mice was impaired (Kaisho et al., 2001; Kawai et al., 2001; Yamamoto et al., 2003a). The existence of a MyD88-independent pathway in signaling initiated by TLR-4 and TLR-3 can be explained by the presence of other adaptor molecules involved in TIR domain-mediated signaling. A total of five such adaptor proteins are known to exist in mammals so far. These proteins are not entirely promiscuous in their interaction with TLRs, but rather, show preferential association with individual family

members, giving a particular character to the signals that distinct micro-organisms initiate.

Other adaptor proteins are involved in IL-1R/TLRs signaling

The second TIR domain containing adaptor protein is identified as MyD88-adaptor like (MAL/TIRAP) (Fitzgerald et al., 2001; Horng et al., 2001). Compared with MyD88, MAL also contains a COOH-terminal TIR domain, but there is no death domain on the NH_2-terminus (figure 4). The TIR domain of MAL interacts with the TIR domain of MyD88 and TLR-4, but not the IL-1R complex. Dominant-negative constructs of MAL/TIRAP specifically block LPS-induced TLR-4, but not IL-1R or TLR-9 signaling. Although MAL knockout mice are impaired in their responses to TLR-4 and TLR-2 ligands, LPS-induced dendritic cell maturation and activation of interferon-inducible genes is normal (Horng et al., 2002; Yamamoto et al., 2004). This finding suggests that MAL plays a role in the MyD88-dependent pathway shared by TLR-2 and TLR-4, instead of a distinct pathway from MyD88.

The third adaptor molecule identified recently is TIR domain-containing adaptor inducing IFN-beta (TRIF) (Yamamoto et al., 2002). TRIF, but neither MyD88 nor MAL/TIRAP, preferentially activates the IFN-ß promoter. Dominant-negative TRIF blocks polyI:C – induced, TLR-3-dependent activation of both the NFκB-dependent and IFN-β-dependent promoters, indicating that TRIF is the adaptor in the MyD88-independent TLR-3 signaling pathway (figure 4). Additional

support for the involvement of TRIF in this pathway was provided by its co-immunoprecipitation with TLR-3. TRIF may also be involved in LPS-induced MyD88-independent signaling in TLR-4 pathway (Hirotani et al., 2005). However, TRIF does not bind TLR-4 directly, suggesting the existence of another adaptor to bridge TRIF and TLR-4.

The fourth adaptor is named TRIF-related adaptor molecule (TRAM), or TIR domain-containing protein (TIRP) (Bin et al., 2003; Fitzgerald et al., 2003; Oshiumi et al., 2003). The interactions between TRAM and the TLRs were examined by yeast two-hybrid analysis, and the results indicate that TRAM binds to TLR-4 as well as to TLR-3 albeit weakly. TRAM has not been found to bind to the TIR domains of TLR-2, TLR-5, TLR-6, TLR-7, TLR-8 and TLR-9 (Oshiumi et al., 2003). TRAM can form homodimers as well as heterodimers with TRIF but can not interact with MyD88 or MAL, indicating that TRAM may play a role in MyD88-independent TLR-4 signaling (figure 4). The involvement of TRAM in TLR-4-initiated signaling is supported by the evidence from a mouse gene knock out study (Yamamoto et al., 2003b). TRAM-deficient mice showed impaired LPS-induced cytokine production but retained a normal response to the ligands for TLR-2, TLR-3, TLR-7, TLR-9 as well as to stimulation with IL-1β. The activation of the MyD88-dependent pathway by LPS was unaffected in the TRAM-deficient mice but the activation of the MyD88-independent pathway was abolished.

Recently, the fifth TIR domain-containing adaptor was discovered. This adaptor is named SARM (SAM and ARM-containing protein). SARM is composed

of an N-terminal series of β-catenin/armadillo motifs and two tandem SAM domains adjacent to a C-terminal TIR domain (Mink et al., 2001). The SAM domain is known to be involved in signaling by homotypic- and heterotypic-oligomerization. The ARM motif is a 40-amino acid tandem repeat that mediates the interaction between β-catenin and its ligand, and can form interactions with other proteins, for example, the small GTPase Ras. Only three *Caenorhabditis elegans* proteins are thought to have TIR domains and two out of three are closely related to SARM. Strikingly, unlike the other adaptor proteins, SARM is the only TIR-containing adaptor that did not induce NFκB-dependent reporter activity (Kaiser and Offermann, 2005). Orthologs of SARM are found in nematode, insect, and fish (Kaiser and Offermann, 2005). Though the function of SARM remains unclear, the nematode ortholog of SARM, TIR-1, is necessary for the cellular response to fungal infection and signals independently of the single TLR expressed in *Caenorhabditis elegans* (Couillault et al., 2004). Overexpression of the TIR domain of SARM partially inhibits IL-1 induced activation of NFκB reporter gene in HepG2 cells (Sethman and Hawiger, unpublished data). Thus, SARM may have a role in IL-1R/TLR-related innate immune responses. The fact that SARM contains both catenin/armadillo motifs and a TIR domain suggests that it may be imported into the nucleus. Further experiments including studies of SARM- deficient mice are needed to unveil the involvement of SARM in TLR signaling. The diagram depicting the domainal structure of these five adaptor proteins discussed above is shown in figure 7. While all adaptor proteins contain

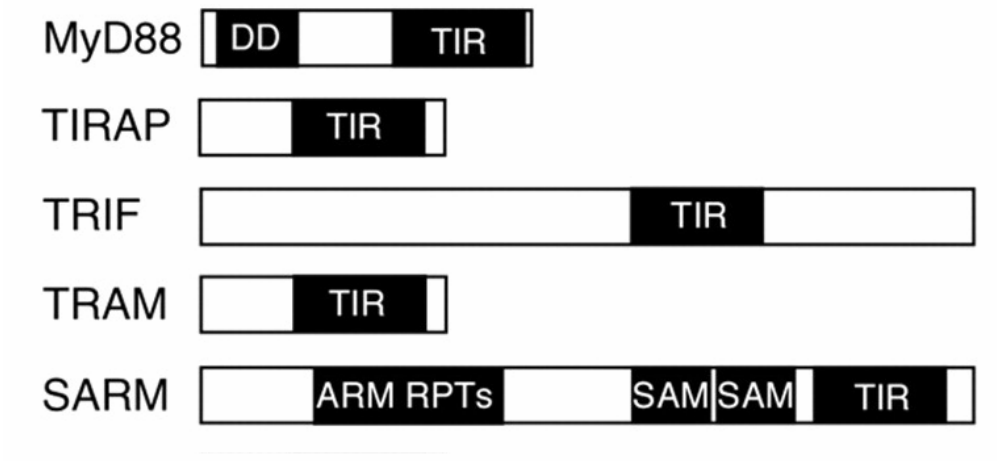

Figure 7. Schematic diagram of five members in the adaptor family of IL1R/TLR superfamily. MyD88 is the only adaptor which contains a death domain (DD). TRIF and SARM are considerably longer than the other TIR domain containing adaptor proteins. Unlike the other four adapter proteins that contain the TIR at the C terminus, TRIF has 400 amino acid at the N-terminus and a C-terminal extension. SARM is composed of an N-terminal series of β-catenin/armadillo motifs and two tandem SAM domain before a C-terminal TIR domain. MAL/TIRAP and TRAM are the smaller in size among the five adaptors, which contain short N-terminal extensions with no known homology to other proteins.

Modified from *Kaiser W.J. et al, The Journal of Immunology*, 2005, 174: 4942-4952.

the TIR domain, only MyD88 bears the death domain (DD) and is uniquely involved in IL-1 beta signaling.

The IL-1β signaling pathway depends on an orchestrated interplay of intracellular protein-protein interactions(Akira and Sato, 2003; Dinarello, 2002; Yamamoto et al., 2004). MyD88 plays a pivotal role in these interactions by directing the flow of signals from IL-1β-occupied cognate receptor complexes to downstream signal transducers (Akira and Sato, 2003; Yamamoto et al., 2004). Within MyD88, its TIR domain provides an interacting surface for heterotypic interaction with the TIR domain of IL1RAcP (Akira and Sato, 2003). Therefore, we embarked on structure-function analysis of the MyD88 TIR domain that is essential for the transduction of IL-1β signaling to downstream effector(s).

Formulation of working hypothesis and experimental strategy

MyD88 integrates signals flowing from IL-1R/IL1RAcP(Akira, 2003). This initial IL-1 receptor – MyD88 adaptor interaction evoked by IL-1β is a critical step in its signaling to the nucleus. Therefore, this interaction represents a potential target for new anti-inflammatory therapeutic agents. MyD88 has a bi-domainal structure comprised of amino terminal death domain and carboxyl terminal TIR domain (McGettrick and O'Neill, 2004). Interaction between IL1RAcP and MyD88 characterized in coimmunoprecipitation studies has indicated that the EE loop and box 3 of the TIR domain in IL1RAcP were required for MyD88 binding (Radons et al., 2002). However, no information was available regarding the

corresponding interactive sites on MyD88. We hypothesize that MyD88 interacts with IL1RAcP via specific surface area(s) in its TIR domain, most likely located within the three conserved boxes.

To study the molecular determinants of MyD88 TIR domain interactions in the IL-1β signaling pathway, a series of truncation/deletion mutants of the MyD88 TIR domain were made. Using an established NFκB reporter assay in HEK293T cells transiently transfected with these mutants, I demonstrated that the TIR domain mediates a dominant negative effect on IL-1β- induced NFκB activation. The integrity of the TIR domain is important for its function in binding to the IL-1R complex. MyD88 TIR mutants containing alanine substitutions of putative interactive sites were generated and the significance of these selected residues was evaluated in NFκB activation, cytokine production, and direct interaction with IL1RAcP. Computational modeling and docking study were applied for further verification of the identified interactive sites. It is anticipated that these structural-functional studies of MyD88 will help to establish the molecular determinants of MyD88 TIR domain interactions in the IL-1β signaling pathway.

CHAPTER II

ANALYSIS OF MYD88 TIR DOMAIN IN IL-1B PATHWAY

Synopsis

Myeloid differentiation primary response gene (MyD88) is the essential adaptor protein that integrates and transduces intracellular signals generated by multiple Toll-like receptors (TLRs) including the receptor complex for interleukin (IL)-1β, a key inflammatory cytokine. The IL-1β receptor complex interacts with MyD88 via the Toll/IL-1 receptor (TIR) domain. Here we report structure-function studies that further define the MyD88 TIR domain binding sites involved in IL-1β-induced protein-protein interactions. The MyD88 TIR domain, employed as dominant negative inhibitor of IL-1β signaling to screen MyD88 TIR mutants, loses its suppressing activity upon truncation of Box 3. Accordingly, mutations of Box 3 residues 285-286 reversed the dominant negative effect of the MyD88 TIR domain on IL-1β-induced and NFκB-dependent reporter gene activity and IL-6 production. Moreover, mutations of residues 171 in helix αA, 195-197 in Box 2, and 275 in βE strand had similar functional effects. Strikingly, only mutations of residues 195-197 eliminated the TIR-TIR interaction of MyD88 and IL1RAcP while substitution of neighboring canonical proline 200 by histidine was without effect. Mutations in Box 2 and 3 prevented homotypic MyD88 oligomerization via the

TIR domain. Based on this structure-function analysis, a 3-dimensional docking model of TIR-TIR interaction between MyD88 and IL1RAcP was developed.

Introduction

The importance of the Toll-like receptor (TLR) family in innate immune responses to microbial pathogenic molecular patterns is well established. Two members of this family recognize key inflammatory cytokines IL-1 and IL-18.

IL-1 is one of the most potent inflammatory cytokines and is responsible for fever, leukocytosis, thrombocytosis, and production of IL-6 and other cytokines (Akira and Sato, 2003; Dinarello, 2002; Yamamoto et al., 2004). The signals generated by the association of IL-1 and its cognate receptor complex, formed by two type 1 transmembrane proteins -- IL-1 receptor I (IL-1RI) and IL-1 receptor accessory protein (IL1RAcP) -- are transduced by their cytoplasmic segments denoted as the Toll/IL-1 receptor (TIR) domain. The TIR domain is shared with *Drosophila* Toll, mammalian TLRs, and cytoplasmic adaptors exemplified by MyD88 (McGettrick and O'Neill, 2004).

Although the biochemical processes of NFκB activation by IL-1 have been well characterized, the elucidation of the IL-1 receptor proximal signaling mechanisms mediated by TIR-TIR domain interaction has just begun within the last few years. Biochemical and genetic studies suggest that the initial IL-1 receptor-MyD88 adaptor interaction evoked by IL-1 binding to its receptor

complex is a critical step in its signaling to the nucleus (Adachi et al., 1998; Kawai et al., 1999).

The bi-domainal structure of MyD88 has been well characterized (McGettrick and O'Neill, 2004). MyD88 adaptor protein is composed of an amino-terminal death domain and a carboxyl-terminal TIR domain with a short intermediate linker segment. The TIR domain of MyD88 is thought to bind with that of the IL-1R, and the death domain interacts with the death domain found at the NH2 terminus of IRAKs. Upon ligand IL-1 binding, IL-1RI/IL1RAcP complex recruits MyD88 via its TIR domain (Wesche et al., 1997a). In addition, IL-1RI-associated kinases are recruited to an IL-1RI/IL1RAcP complex by death domain including IRAK (Huang et al., 1997; Wesche et al., 1997b), IRAK-2 (Volpe et al., 1997), IRAK-4 (Li et al., 2002) and IRAK-M (Kobayashi et al., 2002).

Although biochemical evidence indicates that activation of IL-1R involves the recruitment of specific post-receptor signaling complexes including IL-1R1, IL1RAcP, MyD88 and IRAKs, there is only limited structural information regarding protein-protein interaction within these complexes. In fact, the only structures solved to date are those of the isolated TIRs from TLR-1 and 2 (Xu et al., 2000). The 3-dimensional structures of these molecules have an overall fold with a central five-stranded parallel β-sheets surrounded by five helices, which are similar to the bacterial chemotaxis protein CheY, confirming the prediction made by Rock *et al.*, (Rock et al., 1998). Most of the conserved residues in TIR domains are buried in the center of the molecule, but some are solvent-exposed.

This exposure may form an interaction surface to which other TIR domain containing proteins, such as MyD88 or other adaptor proteins, can bind in response to signaling. Here we report the molecular determinants of MyD88 TIR domain interactions in the IL-1-signaling pathway.

In terms of its structural features, the MyD88 TIR domain contains three highly conserved motifs denoted Box 1, 2, and 3 (figure 8 and 9). Box 2 forms a loop denoted the BB loop that contains an invariant proline residue at position 200. A single amino acid mutation in the corresponding proline residue to histidine in the TLR-4 receptor renders C3H/HeJ mice hyporesponsive to LPS. The BB-loop connects the second β-strand (β-B) and second α-helix (α-B); a corresponding change also abolishes the ability of TLR-2 to interact with MyD88 *in vitro* (Poltorak et al., 1998). This proline residue is thought to be important in multiple TIR domain- mediated signaling pathway from receptors and adaptors based on mutation of invariant proline to histidine (for example, TLR-2, TLR-4, IL1RAcP, and MAL/TIRAP) (Akira, 2003; McGettrick and O'Neill, 2004). These canonical examples indicate that conserved structural motifs in the TIR domain of TLRs and their adaptors play a significant role in proinflammatory ligand-initiated intracellular interactions between these proteins.

Depending on the recognition of distinct ligands by TLRs, the preferential usage of its adaptors may require different interacting sites in the TIR domain of the same adaptor or an alternative adaptor. The latter applies to TLR-3, which requires its adaptor, TRIF, rather than MyD88 for signaling by viral double-

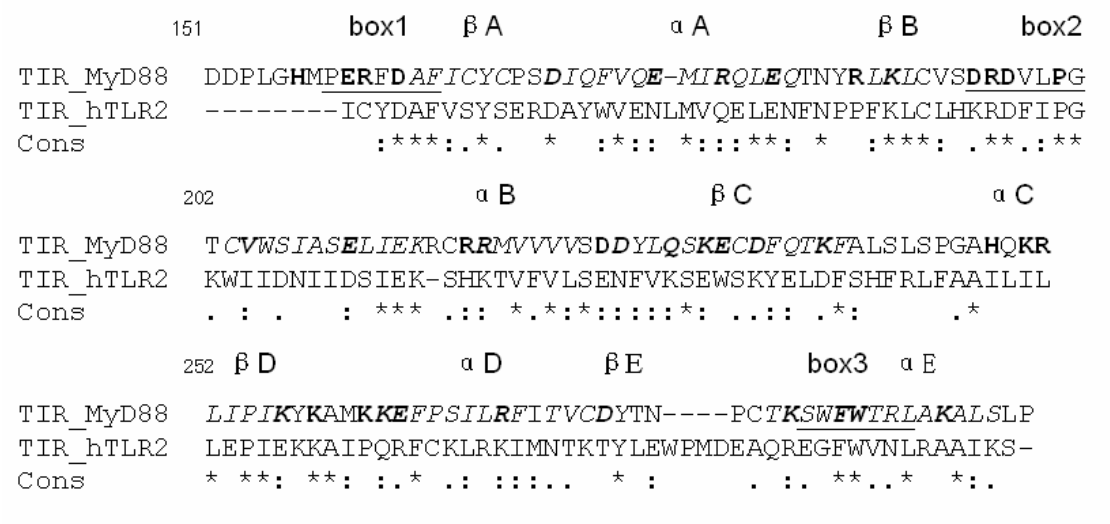

Figure 8. Sequence alignment of the TIR domain of human MyD88 and TLR-2. The crystal structure of the TIR domain of TLR-2 was used for homology modeling of MyD88-TIR performed with T_COFFEE. Box1-3 are underlined. Residues within MyD88 TIR domain substituted with alanine are shown in **bold**. Proline at position 200 is also shown in **bold** and substituted with histidine in this study.

Figure 9. Structural model of the MyD88 TIR domain with conserved box 1-3. Comparative modeling of MyD88-TIR was performed with SWISS-MODEL by aligning to crystal structure of hTLR2 optimized by GROMOS 96 and visualized by DeepView/Swiss-pdb viewer.
A, structural features representing the conserved boxes of the MyD88 TIR domain are shown in *yellow* (Box 1), *purple* (Box 2) and *blue* (Box 3).
B, electrostatic potential of MyD88 TIR with the indicated position of structural features (boxes 1-3) corresponding to same in panel *A*. The color scale is as follows: *red* (most negative) and *blue* (most positive).

A

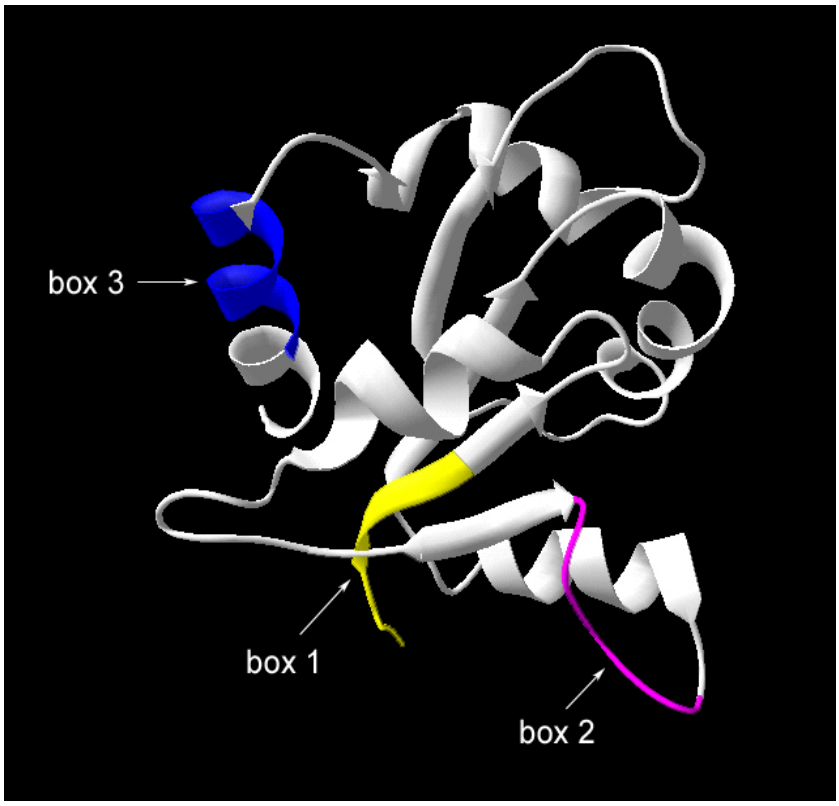

B

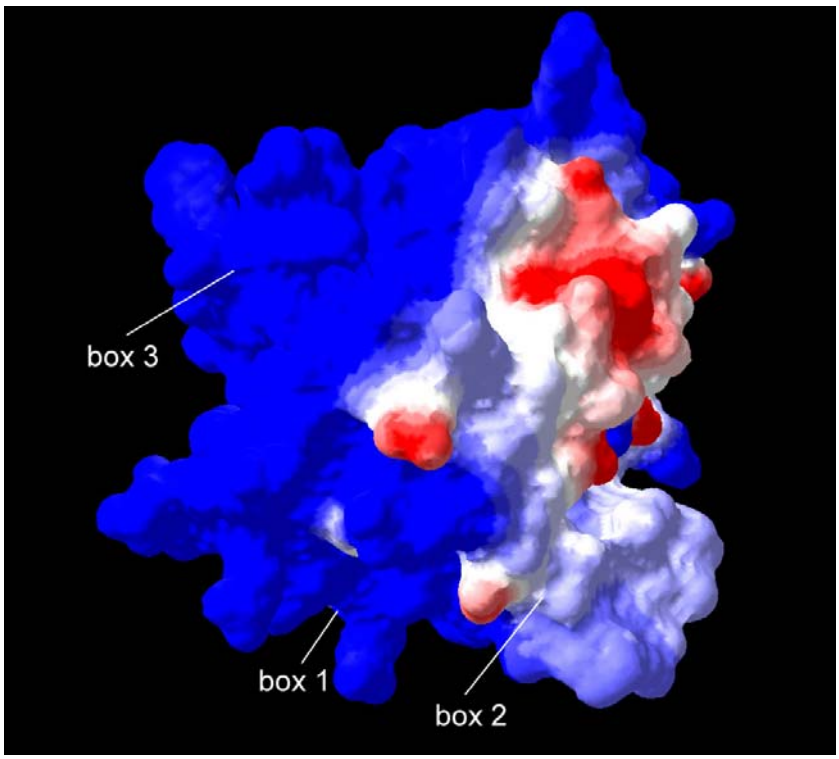

stranded RNA. Conversely, TRIF mediates signaling induced by interaction of LPS with TLR-4 in the absence of MyD88 (Akira, 2003). Different usage of the five currently known adaptor proteins may contribute to the specificity and selectivity of signaling events stimulated by different ligands for IL-1R/TLR family members.

We hypothesized that signaling evoked by IL-1 through its cognate receptor complex may depend on different interactive sites on the TIR domain of MyD88 other than the recently reported sites involved in MyD88 interaction with the TIR domains of TLR-2 and TLR-4 (Dunne et al., 2003).

Results

Our stepwise experimental strategy consisted of analysis of the secondary and tertiary structure of the MyD88 TIR domain. These data were extrapolated from the available crystal structure of TLR-2 TIR domain (Xu et al., 2000), which contains highly conserved Box 1-3 (figure 8), and we used as a comparative template for developing a structural model of the MyD88 TIR domain (figure 9). Drawing from these modeling studies, two series of mutagenesis experiments were performed. In the first set of experiments, a construct containing only the TIR domain of MyD88, as its dominant negative inhibitor, was mutated and the expressed mutants were screened for their inhibitory effect on IL-1β-induced signaling to the nucleus. In the second set of experiments, selected TIR residues were mutated in a full-length MyD88 to assess the impact of specific replacements on the heterotypic interaction of MyD88 with IL1RAcP and on

homotypic MyD88 oligomerization mediated by its TIR domain. The results from these structure-function analysis led us to the development of the 3-dimensional docking model of MyD88 interaction with IL1RAcP mediated by their respective TIR domains (Li et al., 2005).

Activation of NFκB by overexpression of MyD88 and its death domain is abolished in Phe^{56}Asn

Many adaptor proteins involved in signal transduction form homo- and heterotypic interactions through similar domains. MyD88 is composed of N-terminal death domain (DD) and C-terminal TIR domain, each of which promotes similar-domain interactions. As the death domain is a region that frequently promotes such interactions, MyD88 and its deletion mutations were therefore analyzed for NFκB activation using reporter gene activity assay (figure10*A*). To assess whether the death domain mediates NFκB activation, various point and deletion mutants of MyD88 were generated. Phe^{56} was chosen for mutagenesis based on sequence alignment of the MyD88 DD with the DD of Fas (Hofmann and Tschopp, 1995). A similar mutation at this position corresponds to the *lpr^{cp}* mutation known to abolish cytotoxic signaling of Fas by disrupting the conformation of the death domain (DD) as revealed by NMR spectroscopy (Huang et al., 1996). As shown in figure 10*B*, overexpression of MyD88 induces NFκB activation, consistent with a previous report (Burns et al., 1998). Overexpression of death domain can also activate NFκB as well as AP-1, probably

Figure 10. NFκB-dependent reporter gene activation by overexpression of MyD88 and its mutants.

A, schematic diagram of NFκB reporter gene activity assay driven by IL-1β or MyD88 overexpression.

B, the dependence of reporter gene activity on NFκB activation. HEK 293T cells (2×10^5) were transfected with 1 μg of IκBαΔN or control vector together with 1 μg κB-luc and 1 μg of RL-TK, 1 μg of MyD88 (*dark bar*); or 1.5 μg of empty vector (*open bar*). Note that cells transfected with IκBαΔN display minimal reporter gene activation.

C, Full-length MyD88 and MyD88 mutants are schematically represented. The stripped and gray rectangles represent the death and TIR domains, respectively. MyD88 containing a point mutation, F56N, in the death domain is represented by a *black circle*, and P200H, in the TIR domain is represented by a *open circle*.

D, concentration and structure dependenct NFκB activation MyD88 mutants. HEK 293T cells were transfected with 1 μg of κB- luc, 1 μg of RL-TK, and the indicated MyD88 constructs (0.4 and 2 μg of each).

E, Co-expression of TIR domain can inhibit reporter gene activation induced by forced expression of MyD88. Note that the reporter gene activation by ectopically expressed MyD88 is inhibited by co-expression of TIR domain, but not DD-F56N and TIR-P200H mutants. κB-luc activities in C-D were determined 24 h after transfection and normalized on the basis of RL-TK level. Values shown are averages for representative experiments in which each transfection was carried out in triplicate.

A

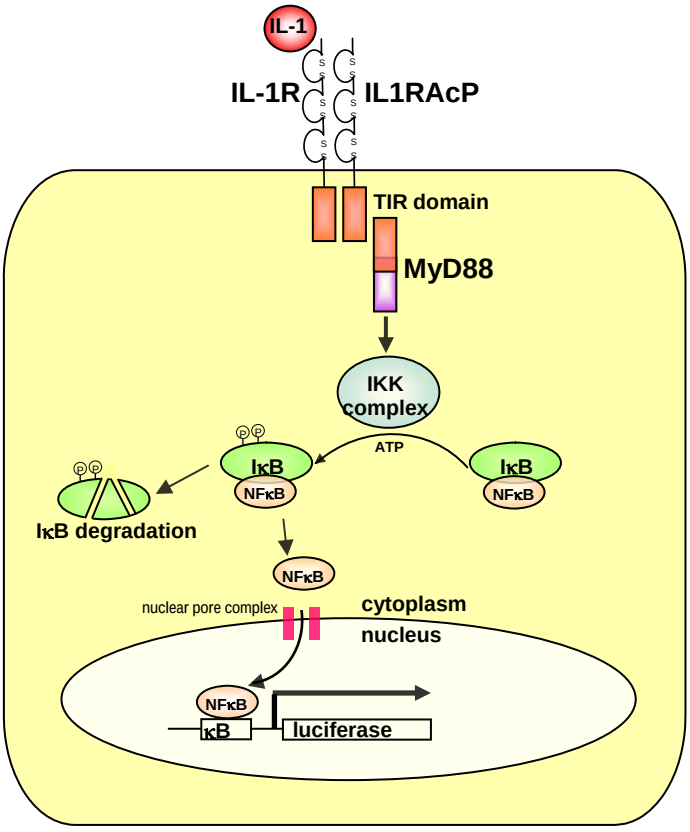
IL-1
IL-1R
IL1RAcP
TIR domain
MyD88
IKK complex
ATP
IκB
NFκB
IκB
NFκB
IκB degradation
NFκB
nuclear pore complex
cytoplasm
nucleus
NFκB
κB
luciferase

B

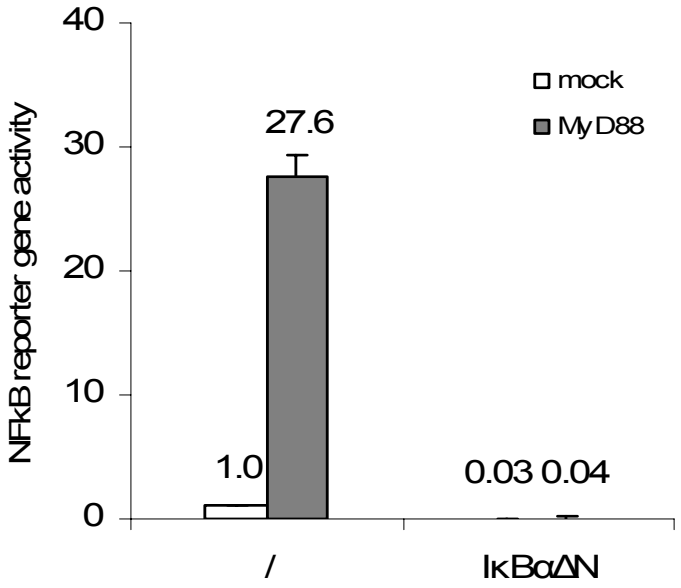
40
30
20
10
0
NFkB reporter gene activity
mock
MyD88
27.6
1.0
0.03 0.04
/
IκBαΔN

C

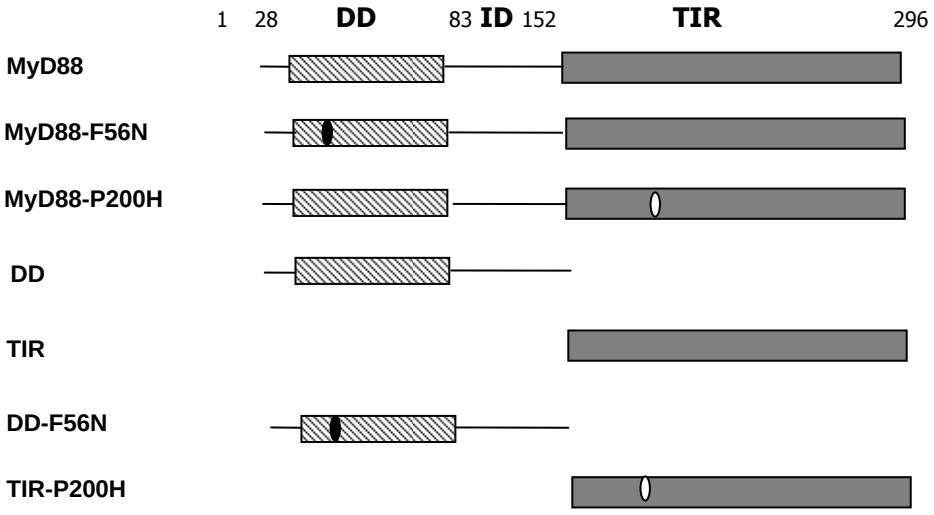
1
28
DD
83
ID
152
TIR
296
MyD88
MyD88-F56N
MyD88-P200H
DD
TIR
DD-F56N
TIR-P200H

D

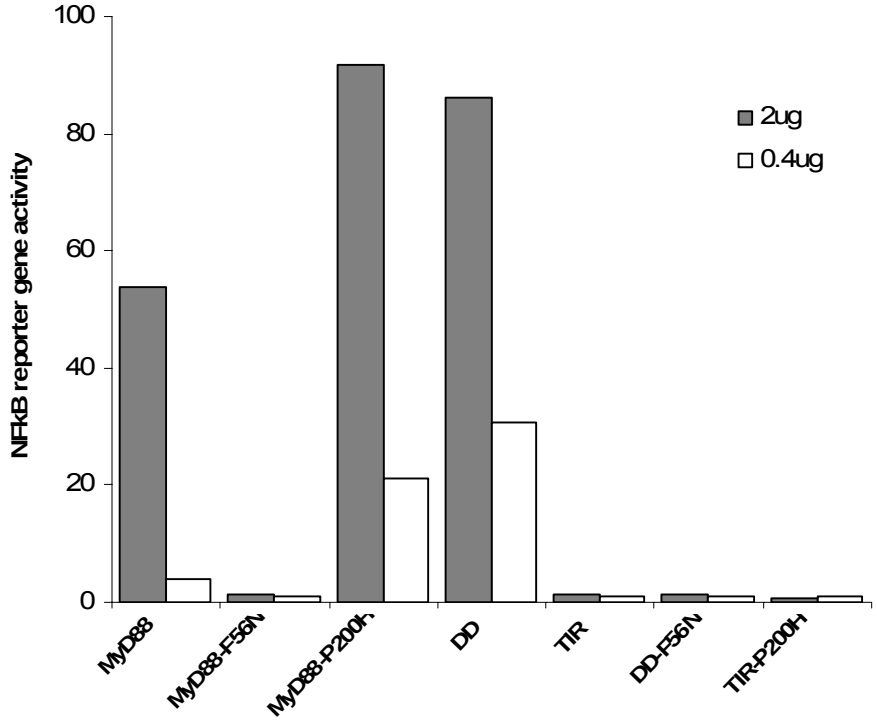
100
80
60
40
20
0
NFkB reporter gene activity
2ug
0.4ug
MyD88
MyD88-F56N
MyD88-P200H
DD
TIR
DD-F56N
TIR-P200H

E

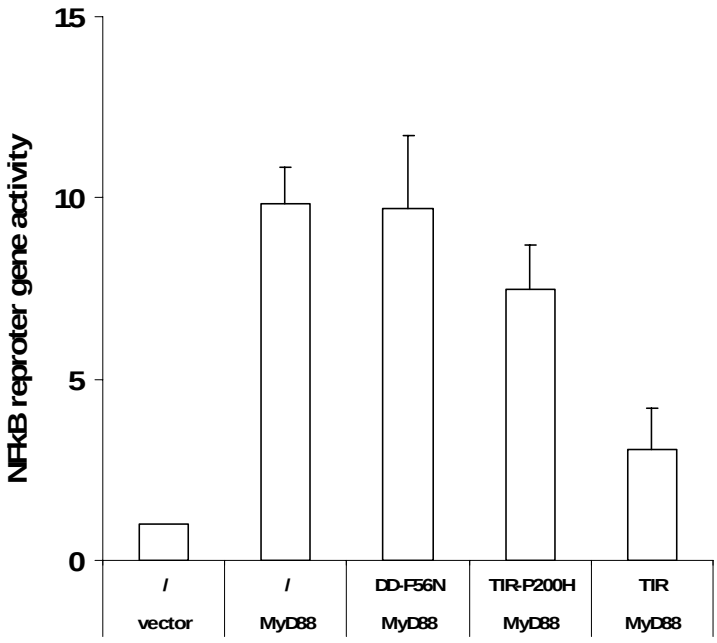
15
10
5
0
NFkB reproter gene activity
/
vector
/
MyD88
DD-F56N
MyD88
TIR-P200H
MyD88
TIR
MyD88

due to homotypic dimerization. However, overexpression of mutants carrying Phe^{56} to Asn in full length MyD88 (MyD88 F56N) and in its death domain (DD-F56N) abolished this activation of NFκB (figure 10*D*). To further assess the function of Phe^{56}, I conducted co-expression experiments with DD-F56N and MyD88 in HEK 293T cells. DD-F56N can not inhibit the NFκB activation induced by overexpression of MyD88, indicating that DD-F56N can not associate with MyD88 (figure 10*E*). There are at least two possible explanations for this loss-of-function mutation: first, Phe^{56} may be involved in the interaction and recruitment of downstream signaling molecules like IRAK; second, the Phe^{56} may be involved in the homotypic dimerization. Burns et al previously reported that the Phe^{56} Asn mutation abolished the interaction of death domains using a yeast two-hybrid assay, suggesting the latter scenario: the Phe^{56}Asn abolished the NFκB activation via disruption of the dimerization mediated through the death domain of MyD88 (Burns et al., 1998).

Although forced expression of full length MyD88 and MyD88-DD strongly induced NFκB activation in 293T cells, as previously reported by others (Burns et al., 1998), the truncation mutants TIR and TIR-P200H were inactive. MyD88 induced the activity of NFκB reporter gene in a dose-dependent manner and this activation was abolished by co-expressed IκBαΔN, an IκBα degradation-resistant mutant form that blocks nuclear translocation of NFκB (Boothby et al., 1997; Liu et al., 2004b). Thus, these results confirmed the dependence of reporter gene activation on NFκB (figure 10*B*).

NFκB activation following transient transfection of MyD88 constructs was also observed with the MyD88-P200H mutant expression vector, suggesting that this canonical proline200 is not involved in MyD88-dependent signaling. However, this result can also be explained by the finding that intact death domain alone is capable of inducing NFκB activation. As described in the previous chapter, the proline 200 residue is highly conserved amongst the members of IL-1R/TLR family. The experimental evidence concerning its potential role in IL-1β signaling will be shown later in this chapter.

Structural characterization of MyD88 TIR domain

To study the TIR-TIR interaction of MyD88, a computational model of its TIR domain was established. This TIR domain is modeled on the basis of the crystal structure solved for TLR-2 (Xu et al., 2000). As shown in figure 6*B*, it has an α-β fold similar to that of the bacterial chemotaxis protein CheY and contains three highly conserved motifs termed Boxes 1, 2, and 3 (Akira and Sato, 2003). On the basis of primary structure alignment obtained with the program T-COFFEE, presented in figure 8, the crystal structure of human TLR-2 TIR domain (Protein Data Bank pdb files of *1O77*) was selected as the best template for the MyD88 TIR domain with 31% identity and >50% similarity. Results obtained from the server were visualized with the DeepView program (Swiss Pdb viewer). As shown in figure 9, the secondary structure of the TIR domain consists of five β strands: β-A, β-B, β-C, β-D and β-E forming the core of molecule which is

surrounded by five α-helices: α-A, α-B, α-C, α-D and α-E. The five loops AA, BB, CC, DD and FF form specific links between β-strand and corresponding α-helix. In terms of its tertiary structure, as depicted in figure 9, the MyD88 TIR domain has a globular shape. Among three highly conserved motifs, Box 1, located at the N-terminus of the TIR domain, partially forms a β-A strand. Box 2 makes the second part of the BB loop, while Box 3 creates the first part of α-E helix, which is located at the C-terminus of MyD88 TIR domain. Analysis of the distribution of charged residues indicates that the molecular surface of MyD88 TIR domain is mostly positively charged (blue) with a few distinct negatively charged knobs (red). They surround a larger swatch of negatively charged surface (red), formed by three loops, AA, BB, and partially DD, and α-C helix. Moreover, the BB loop, projects from the globular TIR domain, forming a quasi-plane on its surface.

Box 3 of MyD88 TIR domain is involved in IL-1β-induced signaling

To study the molecular determinants of MyD88 TIR domain interactions in the IL-1β signaling pathway with its mutants, human embryonic kidney 293T cells were transiently transfected with κB reporter gene. The HEK 293T cells respond to IL-1β in a wide range of concentrations (0.03 – 30 ng/mL) in a dose dependent manner (figure 11*A*). Co-expression of IκBαΔN (kindly provided by Dean W. Ballard, Vanderbilt University), a degradation-resistant mutant form of IκBα with truncation at its N-terminus, resulted in complete inhibition of NFκB reporter gene activity (figure 10*B*). However, HEK 293T cells did not respond to

A.

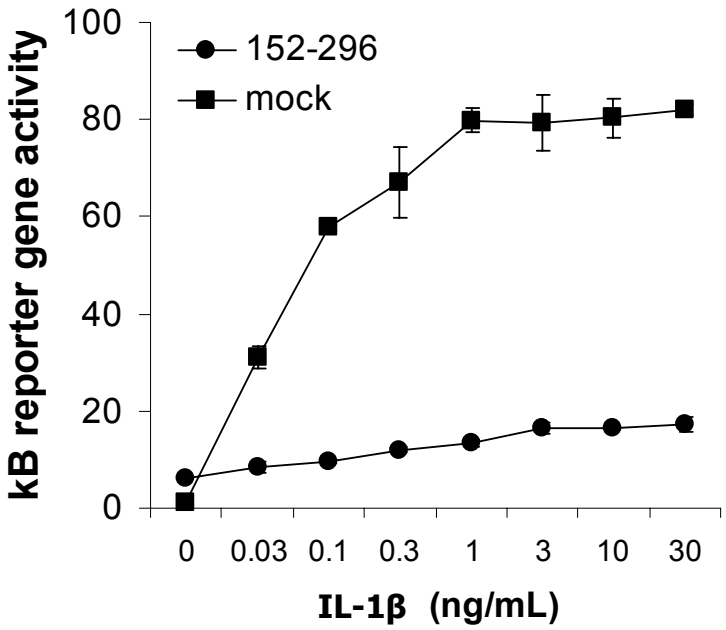

Figure 11. Inhibition of IL1β-induced κB reporter gene activity by MyD88 TIR domain.

A, IL1β-induced κB reporter gene activation was inhibited in HEK 293T cells transfected with MyD88 TIR (152-296). The HEK 293T cells were transfected with MyD88 TIR together with κB-luc (5μg) and RL-TK (2.5μg). After 24 h, IL1β was added at indicated concentrations for 6 h. NFκB-reporter gene activity was determined and normalized on the basis of RL-TK activity.

B, diagram of deletion mutants containing MyD88 TIR domain and the expression level in transfected 293T cells. All these mutants are inserted into pcDNA3.1 using PCR at *BamH* I and *EcoR* I sites. TIR and TIRΔC(152-283) were selected for further study.

C, truncation of the COOH terminal segment of TIR (TIRΔC) reverses the inhibitory effect of the TIR domain. HEK 293T cells were transfected with MyD88-TIR or MyD88-TIRΔC (152-283) constructs together with κB-luc (5 μg) and RL-TK (2.5 μg). After 24 h, IL1β was added at a concentration of 10 ng/mL for 6 h. NFκB reporter gene activity was measured and normalized on the basis of RL-TK activity. *Insets*, Expression levels of MyD88-TIR and MyD88-TIRΔC (152-283) in transfected HEK 293T cells determined by immunoblotting with anti-AU1 antibody. A representative experiment is shown from the series of three performed in triplicate. Error bars indicate the ± S.E. of the mean value of triplicate.

B.

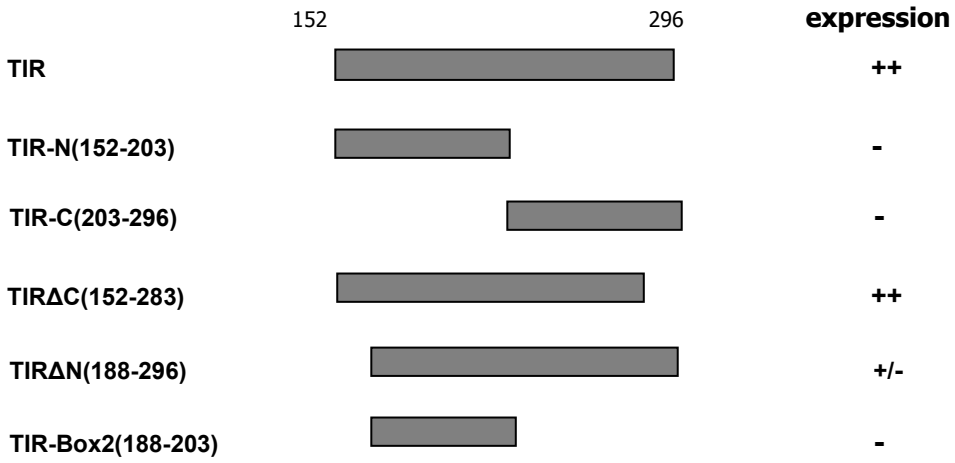
152
296
expression
TIR
++
TIR-N(152-203)
-
TIR-C(203-296)
-
TIRΔC(152-283)
++
TIRΔN(188-296)
+/-
TIR-Box2(188-203)
-

C.

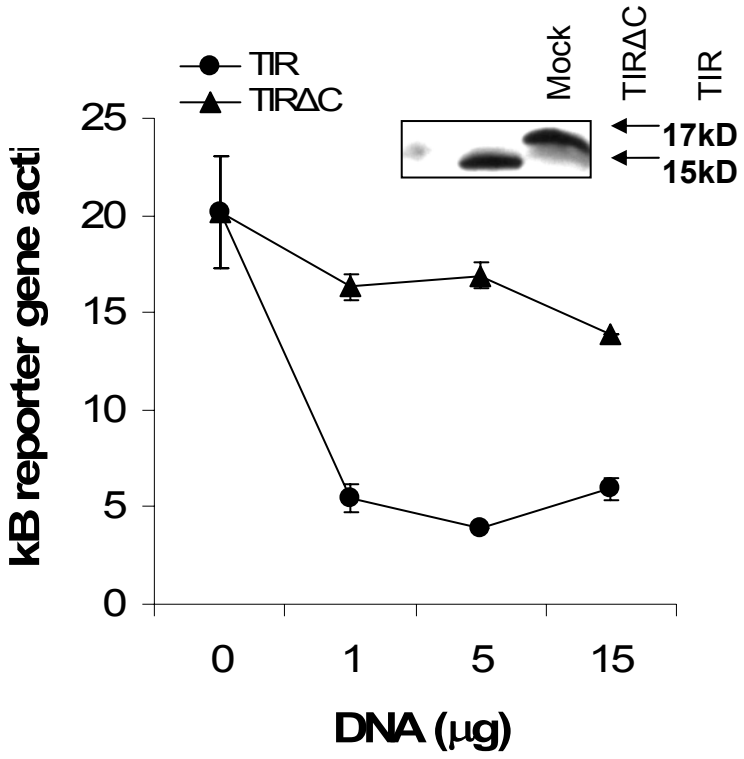
TIR
TIRΔC
Mock
TIRΔC
TIR
17kD
15kD
kB reporter gene acti
25
20
15
10
5
0
0
1
5
15
DNA (μg)

IL-1β in NFκB-dependent reporter gene activity assay after ten passages. Thus, 293T cells freshly thawed were used throughout this study. In previous reports of IL-1β- induced NFκB signaling, the most commonly used cell line is human embryonic kidney cells 293-IL-1RI, which was stably transfected with human IL-1RI (Cao et al., 1996; Radons et al., 2003).

Kappa B reporter gene activity assay was used to test the MyD88 TIR domain as **a** dominant negative inhibitor of IL-1β-induced signaling to the nucleus. As documented in figure 11*A*, HEK 293T cells transfected with plasmid containing NFκB-dependent luciferase gene responded to sub-nanogram doses of IL-1β. This activation reached its maximum at 1 ng/mL of IL-1β attesting to the high sensitivity of transfected 293T cells to this inflammatory cytokine. Consistent with prior studies (Burns et al., 1998; Dupraz et al., 2000), the MyD88 TIR domain, used as a dominant negative inhibitor of IL-1β signaling, almost completely suppressed its activating effect on the reporter gene over a wide range of IL-1β concentrations (figure 11*A*). The TIR domain of MyD88 contains segments of conserved sequences, namely, Box 1, 2, and 3 shared by IL-1R/TLR superfamily members (see previous chapter). Whether all of these boxes are necessary for the function of this dominant negative inhibitor of IL-1β signaling is an important question to address. To study the molecular determinants of the MyD88 TIR domain interactions in IL-1β signaling pathway, I engineered deletion mutants of MyD88 TIR domain to screen them in an established reporter gene activity assay for their inhibitory effect on IL-1β-induced signaling. As depicted in

figure 11*B*, the TIR domain mutants include deletions of N-terminus Box 1 (TIRΔN, 188-296), Box1 and Box 2 (TIR-C, 203-296), Box 1 and Box3 (TIR-Box2, 188-203), C-terminus Box 3 (TIRΔC, 152-283), as well as a deletion of the segments after Box 2 (TIR-N, 152-203). These cDNA fragments were generated by PCR to add an N-terminal AU1-tag and then cloned into pcDNA3.1 at *BamH* I and *EcoR* I sites under control of CMV promoter.

Sequence-verified mutants were transiently transfected into HEK 293T cells to test them for expression and potential inhibitory effect on IL-1β-induced NFκB signaling. As shown in figure 11*B*, only TIRΔC missing a segment encompassing Box 3 (282KSWFWTRLAK291) located at the COOH-terminus of MyD88 TIR domain was expressed at the level comparable to that of intact MyD88 TIR upon transient transfection (see inset). This deletion in TIRΔC caused the loss of the dominant negative inhibitory function of MyD88 TIR (figure 11*C*) suggesting that Box 3 was essential for IL-1β-induced signaling. Other mutants were undetectable in transfected HEK 293T cells by either immunoblotting analysis or immunohistochemical staining with anti-AU1 antibody (data not shown). The fact that the Box 3 deletion mutant was expressed in transfected cells at a level comparable to the intact MyD88 TIR domain but deletion mutants lacking Box 1, Box 1&2, Box 1&3 were not expressed, suggests that Box 1 and 2 are important for TIR domain structural integrity and stability in HEK 293T cells.

Based on the results presented above, Box 3 of the MyD88 TIR domain is essential for IL-1β-induced NFκB signaling. Whether Box 3 is involved in MyD88

interaction with IL1RAcP or in homodimerization of MyD88 was determined in subsequent experiments (see below). Significantly, prior studies based on the yeast - two hybrid assays indicated that MyD88-TIR did not dimerize with a deletion mutant missing 15 amino acids at the C terminus (Burns et al., 1998; Dupraz et al., 2000).

Site-directed mutagenesis of MyD88 TIR domain leads to loss of its inhibitory activity toward IL-1β–induced signaling

The involvement of Box 3, as compared to Boxes 1 and 2, in signaling induced by IL-1β and mediated by the MyD88 TIR domain, was further analyzed in a series of mutagenesis experiments. Mutations of the TIR domain (residues 152-296) included two bulky hydrophobic residues (F285 and W286) in the highly conserved short motif in Box 3 (SWFWTRL) and proline at the position 200. The canonical $Pro^{712}His$ mutation in TLR-4 renders C3H/HeJ mice hyporesponsive to LPS (Poltorak et al., 1998). Furthermore, alignment of members of the TLR family revealed two short motifs in Box 1 (PERFDAF) and Box 2 (DRDVLPG) that are most conserved along with Box 3 motif in MyD88 TIR domain. Alanine substitutions were primarily based on selection of charged residues either in the conserved region or predicted to be on the surface (figure 8). In addition, two mutations, V204 and Q229 were in the region predicted to interact with MAL (Dunne et al., 2003). The expression level of all the TIR domain mutants and their functional analysis of NFκB reporter gene activation are depicted in figure 12.

Figure 12. Selected MyD88 TIR domain mutants with "loss of inhibition" phenotype.

A, functional analysis of MyD88 TIR domain mutants. MyD88 TIR domain mutants that did not inhibit NFκB reporter gene activity 2.5 fold or more were considered "loss of inhibition" phenotype as compared to the dominant negative inhibitory effect of wild type MyD88 TIR domain. Blue, mutants with "loss of inhibition" phenotype, include D171A (T1), D195A/R196A/D197A (T2), D275A (T4), F285A/W286A (T5). Pink, mutants that expressed and displayed similar phenotype as wild type TIR, including P200H (T3). Gray, mutants that were not expressed. T1 to T5 were selected for further functional analysis. Box1-3 are underlined. Residues within MyD88 TIR domain substituted with alanine are shown in **bold**. Proline at position 200 is also shown in **bold**.

B, location of T1, T2, T4 and T5 mutants which displayed "loss of inhibition" phenotype on the ribbon structure of MyD88 TIR domain. Conserved boxes of MyD88 TIR domain are shown in *yellow* (Box 1), *purple* (Box 2) and *blue* (Box 3). P200H (T3) is located on Box 2 (side chain not shown).

A

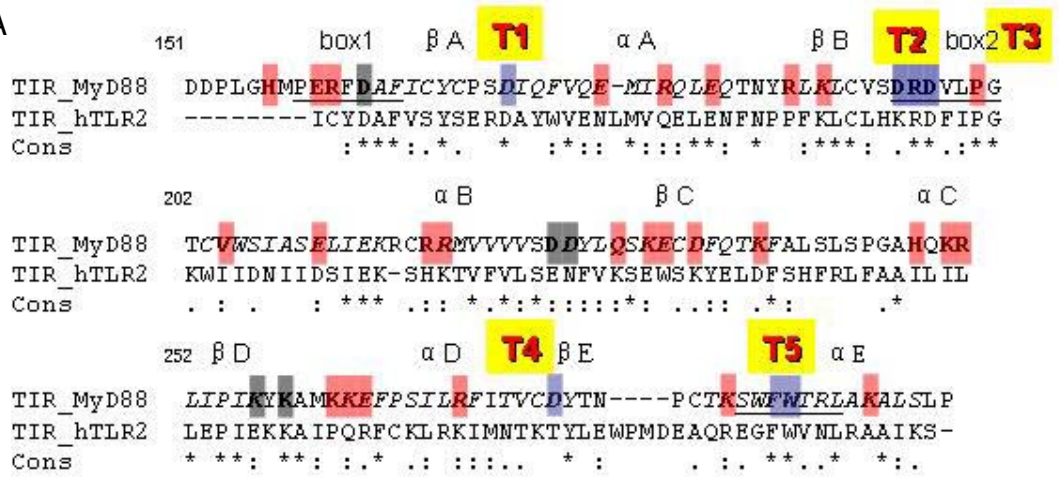
151
box1
β A
T1
α A
β B
T2
box2
T3
TIR_MyD88 DDPLGHMPERFDAFICYCPSDIQFVQE-MIRQLEQTNYRLKLCVSDRDVLPG
TIR_hTLR2 --------ICYDAFVSYSERDAYWVENLMVQELENFNPPFKLCLHKRDFIPG
Cons :***:.*. * :*:: *:::**: * :***: .**.:**
202
α B
β C
α C
TIR_MyD88 TCVWSIASELIEKRCRRMVVVVSDDYLQSKECDFQTKFALSLSPGAHQKR
TIR_hTLR2 KWIIDNIIDSIEK-SHKTVFVLSENFVKSEWSKYELDFSHFRLFAAILIL
Cons . : . : *** .:: *.*:*:::::*: ..:: .*: .*
252
β D
α D
T4
β E
T5
α E
TIR_MyD88 LIPIKYKAMKKEFPSILRFITVCDYTN----PCTKSWFWTRLAKALSLP
TIR_hTLR2 LEPIEKKAIPQRFCKLRKIMNTKTYLEWPMDEAQREGFWVNLRAAIKS-
Cons * **: **: :.* .: :::.. * : . :. **..* *:.

B

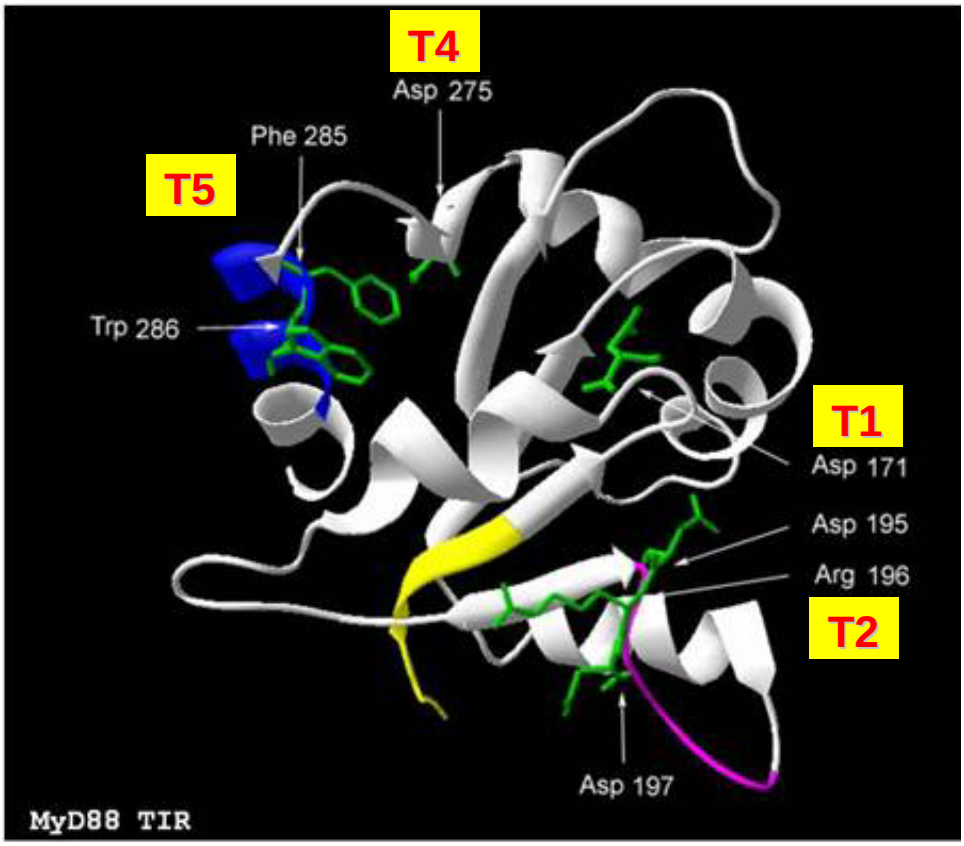
T4
Asp 275
Phe 285
T5
Trp 286
T1
Asp 171
Asp 195
Arg 196
T2
Asp 197
MyD88 TIR

The expression of mutants varied as compared to that of the wild type MyD88 TIR domain (Figure 12). These mutants can be divided into three groups: the first group, TIR mutants that were expressed at a level comparable to that of the wild type MyD88 TIR domain and displayed a loss of inhibition of IL-1β -induced reporter gene activity. They include D171A (T1), D195A/R196A/D197A (T2), D275A (T4), F285A/W286A (T5). The second group encompasses MyD88-TIR mutants that are not expressed presumably due to misfolding and/or degradation. They include D162A, D225A/D226A, K256A and K258A. The third group includes TIR mutants which were expressed and inhibited IL-1β -induced reporter gene activation comparable to that of the wild type TIR. This group included the remainder of the mutants. Of particular significance is the result with the P200H mutant (T3), analogous to the $Pro^{712}His$ mutation in TLR-4, which is responsible for the LPS hyporesponsiveness of C3H/HeJ mice (Poltorak et al., 1998). Similar loss of signaling in other TIR-containing molecules like MAL/TIRAP (Horng et al., 2001) and IL1RAcP (Radons et al., 2003; Radons et al., 2002) were reported, indicating that the invariant proline in the BB loop of Box 2 in these molecules is one of the interactive sites for other TIR domains-containing proteins. In striking contrast, a similar mutation (P200H, T3) in the MyD88 TIR domain, tested over a range of input concentrations, did not change the dominant negative effect of MyD88 TIR on IL-1β-induced reporter gene activation in HEK 293T cells (figure 13*A*). These cells showed a similar level of expression of the intact and mutant TIR proteins (insert in figure 13*A*). This

Figure 13. Functional analysis of MyD88 TIR domain mutants tested in κB reporter gene activity assays.
A, Concentration-dependent inhibition of NFκB reporter gene activity by wild-type and T3 mutant (Proline200Histidine);
B, Inhibition of κB reporter gene activity by mutants T1, T2, T4, and T5. HEK 293T cells were transfected with MyD88-TIR or its mutant constructs (1-15 μg in panel *A* and 12.5 μg in panel *B*) together with κB-luc and RL-TK. After 24 h, IL-1β was added at a concentration of 10 ng/mL for 6 h. Cells were harvested and split for both reporter assay and immunoblotting. κB reporter gene activity was analyzed and normalized on the basis of RL-TK level. The figure shown was a representative of three experiments. *Insets*, expression levels of TIR and TIR mutants as determined by immunoblotting. Data represent combined results from three independent experiments done in triplicate. Error bars indicate the ± S.E. of the mean.

A

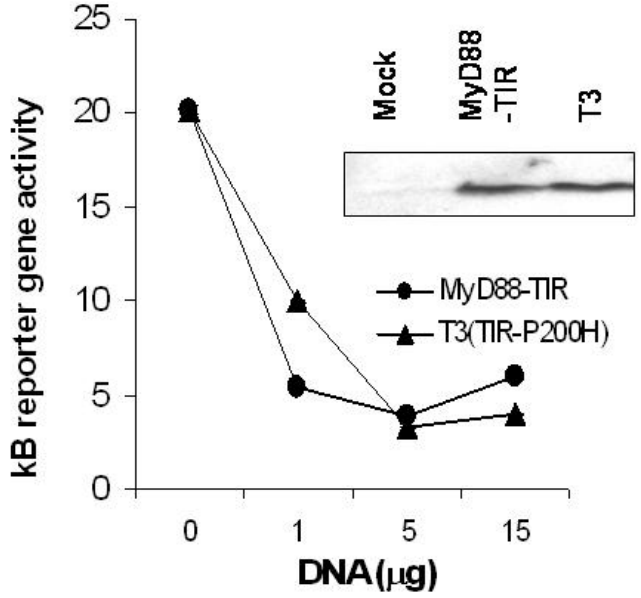
kB reporter gene activity
25
20
15
10
5
0
0
1
5
15
DNA(μg)
Mock
MyD88
-TIR
T3
MyD88-TIR
T3(TIR-P200H)

B

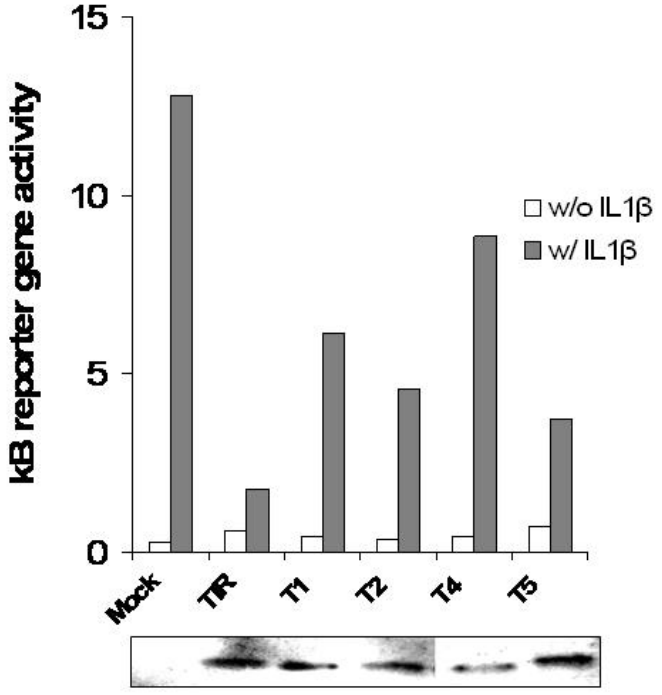
kB reporter gene activity
15
10
5
0
w/o IL1β
w/ IL1β
Mock
TIR
T1
T2
T4
T5

result is consistent with recent modeling studies of the interaction of MyD88 with TLR-2 and 4, which suggested that the highly conserved proline residue may not participate in the protein-protein interactions of MyD88 with TLRs (Dunne et al., 2003).

In contrast to the canonical P200H mutation, the following mutants displayed >2.5 fold loss of the dominant negative effect on IL-1β- stimulated reporter gene activation as compared to the wild type MyD88 TIR domain (figure 13*B*): D171A in helix α-A (T1), triple mutant D195A/R196A/D197A (T2) in Box 2, D275A in β-E strand (T4), and double mutant F285A/W286A (T5) in Box 3. The result with the F285A/W286A mutant is consistent with the loss of inhibition displayed by Box 3-deleted MyD88 TIR domain (figure 11*C*). All these mutants and intact MyD88 TIR domain were expressed at comparable levels in HEK 293T cells (insert in figure 13*B*). Therefore, these mutants were chosen for further validation of the functional significance of mutated residues in the MyD88 TIR domain.

Inhibition of cytokine production by MyD88-TIR mutants

We selected IL-1β-induced expression of an endogenous gene that encodes the inflammatory cytokine, IL-6, in human fibroblast MRC5 cells for testing MyD88 TIR domain mutants. The expression of the IL-6 gene is regulated by NFκB and its mobilization by IL-1β is dependent on MyD88 (Akira and Sato, 2003; Dinarello, 2002; Yamamoto et al., 2004). As shown in figure 14*A*, upon

Figure 14. Inhibition of IL-6 production by MyD88-TIR mutants T1, T2, T4 *(A)* **and T5 as compared to nuclear inhibitor SN50 peptide** *(B)*.

A, IL-1β - induced IL-6 production of MRC-5 cells is specifically inhibited by MyD88-TIR mutants. IL-6 production was analyzed with CBA.

B, IL-1β induced - IL6 production of MRC-5 cells is specifically inhibited by nuclear inhibitor peptide SN50. MRC-5 cells pretreated for 30min with 100 μM SN50 in HBSS or diluent HBSS and then stimulated with 10ng/mL of IL-1β for 6 hrs. Data represent combined results from three independent experiments done in triplicate. Error bars indicate the ± S.E. of the mean. ** $P<0.01$, * $P<0.05$, by two-sided Student's *t* - test.

A

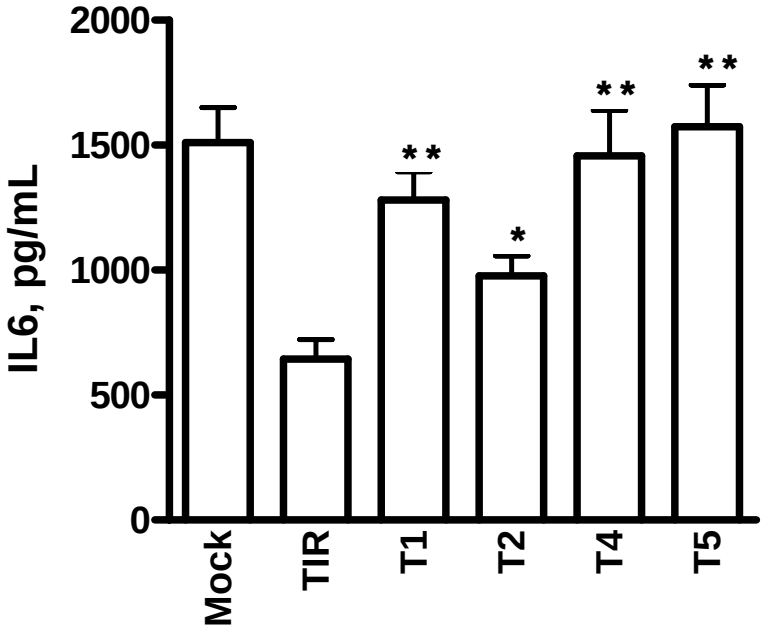
2000
1500
1000
500
0
IL6, pg/mL
**
*
**
**
Mock
TIR
T1
T2
T4
T5

B

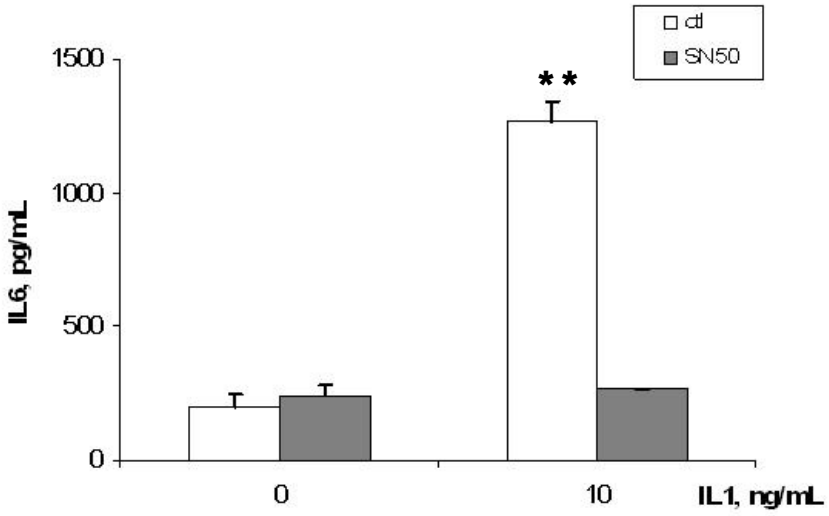
ctl
SN50
1500
1000
500
0
IL6, pg/mL
**
0
10
IL1, ng/mL

stimulation of MRC5 cells with IL-1β, the inflammatory cytokine IL-6 was expressed. To validate its dependence of NFκB and other SRTFs, a nuclear import inhibitor, SN50 peptide, was utilized which is able to block NFκB responses(Lin et al., 1995). Treatment with SN50 completely abolished the IL-1 induced IL-6 production. This expression of endogenous IL-6 gene was suppressed 2.5 fold by dominant negative TIR domain of MyD88 (figure 14*B*). The observed degree of inhibition of endogenous IL-6 gene expression is smaller, albeit still significant, than the suppression of reporter gene activity by MyD88 TIR domain observed in HEK 293T cells. The most likely reason for lower degree of inhibition is lower transfection efficiency of MRC5 cells that minimizes the impact of potential inhibitors on IL-6 expression. Nevertheless, inhibition of IL-1β-induced IL-6 production was depended on residues D171, D275, D195/R196/D197 and F285/W286 because alanine substitutions reduced dominant negative effect of wild-type MyD88 TIR domain. These functional studies of IL-1β-induced IL-6 production are consistent with reporter gene activation (figure 13*B*). Thus, our first series of mutagenesis experiments identified interactive sites within the MyD88 TIR domain responsible for coupling IL-1β signaling to NFκB translocation to the nucleus and induction of endogenous IL-6 gene.

Mutagenesis of full-length MyD88 reveals an interactive site for direct contact with IL-1RAcP

It is still unknown which of the interactive sites identified in the MyD88 TIR domain are responsible for direct contact of MyD88 with the IL-1 receptor complex subunit, IL1RAcP, which is indispensable for IL-1β signaling (Radons et al., 2002). Theoretically, the MyD88 TIR domain may mediate binding to other adaptor proteins also (Dunne et al., 2003). Alternatively, these interactive sites within MyD88 could participate in IL-1β-induced oligomerization of MyD88 through homotypic interactions mediated by its TIR domain.

To sort out these possibilities, a second series of mutagenesis experiments was conducted using a similar strategy. Five selected mutations were engineered in a full length MyD88 to allow a comparative analysis of its direct interaction with IL1RAcP (Table 1). HEK 293T cells were co-transfected with myc-IL1RAcP and AU1-MyD88 or its mutant constructs. We used immunoprecipitation followed by immunoblotting to assess the effect of mutated residues on the receptor TIR-adaptor TIR interaction. As demonstrated in figure 15, only MyD88 D195A/R196A/D197A mutant showed loss of binding to IL1RAcP while other mutants including MyD88 P200H retained their ability to bind IL1RAcP. This result indicates that residues D195A/R196A/D197A may constitute a part of the interacting surface of MyD88 and IL1RAcP, while other alanine-substitutions are without effect. The selective loss of receptor binding function by MyD88 D195A/R196A/D197A mutant led us to develop the 3-D docking model of MyD88 and IL1RAcP and verify the strategic position of these three residues as a main

Table 1

Information about the MyD88 mutants analyzed in this study

Mutant #	Mutation(s)
M1	MyD88-D171A
M2	MyD88-P200H
M3	MyD88-D195A/R196A/D197A
M4	MyD88-D275A
M5	MyD88-F285A/W286A

All the MyD88 mutants in this study were generated as indicated under the Materials and Methods.

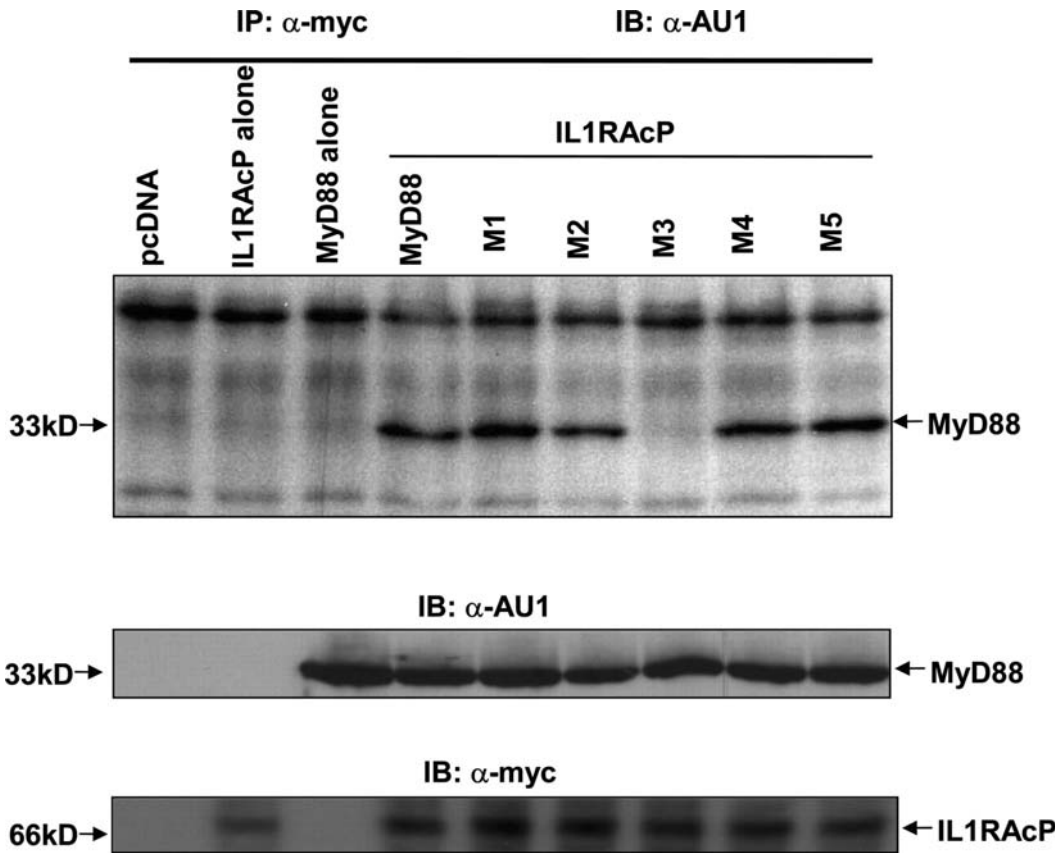

Figure 15. Interaction of MyD88 mutants with IL1RAcP.
HEK 293T cells were transiently transfected with Myc-IL1RAcP (10 μg) and full-length MyD88 or its mutants (10 μg). After 24 h, the cells were stimulated with 100 ng/ml IL-1β for 5 min, harvested, and immunoprecipitated as described under "experimental procedures." Protein samples bound to anti-myc antibody containing protein A beads were subjected to SDS-PAGE, and the immunoprecipitated MyD88 or its mutants were monitored by immunoblotting with anti-AU1 antibody (*top panel*). Expression of MyD88 and its mutants (*middle panel*) and IL1RAcP (*bottom panel*) was analyzed by immunoblotting.

interactive site on the surface of the MyD88 TIR domain for its binding to the TIR domain of IL1RAcP.

The development of the 3-dimensional docking model of MyD88-IL-1RAcP interaction

The 3-D docking model was developed by optimized superposition of two mutually interacting TIR domains of MyD88 and IL1RAcP. IL1RAcP TIR domain has 33% identity with known 3-dimensional structure of human TLR1 (*1fyvA* .pdb); therefore, *1fyvA* was used for generating the computing model of IL1RAcP (figure 16).

Negatively charged side of the MyD88-TIR (figure 8 and figure 9*B*) was selected as a possible interface of the molecule. This side contains D195/R196/D197 residues that are essential, on the basis of mutagenesis studies (figure 15), for MyD88-TIR heterotypic interaction with IL1RAcP-TIR. Then, a suitable positively charged site of the IL1RAcP was selected to conduct the modeling computation process. This modeling was based on geometry optimization by energy minimization followed by molecular dynamic computation using the program SANDER (AMBER software package). Ribbon structure was developed with the Deep View program while the molecular surface of associated proteins was determined by PSSHOW (SYBIL-Tripos software package).

As shown in figure 17, the separation surface indicates that there is no crossing of molecular surfaces and distance between them is within the range of 0.4 - 4.7 Å while their topology is diverse and contains several deep pockets.

```
                395
IL-1RAcP TIR  --TDETILDGKEYDIYVSYARNAEEEEFVLLTLRGVLENEFGYKLCIFDRDSLPGG
Tlr1 TIR      NIPLEELQRNLQFHAFISYS--GHDSFWVKNELLPNLEKE-GXQICLHERNFVPGK
Cons            . * :  . ::. ::**:  ..:. :*   *   **:* * ::*:.:*: :**
               450
IL-1RAcP-TIR  IVTDETLSFIQKSRRLLVVLSPNYVLQGTQALLELKAGLENMASRGNINVILVQYK
Tlr1 TIR      SIVENIITCIEKSYKSIFVLSPNFV-QSEWCHYELYFAHHNLFHEGSNSLILILLE
Cons           :.:: :: *:** : :.*****:* *.  .  **  . .*:  .*. .:**:  :
               507
IL-1RAcP-TIR  AVKETKV----KELKRAKTVLTVIKWKGEKSKYPQGRFWKQLQVAMPVKKSPRRSS
Tlr1 TIR      PIPQYSIPSSYHKLKSLXARRTYLEWPKEKSK--RGLFWANLRAAINIKLTEQAK-
Cons          .: : .: ::**   :  * ::*  ****  :* ** :*:.*: :* : : .
```

Figure 16. Sequence alignment of TIR domain of human IL-1RAcP and TLR-1. IL1RAcP TIR domain has 33% identity with known 3D structure of human TLR1 (1fyvA.pdb); therefore Pdb file 1fyvA was used to generate the computing model of IL1RAcP.

Figure 17. The 3-D models of TIR domain of IL1RAcP and MyD88, and the docking model of their TIR-TIR interaction.

A and *B*, ribbon structure of IL1RAcP TIR domain and MyD88 TIR domain, respectively, obtained from homology computation performed using Swiss-Model and visualized using DeepView (Swiss-PdbViewer). Structural features representing the conserved boxes of the MyD88 TIR domain are shown in *B* in *yellow* (Box 1), *purple* (Box 2), and *blue* (Box 3). The selected side chains of mutated residues in *B* and *C* are marked in *green.*

C, ribbon representation of TIR-TIR interaction optimized with SANDER energy minimization software (AMBER package). The side chains of identified residues on MyD88 TIR (Asp^{195}, Arg^{196}, and Asp^{197}) required for direct binding of MyD88 TIR to IL1RAcP TIR as well as the complementary residues on EE loop of IL1RAcP TIR are shown in *green*. The structural motifs in *A* and *C* are colored as follows: *blue*, α-helices; *red*, β-strands; and *white*, loops.

D, top view of docking superposition presented in molecular surface mode.

A

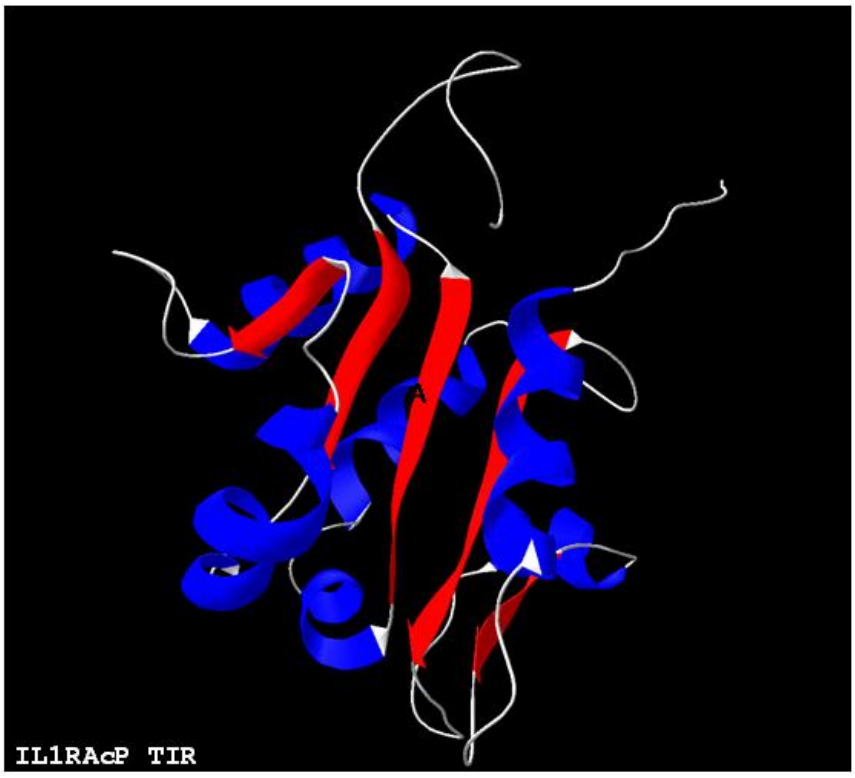
IL1RAcP TIR

B

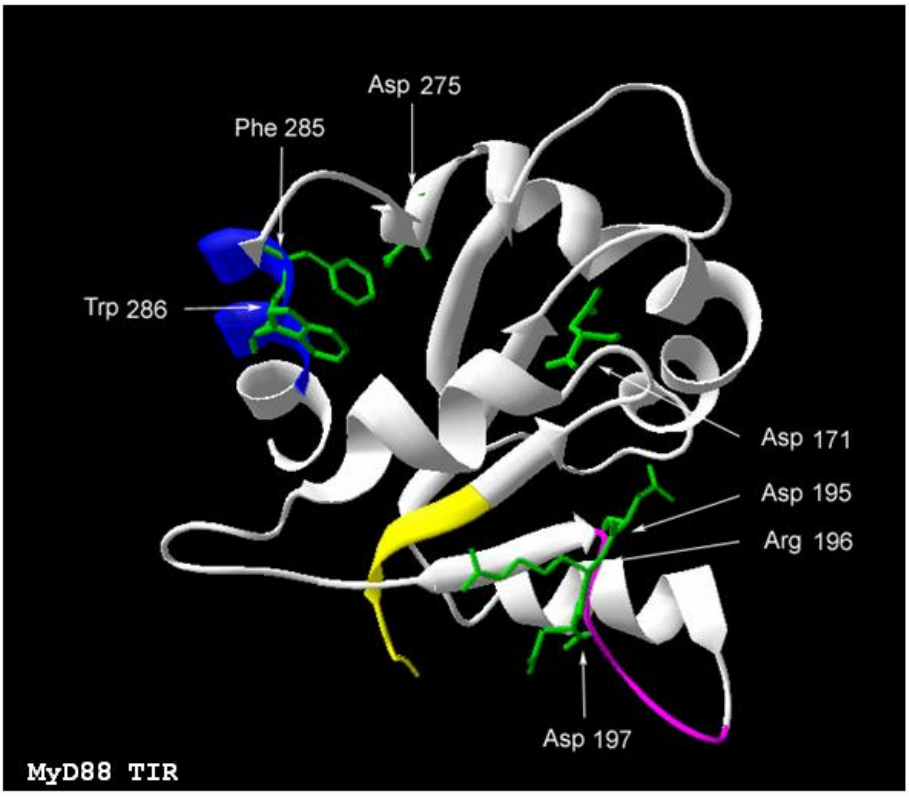
Asp 275
Phe 285
Trp 286
Asp 171
Asp 195
Arg 196
Asp 197
MyD88 TIR

C

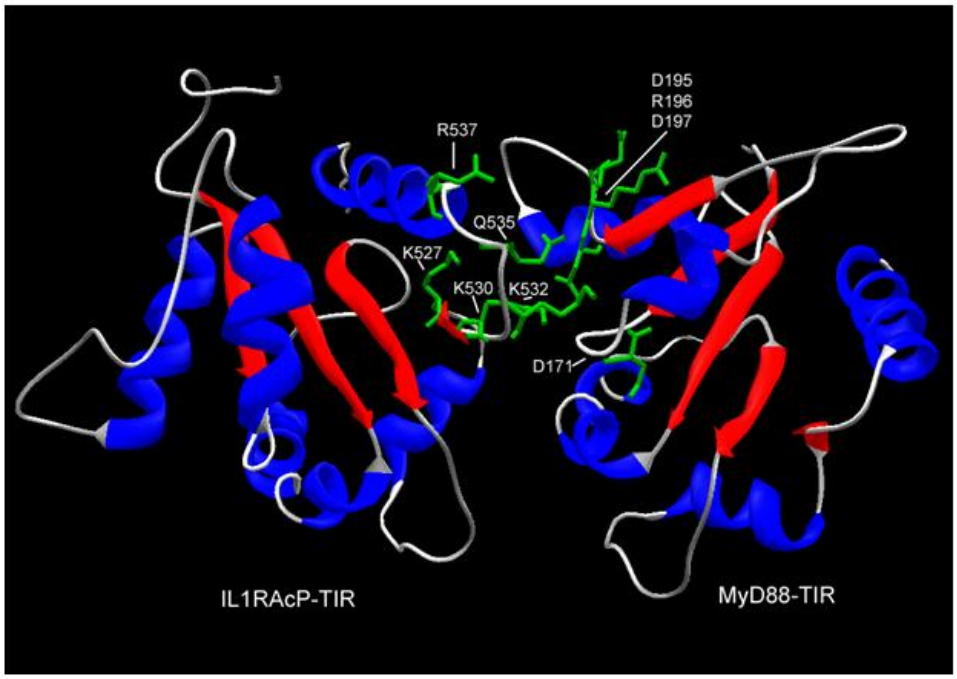
D195
R196
D197
R537
Q535
K527
K530
K532
D171
IL1RAcP-TIR
MyD88-TIR

D

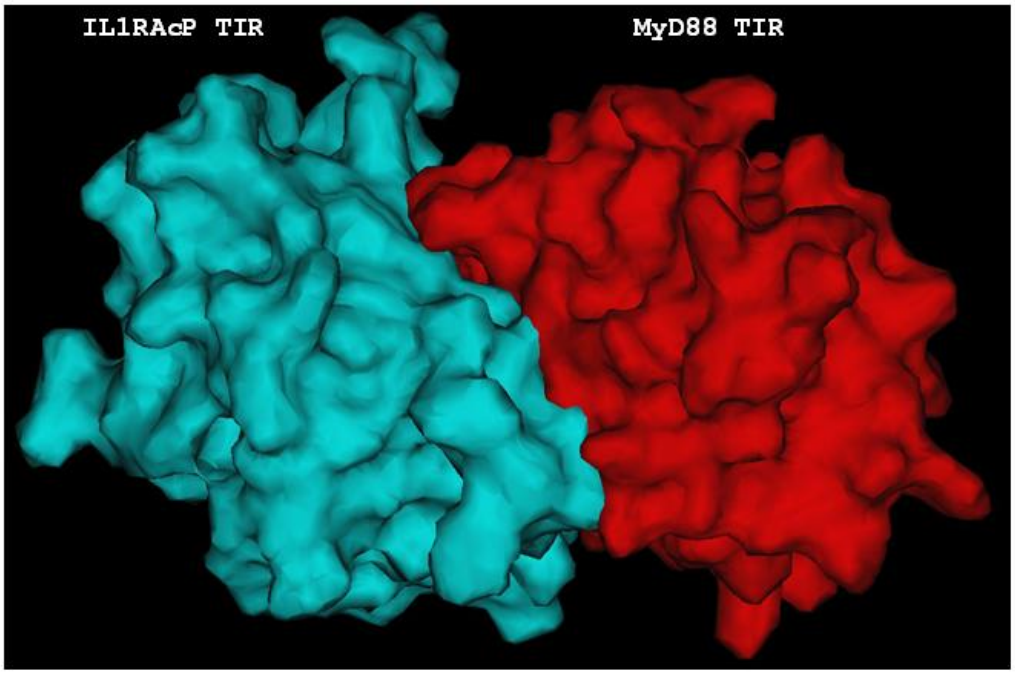
IL1RAcP TIR
MyD88 TIR

Development of this 3-dimensional model allowed us to verify the contribution of the triplet of functionally important residues D195/R196/D197 to the binding reaction with IL1RAcP TIR domain. An analysis of the tertiary structure of two TIR domains that participate in the docking model indicates that three mutated residues (D195/R196/D197) responsible for the loss of MyD88 binding to IL1RAcP, are involved in interaction with residues 527-534 of IL1RAcP previously identified to play a key role in IL-1β signaling pathway (Radons et al., 2003; Radons et al., 2002). Thus, our study identified a complementary site on MyD88 TIR domain that contributes to its interaction with IL1RAcP TIR domain. We therefore postulate that a negatively charged "knob", partially comprised of the BB loop on the surface of MyD88 TIR domain (figure 9*B*), fits into the positively charged lysine patch formed by residues 527, 530, and 532 of the IL1RAcP TIR domain previously identified by Radons et al. as essential for IL-1β signaling (Radons et al., 2003; Radons et al., 2002).

Homotypic oligomerization: interactive sites and docking model of MyD88 TIR domain

Following IL-1β-induced interaction of IL1RAcP with MyD88, this adaptor oligomerizes and interacts with downstream signal transducers (Akira, 2003; Akira and Sato, 2003; Yamamoto et al., 2004). Homotypic oligomerization of MyD88 due to its forced expression resulted in robust activation of NFκB reporter gene activity observed in the absence of IL-1β stimulation (figure 10). This receptor- independent effect of ectopically expressed MyD88 oligomers can be

abolished by cotransfected MyD88-TIR domain (data not shown). Therefore, we examined direct interaction of a full-length MyD88 co-expressed with MyD88 TIR domain or its mutants. We co-transfected HEK 293T cells with full length MyD88 that contained a c-myc epitope tag along with the wild type or mutated TIR domain of MyD88 that contained an AU1 epitope tag. As demonstrated in figure 18, P200H mutant bound to a full-length MyD88 to similar extent as wild-type MyD88 TIR domain. However, mutations in Box 2 (D195A/R196A/D197A) and Box 3 (βE strand D275A and F285A/W286A) caused a loss of binding to MyD88, suggesting that these mutated residues constitute the interactive sites for homotypic oligomerization of the MyD88 TIR domain. Thus, interacting site in Box 2 comprised of residues D195/R196/D197 has potentially an additional function that may encroach on the ability of MyD88 to interact with IL1RAcP. However, in a cascade of signaling steps induced by IL-1β, heterotypic interaction of IL1RAcP TIR domain with MyD88 TIR domain antecedes oligomerization of MyD88. The latter depends on homotypic binding mediated by the MyD88 TIR domain. Therefore, the interactive site in Box 3 is likely uninvolved in binding of MyD88 to IL1RAcP. Rather, this site participates in homotypic MyD88 oligomerization and possibly other transactions involving downstream signal transducers. This interpretation is consistent with the loss of inhibition of IL-1β-induced signaling by MyD88 TIR domain upon truncation of its COOH-terminal segment that contains Box 3.

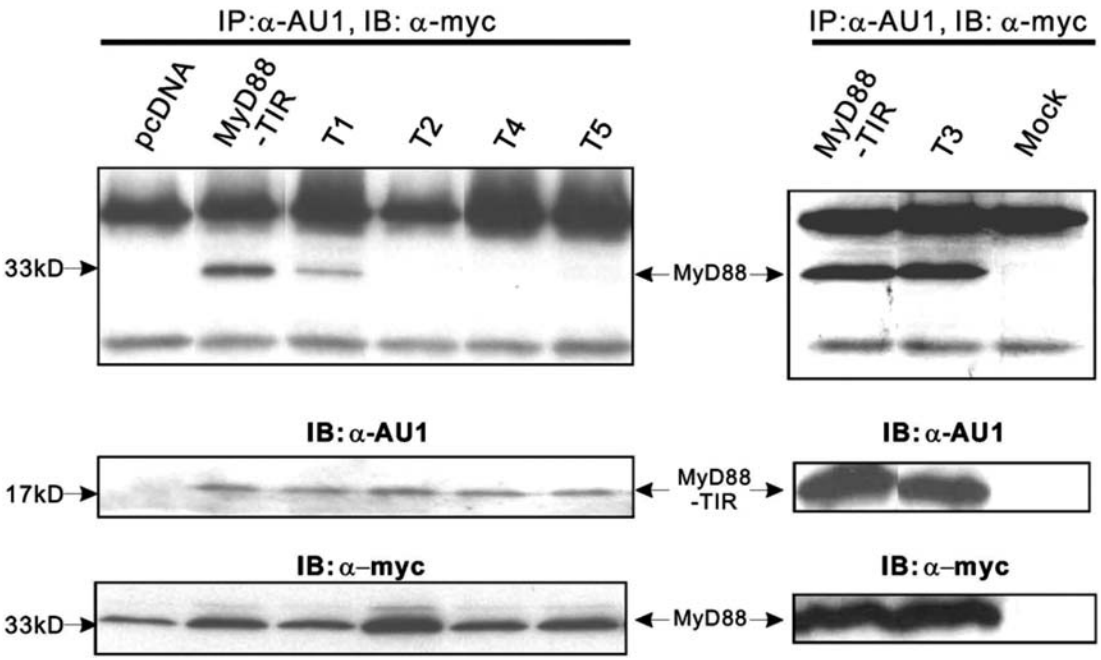

Figure 18. Homotypic interaction of the TIR domain of MyD88 with full-length MyD88. The HEK 293T cells were transiently transfected with c-Myc-tagged full-length MyD88 (5 μg) and AU1-tagged MyD88-TIR (5 μg) or AU1-tagged MyD88-TIR mutants (5 μg). After 24 h, the cells were harvested and immunoprecipitated as described under "Experimental Procedures." Protein samples bound to anti-AU1 antibody containing Protein A beads were subjected to SDS-PAGE and immunoprecipitated. MyD88-TIR or its mutants were detected with anti-myc antibody (*top panel*). Expression of MyD88-TIR and MyD88-TIR mutants (*middle panel*) or MyD88 (*bottom panel*) was analyzed by immunoblotting with indicated antibodies.

On the basis of these studies, a 3-dimensional docking model of MyD88 TIR homotypic interaction was generated with geometry optimization by energy minimization followed by molecular dynamics (AMBER package). Ribbon structures were developed with the Deep View program. Development of this docking model allowed us to verify the contribution of the mutated residues. As presented in figure 19, within this model of the homotypic interaction of MyD88 TIR domain, besides D195R196D197 (BB loop) and D171 that bind to Box 3, especially to K291, another pair of interacting residues was suggested, D275 on the one TIR domain and K231 at the other.

Discussion

In this combined mutagenesis and 3-dimensional modeling study, we identified key residues in the MyD88 TIR domain that are responsible for its heterotypic interaction with IL1RAcP. In addition, we identified interactive sites for homotypic oligomerization of MyD88. These protein-protein interactions evoked by IL-1β are essential for its signaling to the nucleus mediated by NFκB and other proinflammatory stress responsive transcription factors. Mutations identified on the interacting surface of the MyD88 TIR domain are functionally important because they interfere with the induction of the endogenous gene that encodes IL-6. This inflammatory cytokine, along with IL-1β, is responsible for cardinal signs of systemic inflammation: fever, leukocytosis, thrombocytosis, acute phase protein response, and tissue injury (Dinarello, 1996; Dinarello, 2002).

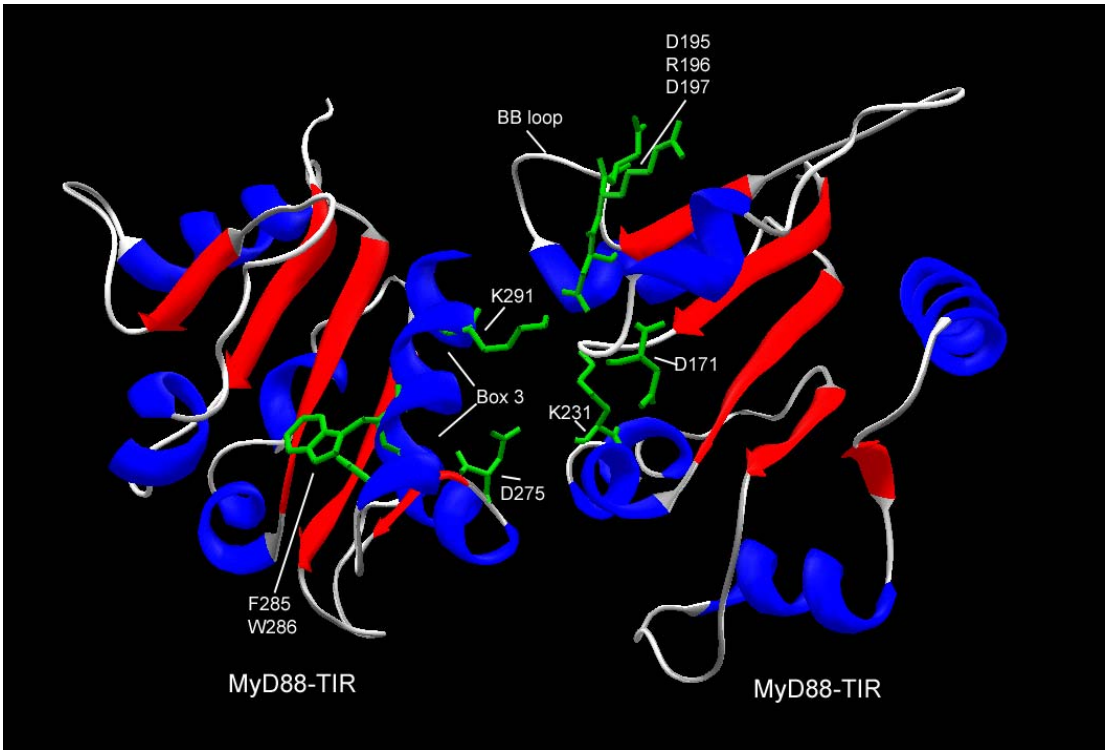

Figure 19. MyD88 TIR–TIR docking model. This homotypic interaction was depicted in ribbon representation optimized with SANDER energy minimization software (AMBER package). The selected side chains of mutated residues are marked in *green* In this homotypic interaction, besides D195R196D197 (BB loop) and D171 that bind to Box 3, especially to K291. Another pair of potential interacting residues was found: D275 at the one TIR and K231 at the other.

The development of the docking 3-dimensional model of MyD88-IL1RAcP binding, in which a cluster of highly charged residues in Box 2 plays a key role, reaffirms their strategic role in contacting a complementary site on IL1RAcP TIR domain. This site is comprised of several positively charged residues identified previously in EE loop residues 527-534 (Radons et al., 2003; Radons et al., 2002). Thus, it is not surprising that the invariant proline 200 is inconsequential for MyD88-ILRAcP interaction. However, mutation of the canonical proline to histidine in TLR-4, which abolishes its signaling by LPS (Poltorak et al., 1998), indicates that different ligands and their cognate TLRs utilize MyD88 in structurally distinct ways. In addition to TLR-4, Proline to Histidine mutation attenuated signaling mediated by TLR-2, MAL, and IL1RAcP (Horng et al., 2001; Poltorak et al., 1998; Radons et al., 2002). We interpret the latter result as indicative of the invariant proline playing a significant role in reshaping the EE loop in IL1RAcP or in interactions with the TIR domain of IL-1RI or with signaling molecules other than MyD88. Further mapping of the MyD88 surface will expand our understanding of its role in integrating signals derived from a variety of Toll-like receptors.

Summary and conclusions

1. MyD88 is the essential adaptor protein that integrates and transduces intracellular signals generated by multiple Toll-like receptors including the receptor complex for IL-1β, a key inflammatory cytokine. As reviewed in Chapter 1, MyD88 plays a key role in IL-1β signaling. This essential role is supported by

other studies with MyD88 -deficient mice which demonstrated the lack of signaling in response to ligands such as IL-1, IL-18, peptidoglycan, LPS, and CpG-DNA (Adachi et al., 1998; Kawai et al., 1999).

2. MyD88 interacts with the IL-1β receptor complex via the Toll/IL1 receptor (TIR) domain. This interaction is a critical step in IL-1β evoked signaling to the nucleus. Previous studies suggested the involvement of direct binding between TIR domain of IL1RAcP and TIR domain of MyD88, as well as homotypic oligomerization of MyD88 via TIR domains (Radons et al., 2003; Radons et al., 2002).

3. I conducted structure-function studies that helped to define the MyD88 TIR domain binding sites involved in heterotypic interaction with IL1RAcP. The MyD88 TIR domain, employed as a dominant negative inhibitor of IL-1β signaling to screen MyD88 TIR mutants, lost its suppressing activity upon the truncation of Box 3. Accordingly, mutations of Box 3 residues 285–286 reversed the dominant negative effect of the MyD88 TIR domain on IL-1β-induced and NFκB-dependent reporter gene activity and IL-6 production. Moreover, mutations of residues 171 in helix α-A, 195–197 in Box 2, and 275 in β-E strand had similar functional effects.

4. Strikingly, based on co-immunoprecipitation studies, only mutations of residues 195–197 eliminated the direct TIR-TIR interaction of MyD88 and IL-1 receptor accessory protein (IL1RAcP), whereas substitution of neighboring canonical Pro^{200} by His in MyD88 TIR domain was without effect.

5. Using NFκB reporter gene activation, cytokine production, and co-immunoprecipitation analysis, I demonstrated that homotypic MyD88 oligomerization via the TIR domain interaction is ablated by mutations in Box 2 and Box 3 of the TIR domain.

6. The above results provided essential structural and functional information for development of a docking 3-dimensional model of MyD88-IL1RAcP interaction, verifying a key role of a cluster of highly charged residues in Box 2. This model is consistent with previous studies, which showed that several positively charged residues(a.a.527-534) within the EE loop of IL1RAcP are the sites responsible for IL1RAcP/MyD88 interaction (Radons et al., 2003; Radons et al., 2002). According to our 3-dimensional docking model, these conserved residues of IL1RAcP are indeed in direct contact with the highly charged residues 195-197 in Box 2 of MyD88 TIR identified in the mutagenesis and co-immunoprecipitation experiments.

7. Based on the co-immunoprecipitation studies of MyD88 TIR domain mutants, a second docking 3-dimensional model was developed to define MyD88 homotypic interaction via its TIR domain. This model points to the essential role of several amino acid residues: D195R196D197 (BB loop) and D171 of one TIR domain were in close proximity to Box 3, especially K291, of its counterpart. Another pair of potential interacting residues was D275 at the one TIR domain and K231 at the other.

In conclusion, my studies based on biochemical characterization and computational modeling analysis led to the establishment of the first 3-dimensional docking models of TIR-TIR interaction between MyD88 and IL1RAcP and of TIR-TIR homotypic oligomerization of MyD88 induced in IL-1β stimulated cells. This new information on the fundamental mechanisms of how MyD88, the key relay station in IL-1β signaling pathway, interacts with IL-1R/IL1RAcP receptor complex, provides a platform for further comparative analysis of MyD88 interaction with other members of Toll-like receptors family. Finally, the results presented here are expected to contribute to the development of therapeutic agents that interfere with IL-1β-induced proinflammatory signaling by disrupting the TIR-TIR interactions as defined in these studies.

Future directions

In this study, I defined the MyD88 TIR domain binding sites involved in heterotypic interaction with IL1RAcP as well as in homotypic interaction. The 3-dimensional docking models of TIR-TIR interaction between MyD88 and IL1RAcP and of TIR-TIR homotypic oligomerization of MyD88 provided fundamental information regarding the interaction between MyD88 and members of the Toll-like receptor family. Further characterization of interactive sites of MyD88 with other TLRs will give more insight regarding how this versatile adaptor protein mediates different Toll-like receptor signaling pathways to achieve distinct signaling outcomes and may eventually reveal the physiological significance of TIR-TIR interaction in inflammation. Comparative analysis of other TIR domain containing adaptors based on the characterization of MyD88 in this study will aid on better understanding of how different adaptor usage by different Toll-like receptors lead to distinct signaling outcomes. The docking studies also established an excellent model for the development of therapeutic agents that can specifically interfere with IL-1 signaling by disrupting the TIR-TIR interaction.

Comparative analysis of heterotypic interactions of MyD88 and TLRs

The MyD88 TIR domain was employed as a dominant negative inhibitor of IL-1β signaling to screen MyD88 TIR mutants. The truncation mutants and point-mutations substituted with alanine were analyzed for IL-1β-induced NFκB reporter gene activation, cytokine production, and direct binding with IL1RAcP.

The TIR domain of MyD88 lost its suppressing activity on IL-1β-induced and NFκB-dependent reporter gene activity and IL-6 production following truncation of Box 3 and mutations of Box 3 residues 285–286. Moreover, mutations of residues 171 in helix α-A, 195–197 in Box 2, and 275 in β-E strand had similar functional effects.

For IL-1R/TLR members other than IL-1R, recruitment of MyD88 may occur at different binding sites of the MyD88 TIR domain. Thus, the functional impact of these mutations on other Toll-like receptor signaling pathways remains an open question. The significance of the interactive sites of the MyD88 TIR domain in LPS-induced TLR-4 signaling pathway is of particular interest. Although it is well established that the binding of LPS from Gram-negative bacteria to TLR-4 on macrophages can induce production of pro-inflammatory cytokines (e.g. IL-1) and provoke the acute phase response to infection (Dunne and O'Neill, 2003), the mechanism of the TIR-TIR interaction between TLR-4 and MyD88 is unknown. In previous computational docking studies, MyD88 was predicted to bind with a surface composed with its AA- and DD-loop to the CD-loop on TLR-4, which is located on the other side of the receptor, opposite its BB-loop (Dunne et al., 2003). Using NFκB reporter gene activation assay and production of IL-6 as described in this thesis, mutants corresponding to AA- and DD- loop are of potential value for testing their involvement in MyD88-TLR-4 interaction. Substitution of D171 in the TIR domain of MyD88 led to the loss of IL-1β-induced NFκB activation and IL-6 production. Comparative analysis of heterotypic

interactions of MyD88 and TLRs will give some insight into whether distinct interactive surfaces of MyD88 are responsible for different TLR signaling cascades. Our model will serve as a matrix to determine how MyD88 can mediate multiple Toll-like receptor signaling pathways.

Developing cell-penetrating peptide/protein as therapeutic agents

The 3-dimensional docking models of TIR-TIR interaction between MyD88 and IL1RAcP and of TIR-TIR homotypic oligomerization of MyD88 provide an excellent platform for the development of therapeutic agents that interfere with IL-1 signaling by disrupting the TIR-TIR interaction. To counteract the effect of IL-1 in inflammatory responses, IL-1 blockade with the recombinant form of the naturally occurring IL-1Ra has been widely accepted (Dinarello, 2004). An alternative strategy is block the downstream signaling pathway by directly targeting key signaling molecules such as MyD88. Therefore, this study may help to develop effective therapeutic agents to treat inflammation-related diseases driven by IL-1.

Bartfai et al. reported that a low molecular weight TIR mimic, hydrocinnamoyl-L-valyl pyrrolidine, modeled on a tripeptide sequence of the BB-loop [(F/Y)-(V/L/I)-(P/G)], can block the IL-1β - induced phosphorylation of the mitogen-activated protein kinase p38 *in vitro*. *In vivo*, a mouse fever model induced by IL-1β is also effectively attenuated by giving intraperitoneal injection of 200 mg/kg of this compound (Bartfai et al., 2003). Pilot experiments of

designing anti-inflammatory cell-penetrating peptide based on TIR-TIR interaction were conducted in our laboratory using conserved structure elements such as the BB loop and box 3 of the TIR domain derived from MyD88, TLR-4, and IL-1R; however, the solubility and functionality were limited. Further experiments to optimize the peptide solubility are needed for proper assessment of their functionality in context of the IL-1β - induced signaling via IL-1R complex as well as LPS-induced signaling via TLR-4.

The TIR domain of MyD88 has been shown to be a potent dominant negative inhibitor of IL-1β – induced NFκB activation and IL-6 production (figure 9 and figure 10). In combination with the cell-penetrating peptide/protein transduction technique developed in our laboratory (Hawiger, 1999; Jo et al., 2005; Lin et al., 1995), recombinant protein comprising MyD88 TIR domain is engineered. The TIR domain of MyD88 in the context of a cell-penetrating motif derived from the hydrophobic region of the signal sequence of Kaposi fibroblast growth factor (K-FGF) has been designed and purified in a prokaryotic expression system of *E. coli.* However, the expressed fusion protein formed inclusion bodies and, therefore, had been limited in the functional evaluations (data not shown). Further experiments are needed to improve the solubility of fusion protein so that it can be tested for inhibition of IL-1β–induced or lipopolysaccharide-induced NFκB nuclear translocation and cytokine production in animal models described previously (Yan Liu et al., 2000).

In summary, the new information on the fundamental mechanism of MyD88 function in multiple IL-1R/TLR signaling pathways will provide a comprehensive understanding of the inflammatory responses mediated by TIR-TIR interactions. These results will help in the development of therapeutic agents that specifically interfere with MyD88-mediated proinflammatory signaling by disrupting the TIR-TIR interactions as defined in these studies.

CHAPTER III

GENE EXPRESSION PROFILING IN RESPONSE TO PROINFLAMMATORY AGONISTS

Synopsis

Inflammation is the major mechanism of cardiac, pulmonary and vascular diseases, the main cause of mortality in the United States. The identification of genes involved in inflammation and the characterization of their functions will help to develop effective treatment for a wide variety of diseases. Genome-wide expression profiling using high-density DNA microarrays provides an unprecedented opportunity for mechanistic studies of inflammation. Animal models of systemic inflammation induced by staphylococcal enterotoxin B (SEB) and lipopolysaccharide (LPS) were used to study genome-wide transcriptional response. Animal models of systemic inflammation induced by staphylococcal enterotoxin B (SEB) and lipopolysaccharide (LPS) were used to study genome-wide transcriptional response.

In vivo treatment with SEB induced 134 and 209 genes in spleen cells and T lymphocytes, respectively. Upregulation of these genes was inhibited by blocking NFκB signaling with a cell-penetrating nuclear import inhibitor cSN50 peptide or the IκBαΔN transgene. *In vivo* treatment of LPS induced upregulation of 1296 genes and downregulation of 1551 genes in the liver and correspondingly, 1109 and 402 genes in the spleen. The genome-wide response

to LPS was ablated in TLR-4-deficent C3H/HeJ mice. The cSN50 peptide blocked 547 LPS-inducible and 669 LPS-downregulated genes in the liver, and 105 LPS-inducible and 230 LPS-suppressed genes in the spleen. Thus, nuclear import of NFκB and other stress-responsive transcription factors plays an important role in genome-wide response to microbial inducers of inflammation.

Gene expression profiling in response to staphylococcal enterotoxin B (SEB)

An animal model of systemic inflammation induced by staphylococcal enterotoxin B (SEB), an agonist for T lymphocytes, was used. In this model, inhibition of nuclear import of NFκB and other stress responsive transcription factors (SRTFs) by cell-penetrating peptide cSN50 has been previously shown to prevent the increase in proinflammatory cytokines and chemokines. Moreover, the mortality induced by SEB in mice was reduced by 87% (Liu et al., 2004b). Here, we analyzed the gene expression profile of spleen cells and T lymphocytes after SEB administration. We identified 134 and 209 SEB-activated genes in the spleen cells and T lymphocytes, respectively. In T lymphocytes, 182 out of 209 activated genes were suppressed upon the treatment with a cell-penetrating peptide cSN50 via intravenous injection. The same treatment abolished the activation of all 134 genes in the spleen. These protective effects of cSN50 were fully recapitulated in the studies of transgenic mice expressing a mutant form of

IκBα which constitutively inhibits NFκB translocation into the nucleus. We concluded that SEB-induced genome-wide transcriptional activation in T lymphocytes is mediated by nuclear import of NFκB and other stress-responsive transcription factors. These findings provide the first evidence that genome–wide transcriptional activation during systemic inflammatory response evoked by SEB in T lymphocytes is dependent of nuclear import of NFκB and other SRTFs.

Systemic inflammation induced by staphylococcal enterotoxin B

SEB is produced by *Staphylococcus aureus* and causes various types of human diseases, including gastroenteritis resulting from consumption of contaminated food and non-menstrual toxic shock syndrome (NMTSS) (Balaban and Rasooly, 2000; Dinges et al., 2000). In addition, SEB is a potent superantigen that stimulates non-specific T-cell proliferation. SEB binds to the Vβ chain (Vβ7, Vβ8 and Vβ11) of the T cell receptor and major histocompatibility complex class II (MHC II) on dendritic cells or macrophages and forms an intercellular "synapse" (Bhardwaj et al., 1993; Seth et al., 1994; White et al., 1989). SEB stimulation leads to a cytokine "storm" from mainly T cells, with massive production of inflammatory cytokines including TNF-α, interferon γ(IFN-γ), interleukin (IL)-1β, IL-2, and IL-6, which leads to massive vascular injury, organ failure, and lethal respiratory distress syndrome or toxic shock (Balaban and Rasooly, 2000; Dinges et al., 2000; Madsen, 2001; Mattix et al., 1995).

The genes that encode inflammatory cytokines are under the control of SRTFs, including nuclear factor kappa B (NFκB), activator protein-1 (AP-1), nuclear factor of activated T cells (NFAT), and signal transducer and activator of transcription 1 (STAT1) (Hawiger, 2001). After mobilization to the nucleus, SRTFs stimulate genome-wide transcriptional activation of multiple genes encoding cytokines, chemokines, and other mediators of inflammation (Goldfeld et al., 1993; Sica et al., 1997; Teague et al., 1999; Tsai et al., 1996). We hypothesize that by combining genome-wide expression profile analysis with inhibition of SRTF cytoplasmic/nuclear translocation, we will be able to develop a global view of SEB-induced signaling to the nucleus via SRTFs and may identify new genes related to inflammatory responses.

To test this hypothesis, we applied cell-penetrating cSN50 peptides to inhibit nuclear import of SRTFs in T cells stimulated by SEB (Lin et al., 1995; Yan Liu et al., 2000). The inhibitors of nuclear import used in the animal model for SEB toxicity contain a cyclized form of the nuclear localization signal (NLS) from the p50/NFκB1 subunit of NFκB and membrane-translocating motif (MTM) from the signal sequence hydrophobic segment of fibroblast growth factor 4 (Yan Liu et al., 2000). MTM enables peptide or protein cargoes to cross the plasma membrane of multiple cell types in various organs via a receptor/transporter-independent mechanism (Hawiger, 1999; Jo et al., 2005; Jo et al., 2001; Torgerson et al., 1998; Veach et al., 2004; Yan Liu et al., 2000). These cell-penetrating peptides carrying NLS have been shown to simultaneously block the

nuclear import of multiple SRTFs by targeting Rch1/importin α/karyopherin-α2 in a Jurkat T cell line (Torgerson et al., 1998). Thus, we used cSN50-mediated inhibition of SRTFs as a novel platform to investigate the role of SRTFs nuclear import in the global regulation of inflammation related genes in T lymphocytes, the essential target for SEB-induced toxicity (Aoki et al., 1995; Marrack et al., 1990).

cSN50 blocks the cytokine storm induced by superantigen SEB in vivo

Most of the lethal effects of SEB have been attributed to superantigenicity and subsequent T-cell proliferation with massive inflammatory cytokine release. BALB/c mice with both I-A and I-E major histocompatibility complex class II isotypes of the H-2^{d} haplotype are 50 times more susceptible to SEB than the C57BL/6 strain (Taub et al., 1992). Thus, BALB/c mice were chosen to study the deleterious effects of SEB-induced cytokine "storm". In this murine model, administration of SEB via an intravenous route evokes massive production of cytokines which mediates the acute systemic inflammatory disorder. Under this condition, cytokine "storm" by SEB treatment does not lead to lethality, unless mice are either genetically manipulated (Anderson and Tary-Lehmann, 2001; Chen et al., 1994; Yeung et al., 1996) or previously sensitized with D-galactosamine or endotoxin (Liu et al., 2004b). Injection of 150ug of SEB into BALB/c mice caused a rapid rise in plasma TNF-α and IL-2 levels that peaked around 1hr, followed by a more progressive increase in IFN-γ (figure 20*A*).

Figure 20. Cytokine production and genome-wide expression profiling in the spleen induced by SEB and regulated by nuclear import inhibitor CSN50 or IκBαΔN transgene.

A, Suppression of SEB-Induced cytokine expression by nuclear import inhibitor cSN50 (significance was assessed by two-way AVOVA).

B, Suppression of cytokine expression in IκBαΔN transgenic mice which bear a dominant negative inhibitor of NFκB in T-lymphocytes. Cytokine levels were measured by CBA as described in experimental procedures. Data shown here represent Mean ± SE from at least 3 mice in each group. P value was calculated using two-way Anova with Bonferroni post-test.

C, Venn diagram of SEB-induced gene expression in whole spleen regulated by nuclear import inhibitor.

D, Venn diagram of regulated gene expression in spleen of IκBαΔN transgenic mice. Only genes that showed at least 2-fold induction or suppression with a minimum of 66% reproducibility as compared with control samples are included in the analysis. Each of these spots has a coefficient of variance(COV) less than or equal to 30%.

A

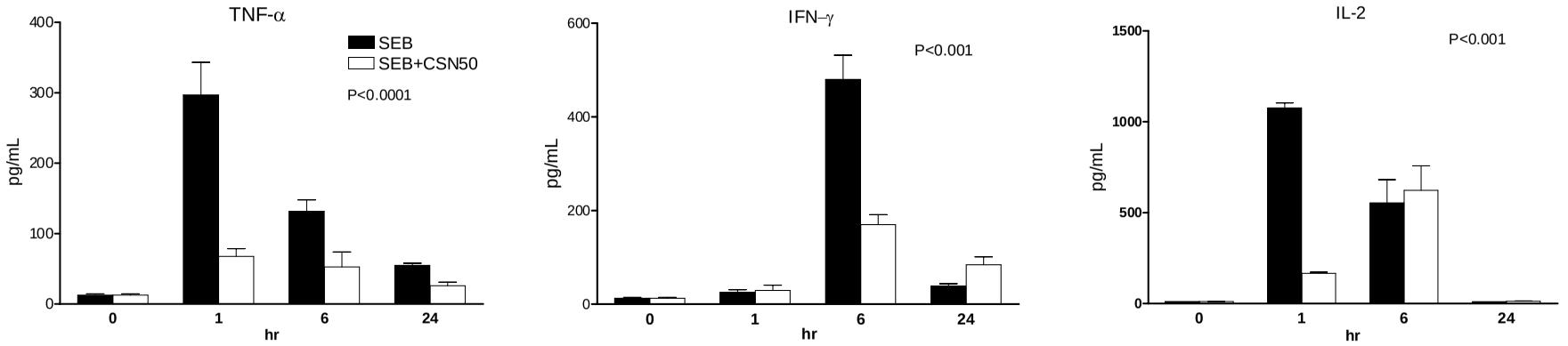
TNF-α
SEB
SEB+CSN50
P<0.0001
pg/mL
400
300
200
100
0
0
1
6
24
hr
IFN–γ
P<0.001
600
400
200
IL-2
P<0.001
1500
1000
500

B

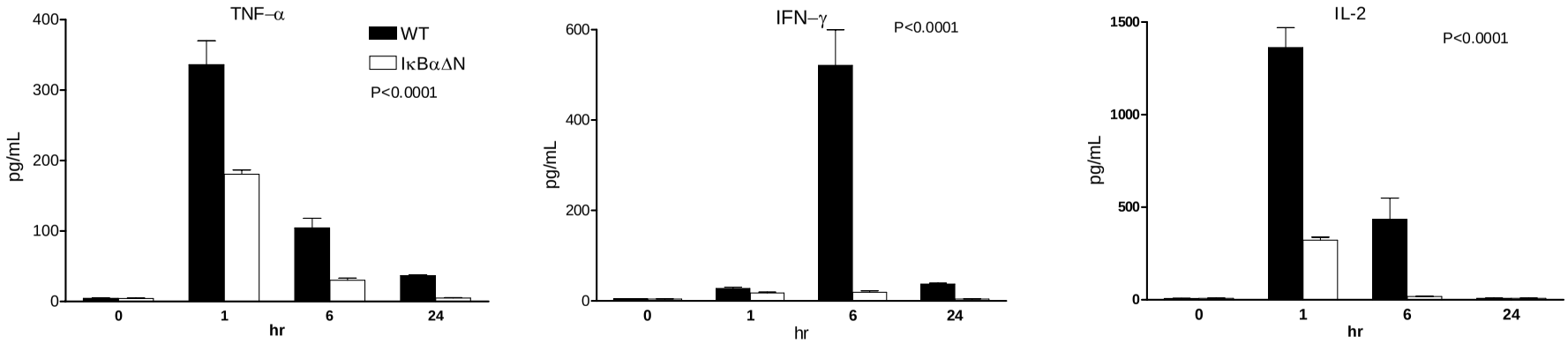
TNF–α
WT
IκBαΔN
P<0.0001
pg/mL
400
300
200
100
0
0
1
6
24
hr
IFN–γ
P<0.0001
600
400
200
IL-2
P<0.0001
1500
1000
500

C

SEB-regulated genes and their blockade by nuclear import inhibitor

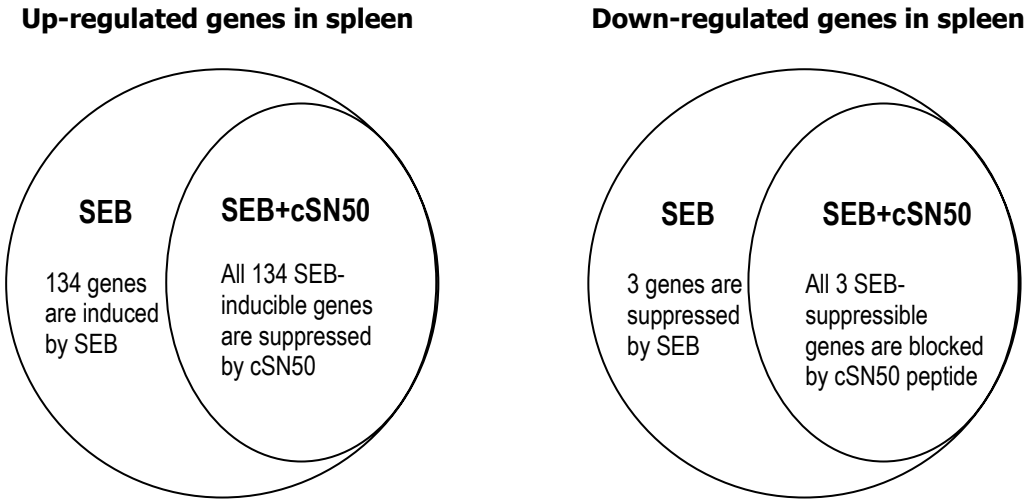

D

Blockade of SEB response in IκBαΔN transgenic mice

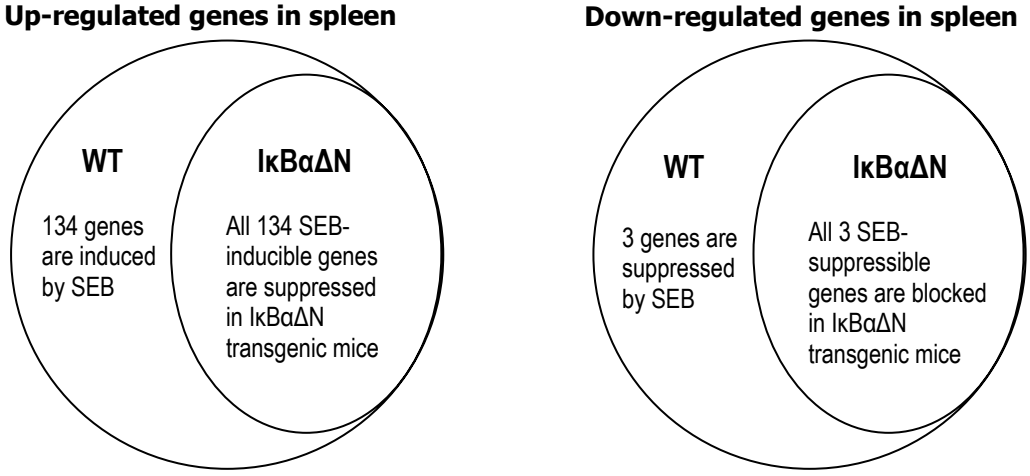

Administration of cSN50, before and after SEB exposure, suppressed the induction of inflammatory cytokines. Plasma levels of inflammatory cytokines including TNF-α, IFN-γ, and IL-2 were significantly decreased. This inhibition of cytokine production was fully recapitulated in IκBαΔN transgenic mice which bear a dominant negative inhibitor of NFκB in T lymphocytes in the C57BL/6 background (Liu et al., 2004b) (figure 20*B*). Therefore, whole spleen and splenic T cells were isolated from the mice to study further the regulation of SEB-induced genes.

Gene expression in the whole spleen correlates with SEB-induced toxic shock syndrome

SEB induces a "storm" of inflammatory cytokines, including TNF-α and IFN-γ, which contribute to the widespread systemic damage, multiorgan failure and even shock and significant morbidity. To elucidate the gene expression regulation underlining these events, we performed microarray profiling of whole mouse spleen harvested from BALB/c mice challenged with SEB and not treated or treated with cSN50 peptide. The experimental design is described in the Materials and Methods. The microarray included 22,172 cDNAs from the National Institute on Aging (NIA) set.

The examination of the overall gene expression patterns indicates that 134 genes became strongly up-regulated while very few (3 genes) were downregulated (figure 20*C*). Strikingly, all 134 activated genes, as based on an over2-fold increase in their expression in SEB-stimulated mice, were blocked in

mice treated with nuclear import inhibitor, cSN50 peptide (figure 20*C*). Since cSN50 has been previously shown to target nuclear import complex shuttling SRTFs to the nucleus, it is reasonable to interpret that these transactivators are required for SEB-induced gene expression in T lymphocytes *in vivo*. This notion is further supported by the analysis of gene expression in whole spleen of IκBαΔN transgenic mice. IκBαΔN is the dominant negative mutant of IκBα and the transgene leads to inhibition of NFκB nuclear translocation. The SEB-induced genome-wide activation is completely ablated in SEB treated transgenic mice as compared to wild-type animals. Our data indicate that NFκB is the essential transcription factor among all SRTFs for signaling to the nucleus and genome-wide activation in response to SEB *in vivo*.

We performed further analysis and functional clustering studies of SEB-upregulated genes. All of the information regarding this microarray analysis is available as supplementary data on the VUSR website (http://array.mc.vanderbilt.edu/). The majority of the SEB-activated genes could be classified by grouping them into functional groups encompassing metabolism, including protein metabolism and nucleobase, nucleoside, nucleotide and nucleic acid metabolism, response to stimulus, cell cycle, transcriptional regulation and structural molecules.

Gene expression in spleen T cells correlates with SEB-induced toxic shock syndrome

T cells constitute one third of the total spleen cells and are the main source for cytokines responsible for SEB toxicosis and toxic shock. SEB-induced lethal shock is T-cell dependent in mice models with or without co-administration of D-Gal (Anderson and Tary-Lehmann, 2001). Upon SEB stimulation, proliferation of T cells bearing Vβ8 and CD69 peaks at 18-24 hrs in both spleen and lymphnodes, at 48-72hrs the percentage of this T cell population is back to normal as a result of apoptosis (Liu and Hawiger, unpublished data). To address the SEB-induced gene expression regulation in T cells, we performed a comprehensive analysis of gene expression in T cells isolated from the spleen of BALB/c mice 24hrs after SEB injection.

The overall patterns (figure 21*A*) demonstrated that 209 genes became strongly up-regulated while 3 genes were downregulated. Boolean operation showed in T cells, which are the main cell population responsible for SEB toxicosis, 45% (97 out of 209) of the SEB-induced genes were also activated in the spleen. This subset of genes represent 75% (97 out of 134) of the whole spleen SEB-inducible genes (figure 21*B*). Consistent with the analysis in the whole spleen, most of the upregulated genes in T cells (182 out of 209) were inhibited by cSN50 treatment (figure 21*A*), further confirming the essential role of SRTFs nuclear import in SEB-induced transcriptional regulation. Moreover, the effectiveness of cSN50 as an inhibitor of the SEB-mediated response is based on transcriptional "silencing" of inflammatory response in T cells.

Figure 21. SEB-induced gene expression profile in spleen T cells.

A, Venn diagrams of SEB-induced (left) and SEB-suppressed (right) genes in T lymphocytes of mice treated with and without nuclear import inhibitor peptide cSN50 *in vivo*.

B, Venn diagram of SEB-induced genes in whole spleen and T lymphocytes. Boolean operation showed 45% (97 out of 209) of the SEB-induced genes in T cells are also activated in the spleen, and this subset of common genes represents 75% (97 out of 134) of the whole spleen SEB-inducible genes.

C, Venn diagram of SEB-induced, nuclear import-dependent genes in whole spleen and T lymphocytes. Only genes that showed at least 2-fold differences at a minimum of 66% of replicates as compared with control are included in the analysis. Each of these spots has a coefficient of variance (COV) less than or equal to 30%.

A

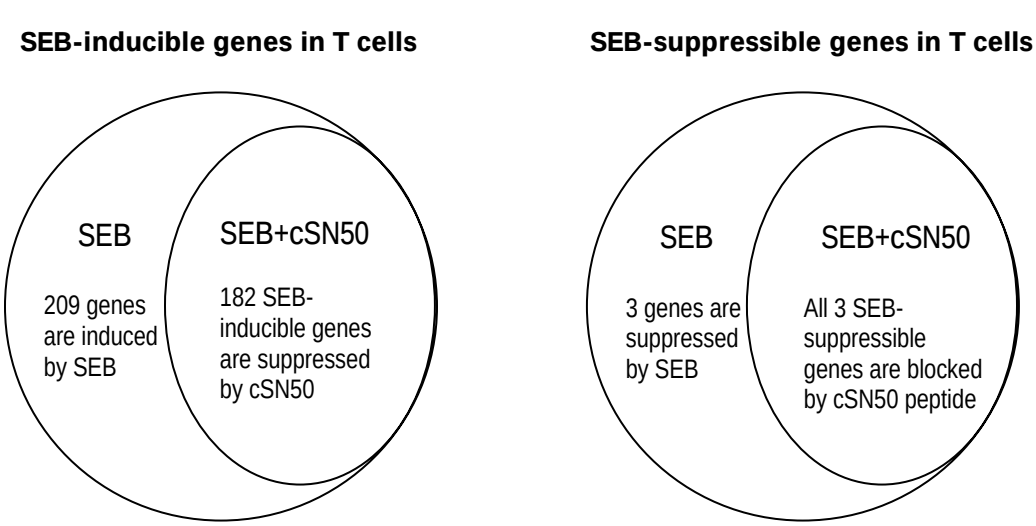
SEB-inducible genes in T cells
SEB
SEB+cSN50
209 genes are induced by SEB
182 SEB-inducible genes are suppressed by cSN50
SEB-suppressible genes in T cells
SEB
SEB+cSN50
3 genes are suppressed by SEB
All 3 SEB-suppressible genes are blocked by cSN50 peptide

B

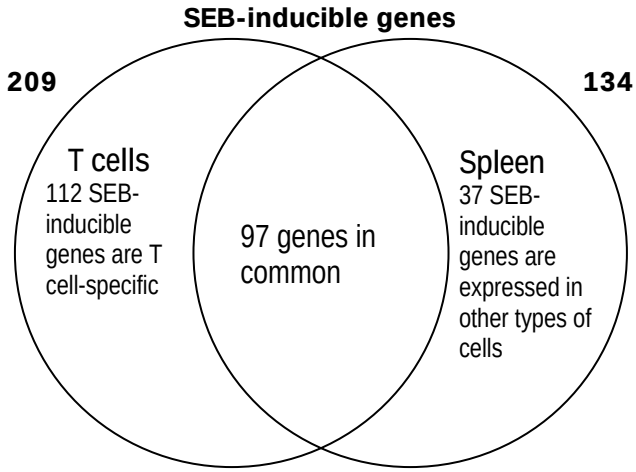
SEB-inducible genes
209
134
T cells
112 SEB-inducible genes are T cell-specific
97 genes in common
Spleen
37 SEB-inducible genes are expressed in other types of cells

C

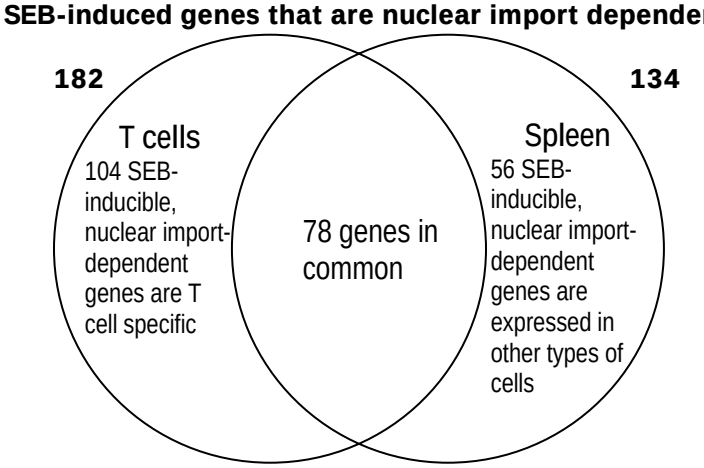
SEB-induced genes that are nuclear import dependent
182
134
T cells
104 SEB-inducible, nuclear import-dependent genes are T cell specific
78 genes in common
Spleen
56 SEB-inducible, nuclear import-dependent genes are expressed in other types of cells

The 182 genes which were inhibited by cSN50 were then classified into functional groups. All of the data are available as supplementary material on the VMSR website (http://array.mc.vanderbilt.edu/). Three-fourth of the upregulated genes were functionally classified by metabolism, including protein metabolism and nucleobase, nucleoside, nucleotide and nucleic acid metabolism. Genes linked to transcription regulation, response to stimulus, and cell cycle are also significantly represented. Thus, our study provided new *in vivo* evidence of the dependence of genome-wide transcriptional regulation on SRTFs nuclear import in response to superantigen SEB.

Gene expression profiling in response to LPS

Systemic inflammation caused by endotoxic LPS, the most potent proinflammatory pathogen-derived ligand that interacts with TLRs on monocytes, macrophages, dendritic cells, and B cells, leads to the induction of a robust production of cytokines and chemokines. These inflammatory mediators include TNF-α, IL-1, IL-6, IL-8, IL-10, IL-12, and IL-18 (Liu et al., 2004a). In addition, other chemokines (e.g. MIP-1, macrophage inflammatory protein-1), inflammatory prostanoids, leukotrienes, and reactive oxygen and nitrogen intermediates are produced upon LPS stimulation (Hawiger, 2001). The robust activation of the mouse transcriptisome is primarily dependent on the interaction of LPS with Toll-like receptor (TLR-4) (see detailed description in chapter I). Previous studies from our laboratory have demonstrated that the LPS-induced

cytokine and chemokine production is blocked by the cell-penetrating cSN50 peptide inhibitor of nuclear import (Liu et al., 2004a). The cSN50 peptide administration can also prevent inflammation-associated liver apoptosis, DIC, and promote increased survival of LPS-challenged mice from 7% to 71%. Therefore, we reasoned that genome-wide transcription activation is dependent on nuclear import of SRTFs including NFκB, AP-1, STAT1 and NFAT (Torgerson et al., 1998).

The LPS-evoked inflammatory response is dependent on expression of TLR-4 in phagocytes (macrophages) which are abundantly present in the liver and known as Kupffer cells (Liu et al., 2004a). In the spleen, the most abundant cells that respond to LPS are B lymphocytes. They express not only TLR-4 and TLR-3 but also another member of TLR family denoted RP105 which can potentially participate in the response to LPS (Kimoto et al., 2003; Kusumoto and Miyake, 2002; Miyake et al., 2000; Ogata et al., 2000). In response to a high dose of LPS (40 mg/kg), mice produce robustly inflammatory cytokines/chemokines and succumb within 72 hours (Liu et al., 2004a). We conducted an extensive analysis of genes induced by LPS (40 mg/kg) in TLR-4-sufficient C3H/HeN and TLR-4-deficient C3H/HeJ mice. Genome-wide expression profiles in the liver wherein Kupffer cells are targeted, and the spleen wherein B lymphocytes are predominantly targeted, were analyzed and compared between C3H/HeN and TLR-4-deficient C3H/HeJ mice.

The role of Toll-like receptor 4 (TLR4) in LPS-induced inflammatory response in vivo

A systemic inflammatory response in C3H/HeN mice was induced by intraperitoneal injection of 40 mg/kg LPS. RNA was purified from the liver or spleen harvested at 24 hours post-injection. RNA samples were used to interrogate a high-density Affymetrix oligonucleotide array containing over 39,000 transcripts, approximate the size of the protein coding capacity of the mouse genome. As depicted in figure 22, LPS induced upregulation of 1296 genes and downregulation of 1551 genes in the liver. Thus, a genome-wide analysis of LPS induced gene alteration documents an adaptation to endotoxic challenge involving about 10% of the mouse genome. Metabolic adjustments, innate immunity components, and adaptive immunity mediators are well represented in the LPS-regulated genes. In the spleen, LPS-induced transcriptional response involved upregulation of 1109 genes and suppression of 402 genes. This genome-wide transcriptional regulation by LPS is dependent almost entirely on LPS-induced signaling through TLR-4. Surprisingly, induction of 1109 genes and suppression of 402 genes in the spleen is also dependent on TLR-4 without significant usage of alternative signaling pathways evoked by LPS interaction with TLR-3 or RP105. Thus, TLR-4 plays the essential role in LPS-induced systemic inflammatory response involving primarily macrophages in the liver and B lymphocytes in the spleen. The lack of genome response in C3H/HeJ mice with defective TLR-4 signaling indicates that over 98% of the genome-wide adaptation to LPS *in vivo* is TLR-4-dependent.

Figure 22. TLR-4 mutation in C3H/HeJ mice render the LPS response in gene profiling compare with C3H/HeN mice.
A, LPS-induced gene activation in spleen and liver of C3H/HeN mice is abolished by TLR-4 deficiency in C3H/HeJ mice.
B, Venn diagrams of LPS-inducible genes in liver and spleen, showing over 98% of the genome-wide transcription activation is TLR-4-dependent.
C, LPS-induced gene suppression in spleen and liver of C3H/HeN mice is abolished by the deficient TLR-4 gene in C3H/HeJ mice. D, Venn diagrams of LPS-suppressible genes in liver and spleen, demonstrating over 98% of transcription suppression is TLR4-dependent.

A

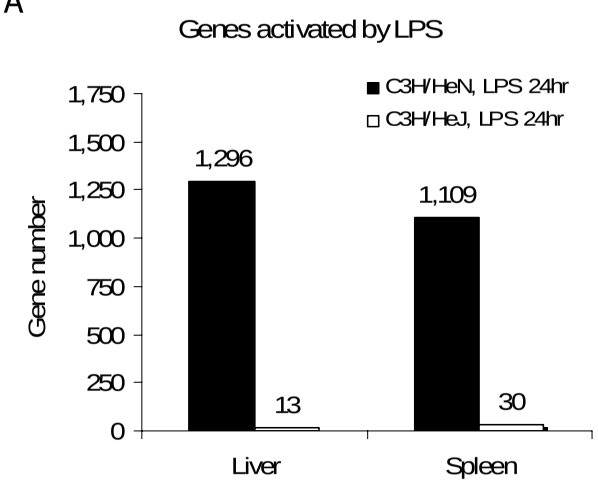
Genes activated by LPS
C3H/HeN, LPS 24hr
C3H/HeJ, LPS 24hr
Gene number
1,750
1,500
1,250
1,000
750
500
250
0
1,296
13
1,109
30
Liver
Spleen

B

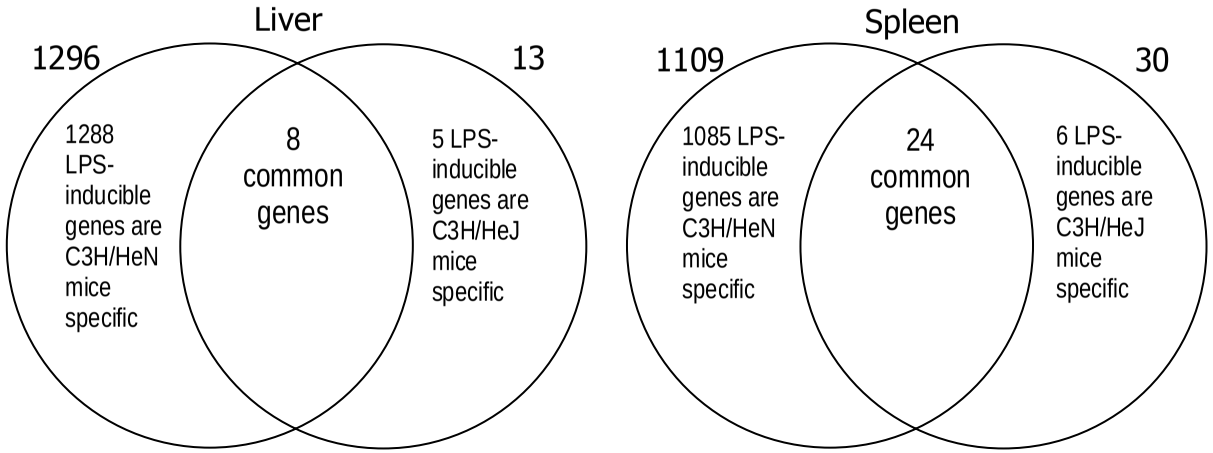
Liver
1296
13
1288 LPS-inducible genes are C3H/HeN mice specific
8 common genes
5 LPS-inducible genes are C3H/HeJ mice specific
Spleen
1109
30
1085 LPS-inducible genes are C3H/HeN mice specific
24 common genes
6 LPS-inducible genes are C3H/HeJ mice specific

C

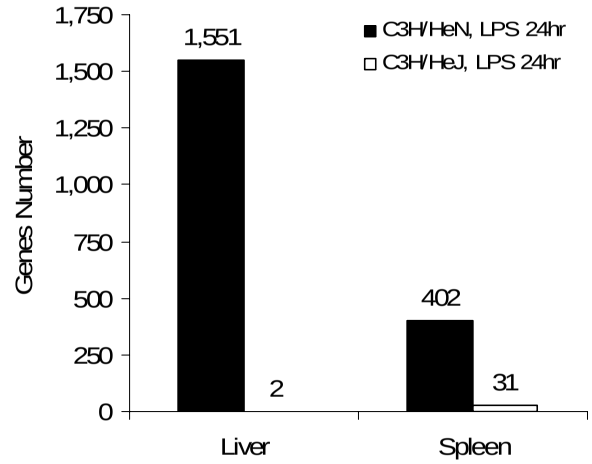
Genes suppressed by LPS
C3H/HeN, LPS 24hr
C3H/HeJ, LPS 24hr
Genes Number
1,750
1,500
1,250
1,000
750
500
250
0
1,551
2
402
31
Liver
Spleen

D

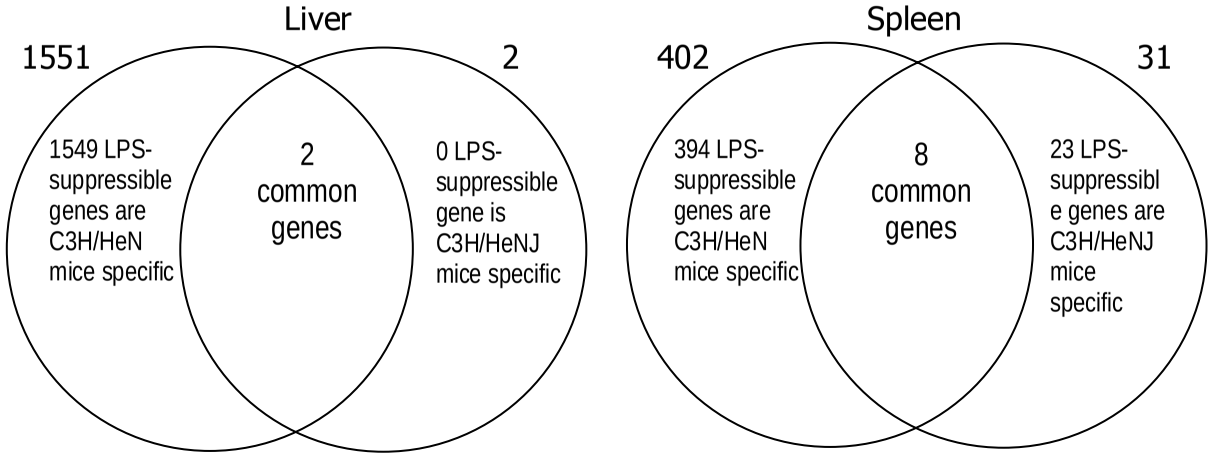
Liver
1551
2
1549 LPS-suppressible genes are C3H/HeN mice specific
2 common genes
0 LPS-suppressible gene is C3H/HeNJ mice specific
Spleen
402
31
394 LPS-suppressible genes are C3H/HeN mice specific
8 common genes
23 LPS-suppressible genes are C3H/HeNJ mice specific

The role of SRTFs in LPS-induced inflammatory response in vivo

Signaling to the nucleus mediated by NFκB and other SRTFs play a significant role in transcriptional regulation evoked by LPS (Hawiger, 2001). As demonstrated in figure 23, nuclear import inhibitor, cSN50, suppressed almost 50% (547 out of 1296) of LPS-inducible genes in the liver and about 10% (105 out of 1109) in the spleen. Among LPS-suppressed genes, cSN50 administration blocked the suppression of almost 45% of genes (669 out of 1551) in the liver and more than 50% (230 out of 402) in the spleen. A reciprocal relationship is observed between the response of metabolic genes (carbohydrate, lipid, fatty acid and steroid metabolism) and intracellular signaling genes (genes related to cytokine/chemokine pathway, and genes involving pre-mRNA modification and mRNA splicing). Genes involved in intracellular signaling are more prominently presented in the LPS-induced pool while genes involved in metabolism are predominant in the LPS-suppressed pool. The adjustment of metabolic gene expression in the liver is consistent with the observation that systemic inflammation is often accompanied by alterations of triglyceride-rich lipoproteins, high-density lipoproteins cholesterol, and cholesterol transport (Khovidhunkit et al., 2000).

This hitherto unreported comprehensive analysis of the nuclear import-dependent genome response to a proinflammatory agonist is consistent with our previous data demonstrating the highly protective effect of cell-penetrating nuclear import inhibitor in a murine model of LPS-induced lethal inflammation,

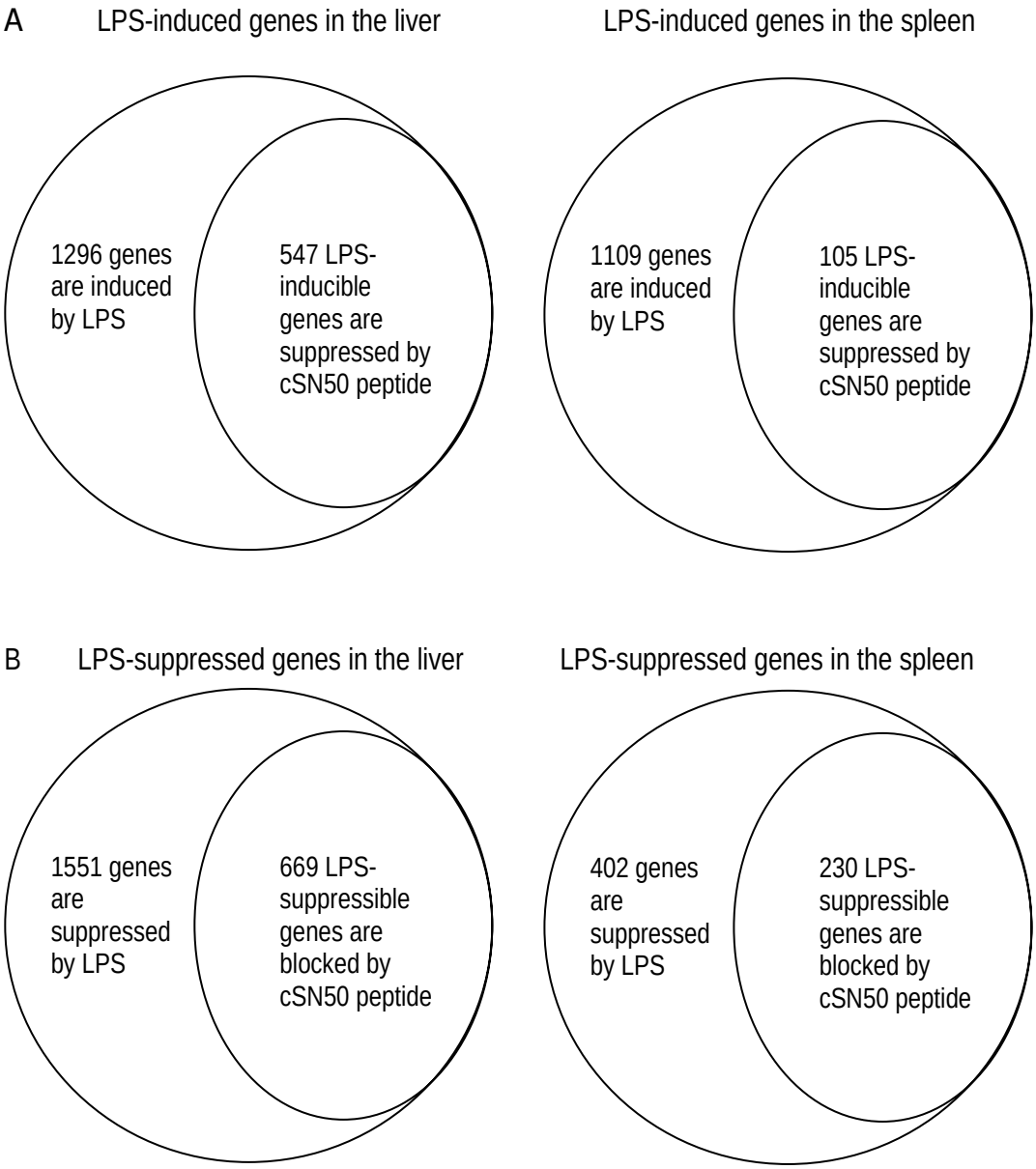

Figure 23. Genome-wide expression profiling in the liver and spleen induced by LPS and regulated by nuclear import inhibitor CSN50.

A, Venn diagram of LPS-induced genes in the liver and the spleen regulated by nuclear import inhibitor.

B, Venn diagram of LPS-suppressed genes in the liver and the spleen regulated by nuclear import inhibitor. Only genes that showed at least 2-fold induction or suppression with a minimum of 66% reproducibility as compared with control samples are included in the analysis. Each of these spots has a coefficient of variance (COV) less than or equal to 30%.

apoptosis, microvascular thrombosis, and hemorrhagic necrosis (Liu et al., 2004a). The survival rate of mice challenged with LPS and D-galactosamine was increased by 10 fold (from 7% to 71%) in mice treated with the nuclear import inhibitor, cSN50 (Liu et al., 2004a).

Discussion

Inflammation is the major mechanism of diseases caused by biological, chemical, and physical agents. Cumulatively, the morbidity and mortality due to inflammation-mediated diseases including coronary heart diseases, sepsis, and acute respiratory distress syndrome far exceeds that caused by cancer, neurodegeneration, and inborn errors of metabolism. Signaling to the nucleus induced by proinflammatory agonists is responsible for an extensive reprogramming of the genome. The "inflamed" genes encode mediators and suppressors of inflammation and apoptosis (Vanderbilt Program on Functional Genomics of Inflammation website, http://www.inflamedgene.org/). This burst of transcriptional activity can be suppressed by cell-penetrating peptide inhibitor of nuclear import validating a new "nuclear paradigm of inflammation" (Hawiger, 2001). The nuclear import inhibitor (cSN50) is effective in animal models of systemic inflammation triggered by pathogen-derived endotoxin LPS and staphylococcal enterotoxin B (a class B agent) (Liu et al., 2004a; Liu et al., 2004b).

Detailed information of the genes described in this chapter can be found on VMSR website (http://array.mc.vanderbilt.edu/). Selected genes have been verified by real-time RT-PCR and the results are consistent with the microarray study (data not shown). A few genes from the list of nuclear import-dependent, LPS-inducible genes in the liver of C3H/HeN mice were chosen for further study for their role in inflammation in mice deficient in these genes. The lessons drawn from our analysis will be extremely useful for the conceptual development of new therapeutic approaches toward systemic and organ-based inflammatory diseases.

Summary and conclusions

Inflammation is the major mechanism of cardiac, pulmonary and vascular disease. Animal models of systemic inflammation induced by SEB and LPS were used to study inflammatory responses through high-density DNA microarrays.

In an animal model of systemic inflammation induced by SEB, 134 and 209 SEB-activated genes were identified in spleen cells and T lymphocytes, respectively. In T lymphocytes, 182 out of 209 activated genes were suppressed upon the treatment with a cell-penetrating peptide cSN50 while the same treatment abolished the activation of all 134 genes in the spleen. SEB-induced genome activation was also ablated in IκBαΔN transgenic mice. As this transgenic supersuppressor interferes with NFκB-mediated signal transduction, our data indicate that SEB-induced genome-wide transcriptional activation in T

lymphocytes is mediated by nuclear import of NFκB and other stress-responsive transcription factors.

In an animal model of systemic inflammation induced by LPS in C3H/HeN mice, we observed upregulation of 1296 genes and downregulation of 1551 genes in the liver. In the spleen, LPS induced upregulation of 1109 genes and downregulation of 402 genes. This genome-wide regulation by LPS is dependent on TLR-4 since C3H/HeJ mice with defective TLR-4 signaling demonstrated the lack of genome-wide response. Moreover, nuclear import inhibitor cSN50 blocked 547 LPS-upregulated and 669 LPS-downregulated genes in the liver. In the spleen, same treatment blocked 105 LPS-upregulated and 230 LPS-downregulated genes. Thus, nuclear import of SRTFs plays an important role in the LPS-induced and TLR-4-dependent genome-wide transcriptional regulation in the liver and the spleen.

CHAPTER IV

MATERIALS AND METHODS

Cell lines

Human embryonic kidney 293T cells and MRC-5 cells were obtained from the American Type Culture Collection (Manassas, VA). HEK293T were cultured in Dulbecco's modified Eagle's medium (DMEM; Cellgro, VA) supplemented with 10% heat-inactivated fetal bovine serum (HI-FBS) containing no detectable LPS (< 6 pg/mL as determined by the manufacturer, Atlanta Biological, Norcross, GA), L-glutamine (2mM), penicillin (100 U/mL) and streptomycin (100 µg/mL). MRC-5 cells were maintained in Minimum essential medium (Eagle) supplemented with 10% HI-FBS, L-glutamine (2mM), penicillin (100 U/mL) and streptomycin (100 µg/mL). All cells were maintained at 37°C in a humidified atmosphere of 5% CO_2.

Plasmids and reagents

The NFκB-luciferase reporter construct (κB-luc) containing five κB elements were a generous gift from Dean Ballard (Vanderbilt University, Nashville, TN). The Renilla-TK-luciferase reporter constructs (RL-TK) was purchased from Promega. The AU1-tagged MyD88 expressing plasmid was a gift from Marta Muzio (Mario Negri Institute, Italy, ref: (Muzio et al., 1997)). All

MyD88-TIR constructs were cloned into pcDNA3.1. An AU1-tag or Myc-tag was introduced at N-terminus of MyD88 or MyD88-TIR by Polymerase Chain Reaction (PCR). All constructs were verified by sequencing.

Generation of mutants

$Pro_{712}His$ mutation in TLR-4 renders the LPS response in C3H/HeJ mice (Poltorak et al., 1998). Similar mutation in MyD88 and MyD88-TIR[1-296($P_{200}H$) and 152-296($P_{200}H$)] were generated by PCR and subcloned into pcDNA3.1 (Invitrogen, Carlsbad, CA). Alignment of members of TLR family reveals that three short motifs in MyD88 that are most conserved among family members: Box 1 (PERFDAF), Box2 (DRDVLPG) and Box 3 (SWFWTRL). Alanine substitution were performed by selecting charged residues either in the conserved region or predicted to be on the surface. There were 3 exceptions, V204, Q229 and F285W286. The first two were in the region predicted to interact with MAL (Dunne et al., 2003), and the third was conserved hydrophobic residues. All mutations were made *in vitro* using site-directed PCR mutagenesis as previously described (Kunkel, 1985). Briefly, PCR was utilized with a supercoiled dsDNA template and two synthetic complementary oligonucleotides containing the desired mutation and followed by removing methylated parental DNA template with *Dpn* I. The nicked DNA containing the desired mutations was transformed into DH5α competent cells. Mutants were confirmed by sequencing. Primers used in the PCR mutagenesis are listed in Table 2.

Table 2. Oligonucleotides used for alanine substitution

Primer	Sequence
H156-S	5′-CATCGACCCCCTGGGGGCCATGCCTGAGCGTTTCG-3′
H156-A	5′-CGAAACGCTCAGGCATGGCCCCCAGGGGGTCGA-3′
ER159S	5′-CCTGGGGCATATGCCTGCCGCTTTCGATGCCTTCATCTG-3′
ER159-A	5′-GCACATGAAGGCATCGAAAGCGGCAGGCATATGCCCCAG-3′
D162S	5′-GCCTGAGCGTTTCGCTGCCTTCATCTGCTATTG-3′
D162A	5′-CAATAGCAGATGAAGGCAGCGAAACGCTCAGGC-3′
D171S	5′-GCTATTGCCCCAGCGCCATCCAGTTTGTGCAGG-3′
D171A	5′-CCTGCACAAACTGGATGGCGCTGGGGCAATAGC-3′
E177S	5′-CATCCAGTTTGTGCAGGCCATGATCCGGCAACTGG-3′
E177A	5′-CCAGTTGCCGGATCATGGCCTGCACAAACTGGATG-3′
R180S	5′-GTGCAGGAGATGATCGCGCAACTGGAACAGACAAAC-3′
R180A	5′-GTTTGTCTGTTCCAGTTGCGCGATCATCTCCTGCAC-3′
E183-S	5′-GATGATCCGGCAACTGGCACAGACAAACTATCGACTG-3′
E183-A	5′-CAGTCGATAGTTTGTCTGTGCCAGTTGCCGGATCATC-3′
R188S	5′-CTGGAACAGACACAACTTCAGTGCATAGTTTGTCTGTTCCAG-3′
R188A	5′-GTCAGACACACACAACTTCAGTGCATAGTTTGTCTGTTCCAG-3′
K190S	5′-CAGACAAACTATCGACTGGCCTTGTGTGTGTCTGACCGCG-3′
K190A	5′-CGCGGTCAGACACACACAAGGCCAGTCGATAGTTTGTCTG-3′
DRD195S	5′-CTGCCGTTGTGTGTGTCTGCCGCCGCTGTCCTGCCTGGCACCTG-3′
DRD195A	5′-CAGGTGCCAGGCAGGACAGCGGCGGCAGACACACACAACTTCAG-3′
V204S	5′-GCCTGGCACCTGTGCCTGGTCTATTGCTAG-3′
V204A	5′-CTAGCAATAGACCAGGCACAGGTGCCAGGC-3′
E210S	5′-CTGGTCTATTGCTAGTGCCCTCATCGAAAAGAGGTGCC-3′
E210A	5′-GGCACCTCTTTTCGATGAGGGCACTAGCAATCGACCAG-3′
EKS213S	5′-GCTAGTGAGCTCATCGCAGCCGCGTGCCGCCGGATGGTGGTGG-3′
EKS231A	5′-CCACCACCATCCGGCGGCACGCGGCTGCGATGAGCTCACTAGC-3′
RR218S	5′-GCTCATCGAAAAGAGGTGCGCCGCGATGGTGGTGGTTGTCTCTG-3′
RR218A	5′-CAGAGACAACCACCACCATCGCGGCGCACCTCTTTTCGATGA-3′
DD225S	5′-GATGGTGGTGGTTGTCTCTGCTGCTTACCTGCAGAGCAAGG-3′
DD225A	5′-CCTTGCTCTGCAGGTAAGCAGCAGAGACAACCACCACCATC-3′
Q229S	5′-GTTGTCTCTGATGATTACCTGGCCAGCAAGGAATGTGACTTCC-3′
Q229A	5′-GGAAGTCACATTCCTTGCTGGCCAGGTAATCATCAGAGACAAC-3′
KE231S	5′-CTGATGATTACCTGCAGAGCGCGGCATGTGACTTCCAGACC-3′

Table 2. continued

KE231A	5′-GGTCTGGAAGTCACATGCCGCGCTCTGCAGGTAATCATCAG-3′
D234S	5′-GCAGAGCAAGGAATGTGCCTTCCAGACCAAATTTGC-3′
D234A	5′-GCAAATTTGGTCTGGAAGGCACATTCCTTGCTCTGC-3′
K238S	5′-GGAATGTGACTTCCAGACCGCATTTGCACTCAGCCTCTC-3′
K238A	5′-GAGAGGCTGAGTGCAAATGCGGTCTGGAAGTCACATTCC-3′
H248S	5′-CCTCTCTCCAGGTGCCGCTCAGAAGCGACTGATC-3′
H238A	5′-GATCAGTCGCTTCTGAGCGGCACCTGGAGAGAGG-3′
KR250S	5′-CTCTCCAGGTGCCCATCAGGCCGCACTGATCCCCATCAAGTAC-3′
KR250A	5′-GTACTTGATGGGGATCAGTGCGGCCTGATGGGCACCTGGAGAG-3′
K256S	5′-GAAGCGACTGATCCCCATCGCCTACAAGGCAATGAAGAAAGAG-3′
K256A	5′-CTCTTTCTTCATTGCCTTGTAGGCGATGGGGATCAGTCGCTTC-3′
K258S	5′-CGACTGATCCCCATCAAGTACGCCGCAATGAAGAAAGAGTTCC-3′
K258A	5′-GGAACTCTTTCTTCATTGCGGCGTACTTGATGGGGATCAGTCG-3′
KKE261S	5′-CATCAAGTACAAGGCAATGGCGGCAGCGTTCCCCAGCATCCTGAGG-3′
KKE261A	5′-CCTCAGGATGCTGGGGAACGCTGCCGCCATTGCCTTGTACTTGATG-3′
R269S	5′-GTTCCCCAGCATCCTGGCCTTCATCACTGTCTGCGAC-3′
R269A	5′-GTCGCAGACAGTGATGAAGGCCAGGATGCTGGGGAAC-3′
D275S	5′-GTTCATCACTGTCTGCGCCTACACCAACCCCTG-3′
D275A	5′-CAGGGGTTGGTGTAGGCGCAGACAGTGATGAAC-3′
K282S	5′-CACCAACCCCTGCACCGCATCTTGGTTCTGGACTC-3′
K282A	5′-AGATCCAGAACCAAGATGCGGTGCAGGGGTTGGTG-3′
FW285S	5′-CCTGCACCAAATCTTGGGCCGCCACTCGCCTTGCCAAGGCC-3′
FW285A	5′-GGCCTTGGCAAGGCGAGTGGCGGCCCAAGATTTGGTGCAGG-3′
R288S	5′-CAAATCTTGGTTCTGGACTGCCCTTGCCAAGGCCTTG-3′
R288A	5′-CAAGGCCTTGGCAAGGGCAGTCCAGAACCAAGATTTG-3′
K291S	5′-CTGGACTCGCCTTGCCGCCGCCTTGTCCCTGCCC-3′
K291A	5′-GGGCAGGGACAAGGCGGCGGCAAGGCGAGTCCAG-3′

Transient transfection, reporter assay and cytokine cytometric beads array (CBA)

Transfection of HEK 293T cells was performed with the indicated cDNAs by a conventional calcium phosphate method. One day before transfection, cells were seeded $2.5X10^5$ /mL per 100mm plate. At 18 h after transfection, the culture media was replaced with fresh media, and on the following 24 h the cells were treated as indicated, harvested and submitted to subsequent analysis. When the cells were to be stimulated with IL-1β, the culture media was changed to media containing IL-1β (10ng/mL or indicated otherwise; Cellsciences, Canton, MA) and further cultured for 6 h or left untreated for the indicated period of time. One million MRC-5 cells were transfected with Cell Line Nucleofector Kit R (Amaxa, Gaithersburg, MD) program U23 following manufacture's protocol. At 8 h after transfection, cells were washed with HBSS and fresh media added. Cells were stimulated with IL-1β for 6h next day, and culture media were collected and analyzed for production of cytokines and chemokines.

SN50 which inhibit nuclear translocation of NFκB and other SRTFs has been described elsewhere (Hawiger, 1999; Lin et al., 1995). SN50 peptide was synthesized, purified and prepared as described before (Yan Liu et al., 2000). One million MRC-5 cells in 6-well plates were seeded and treated with diluent or SN50(100 μM) in HBSS for 30 minutes before and followed by IL-1 10ng/mL treatment for 6 h. Culture media were collected and IL-1β-stimulated cytokines/chemokines production of MRC-5 cells was analyzed by Human

Inflammation cytometric beads array Kit (BD Biosciences, San Diego, CA) according to manufacture's protocol.

For reporter gene activity assay, HEK 293T cells were transfected with the NFKB-dependent luciferase reporter gene (NFKB-Luc) together with pRL-TK (Promega). The NFκB-Luc vector contains firefly luciferase gene controlled by five reiterated κB sites. The pRL-TK Vector, as an internal control reporter, contains a renilla luciferase gene under the herpes simplex virus thymidine kinase (HSV-TK) promoter. HEK 293T cells were harvested and submitted to subsequent Dual-luciferase assay according to manufacture's protocol (Promega technical manual #TM040).

Immunoblotting and indirect immunofluorescence

To check the protein expression after transient transfection, 293T cells were seeded ($2.5X10^5$ mL^{-1}) onto 100-mm dishes 24 h prior to transfection with combinations of plasmids (20 μg total) as indicated using calcium phosphate method. 36 h post-transfection cells were washed by the addition of 5 mL of ice-cold phosphate-buffered saline. Cells were lysed on ice for 10 min in lysis buffer containing 150 mM NaCl, 2 mM EDTA, 10% glycerol, 0.1% NP-40, 0.2 mM phenylmethylsulfonyl fluoride, 0.2 mM Na_3VO_4, and 1 μg of leupeptin mL^{-1}. 50 μg of cell lysate was separated by SDS-PAGE, and then analyzed by immunoblotting. Monoclonal antibodies against the epitope tags myc and AU1 were obtained from Covance(Berkeley, CA). For indirect immunofluorescence —10^5 transfected HEK

293T cells were cytocentrifuged onto glass slide and fixed with 3.5% paraformaldehyde. After washing with PBS, cells were permeablized with 0.25% Triton X-100 for 10 min and then probed with anti-AU1 antibody followed by Rhodamine Red-X labeled goat anti mouse IgG antibody (Jackson ImmunoResearch Lab, West Grove, PA) as described (Lin et al., 1995). Slides with stained cells were mounted in Poly/Mount (Polysciences, Warrington, PA) and analyzed in an Olympus fluorescence microscope using a X 100 oil immersion lens.

Co-immunoprecipitation

HEK 293T cells were plated $5X10^6$per 100 mm plate. 24h later, cells were transfected with 10mg of myc-MyD88 and 10 mg of AU1-TIR or TIR mutants using Calcium phosphate method. Fresh media was added 18 h later and incubated for 24h. Cells were washed with PBS and resuspended in 400 µL hypotonic gentle lysis buffer (10 mM Tris-HCl pH 7.5, 10 mM NaCl, 10 mM EDTA, 0.5% Triton-X100, 1 mM PMSF, 1 µM aprotinin, 1 µM leupeptin). 200 mg of lysate was incubated with 10 µg anti-AU1(Covance, Berkeley, CA) at 4°C overnight. 10 µl Protein G Sepharose 4 fast flow slurry (Amersham) were added and incubated for 3 h at 4°C. Beads were washed 8 times with 0.5 mL of wash buffer (10 mM Tris-HCl pH 7.5, 150 mM NaCl, 10 mM EDTA, 0.5% Triton-X100, 1 mM PMSF, 1 µM aprotinin, 1 µM leupeptin). Beads were resuspended in 2X Laemmli buffer. The samples were fractionated on 15% SDS-PAGE, transferred

to a PVDF membrane and subjected to immunoblotting analysis with specific antibody (anti-myc, Covance; Berkeley, CA). As a control, 50 μg of total cell lysate was applied to immunoblotting with same antibody. As a second control, counter immunoprecipitations were also performed.

Modeling studies

The 3-dimensional models of MyD88 and IL1RAcP TIR domain structure were established by comparative modeling computation using Swiss-Model homology-modeling server(Guex and Peitsch, 1997; Schwede et al., 2003). Within known 3-dimensional structures of TIR domain from highly homologous TLR family members, there are at least 7 PDB records (Tao et al., 2002; Xu et al., 2000). TIR domain of human TLR-2 with an alignment identity 31% and over 50% of similarity comparing with MyD88 was used for MyD88 TIR domain comparative modeling (PDB file of *1o77*). TIR domain of human TLR1 with an identity 33% compare with MyD88 was used for comparative modeling of IL1RAcP(PDB file of *1fyvA*).

Peptide synthesis

The cell-permeable peptide cSN50 was synthesized, purified, filter-sterilized, and analyzed as described elsewhere(Torgerson et al., 1998; Yan Liu et al., 2000). The cSN50 peptide carries a nuclear localization sequence (NLS)

derived from p50/NFκB1 and membrane-translocating motif (MTM) which leads the functional cargo into across cell membrane.

Delivery of cell-penetrating peptides *in vivo*

C57BL/6 mice were purchased from the Jackson Laboratory. Transgenic C57BL/6 mice expressing IκBαΔN in T cell lineage were engineered as previously described(Boothby et al., 1997; Liu et al., 2004b). Unlike wild type IκBα, the IκBαΔN mutant protein is resistant to degradation and functions as constitutive repressor of NFκB (Boothby et al., 1997; Liu et al., 2004b). All of the mice were female (8 - 12 weeks old) with an average weight of 20 grams. Unless noted otherwise, mice were injected intravenously with 150 μg of SEB (Toxin Technology). SEB has been purified with additional procedure by the manufacturer so that it contains less than 1 endotoxin unit (EU) of LPS per mg. Cell-permeable peptide cSN50 (0.7 mg) was dissolved in pyrogen-free water containing 5% DMSO. Animal handling and experimental procedures were performed in accordance with the American Association of Accreditation of Laboratory Animal Care Guidelines and were approved by the Institutional Animal Care Committee.

Measurement of cytokine/chemokine expression

Blood samples were collected from the saphenous vein in heparinized tubes before (30 mins.) and after (1, 6, and 24 hours) SEB challenge. Plasma

levels of TNF-α, IFN-γ, and IL-2 were measured by cytometric bead array (CBA) according to the manufacturer's protocol as described previously (Liu et al., 2004b).

Isolation of T lymphocytes from the spleen

Murine lymphocytes were isolated from the spleens of wild type C57BL/6 mice and transgenic C57BL/6 mice that express IκBαΔN (inhibitor of NFκB nuclear translocation) as previously described (Yan Liu et al., 2000). By depletion of MHC Class II expressing cells, the intact T cells enriched from spleen contained 83-90% of CD3 positive cells.

RNA extraction and reverse transcriptase reaction

Total RNA was extracted from mouse tissue and enriched T cells using Trizol Reagent (Invitrogen) following the manufacturer's instructions with slight modification to eliminate the contamination of polysaccharides and proteoglycons. The RNA samples were DNase-treated (Promega) and treated with phenol/chloroform two times to remove DNase. The RNA samples were then cleaned up using RNeasy kit (Qiagen). RNA isolated from T cells isolated from a group of C57BL/6 or IκB.DN mice were pooled to get sufficient amount and analyzed as one sample. RNA from spleen isolated from each mouse is not pooled. RNA was quantified by spectrophotometry and its integrity was assured

by analysis using an Agilent Bioanalyzer 2100 (Agilent Technologies, Palo Alto, CA).

Construction of microarray containing 22k genes

Microarrays containing 22,172 cloned genes from the National Institute on Aging 15k cDNA clone set, mouse sequence-verified clones from Research Genetics and several control genes were generated by the Vanderbilt Microarray Shared Resource. Full gene lists and protocols are available at http://array.mc.vanderbilt.edu. Briefly, all cDNA clones were amplified and verified by gel electrophoresis. The dried PCR products were then resuspended in 40 μl VMSR buffer A [Vanderbilt Microarray Shared Resource, Nashville, TN] resulting in an average concentration of 400 – 700 μg/ml per product. The PCR products were then transposed to 384 well plates and robotically arrayed using a BioRobotics MicroGrid II microarray printing robot (Apogent Discoveries, Hudson, NH) onto amine-coated glass slides (TeleChem International, Sunnyvale, CA). The microarrays were then crosslinked using 80mjoules of ultraviolet energy (Stratagene Stratalinker, LaJolla, CA). Following crosslinking, the arrays were baked for two hours at 70°C in a standard oven and stored under low humidity conditions until use.

Target labeling and coupling

All RNA Preps were run on an Agilent 2100 Bioanalyzer to assess RNA integrity. Those samples meeting minimum requirements of RIN value of 7.0 and greater were used to generate cDNA targets for hybridization to spotted arrays in the following manner: 5-10µg of total RNA from each sample was reverse transcribed at 42 °C using 400 units Superscript II (Invitrogen) in the presence of 6ug anchored oligo dT and an Amino-allyl tagged dUTP (Sigma, A0410). Additionally, RNA Spike- In controls (Ambion, cat#1780) were added at concentrations ranging from 0 – 200pg per spike per reverse transcriptase reaction. These 8 control spike-ins hybridize to the Ambion control spots on VMSR arrays. Final concentrations of dNTP's in the reaction were 200µM dA, dG, dC, 51µM dT, and 149µM AAdUTP (Sigma A 0410). cDNA targets generated were incubated with NaOH to hydrolyze any remaining total RNA, then neutralized with HCl, and cleaned over Qiaquick columns (Qiagen, 28106). The targets were dried to completion and then coupled to ester-linked Cy5 and Cy3 dyes (Amersham PA23001 Cy3, and PA25001 Cy5) in 0.1M Sodium Bicarbonate (pH. 9.0) for 60 minutes in a 6µl volume to facilitate the coupling reaction. After quenching of unbound dye with 4M Hydroxylamine (Aldrich 43,136-2) Cy3 and Cy5 pairs were combined and the target pairs were cleaned up over Qiaquick columns again (Qiagen, 28106) and then dried to completion in a speed-vac. The targets were then resuspended in 50µl of MWG Hyb Buffer (Ocimum Biosolutions, cat#1180-200000) and 1 µg of Poly A RNA (Sigma, P9403) was added to each

target. The targets were heat denatured and then hybridized 16 hours at 42°C on a Maui Hyb Station (BioMicro Systems, Inc.). Following post hybridization washes all arrays were scanned on an AXON 4000b scanner.

Data analysis of microarray

Microarrays were scanned and the raw data was generated by the accompanying software, GenePix 4.1. Raw data were then analyzed using GeneTraffic 2.6 by Iobion Informatics, LLC. All 20,996 spots were first filtered and removed from analysis if the following criteria were not met: *(i)* Cy5 signal to background intensity ratio less than 2; *(ii)* Cy3 signal to background intensity ratio less than 2; *(iii)* Cy5 signal less than 200; *(iv)* Cy3 signal less than 200.

The arrays were performed in at least triplicate for each group (SEB Spleen, SEB+cSN50, SEB-T cell, SEB+cSN50 T cell, SEB-Transgenic, Trans-no SEB, all at 24hr). Between three and six RNA samples were collected from experimental time point (SEB Spleen, SEB+cSN50, SEB-T cell, SEB+cSN50 T cell, SEB-Transgenic, Trans-no SEB, all at 24hr) and matched control samples were labeled with Cy3 and Cy5 dyes. Labeling of these RNA samples yielded equal amounts of labeled probes indicating the initial RNA quantity was equal and there was no artifact introduced during the labeling procedure. Therefore, possibility of general decline in the abundance of transcript can be excluded. The possibility of introduction of variation due to sample-to-sample variation was

reduced because of the number of replicate RNA samples. The average statistically significant intensities were obtained by using GeneTraffic software.

Data was normalized using the Lowess sub-grid method. Lists of features with a fold change of greater than 2.0 fold and a coefficient of variance of less than 30% (across multiple arrays) that repeated expression in the hybridizations under the same conditions were generated for each condition. These gene lists were then compared to each other in order to identify genes with interesting expression profiles across each condition.

In addition to GeneTraffic, GeneSpring (Silicon Genetics) was also used to illustrate the hierarchical correlation between the genes. This data analysis software uses numerical expression data from microarray results and illustrates the possible correlation between the expression profiles amongst the genes based on their expression levels. We analyzed the genes suppressed and expressed in whole spleen cells treated with SEB when cSN50 was added at 24hrs, and studied their expression profile by clustering. Similar analysis was also performed on the changing expression of the genes in T cells when the cSN50 peptide was added at 24 hrs. We also studied the cluster analysis of the genes that are commonly expressed among the whole spleen cells and T cells in response to the addition of cSN50 at 24 hrs.

Affymetrix-based microarray analysis

Affymetrix mouse gene chip platform is provided by the Vanderbilt Microarray Shared Resource (VMSR). This high-density oligonucleotide chip contains over 39,000 transcripts, within which 34,000 are annotated as well-defined genes. Following hybridization, arrays are washed and scanned according to Affymetrix protocols (Affymetrix Inc, Santa Clara, CA). All instrument control and initial data analysis is performed using GCOS. Additional analysis employing alternative probe-level methods is performed in GeneTraffic (Iobion Informatics). Following data collection, all arrays will be analyzed using both the MAS5.0 algorithm (default Affymetrix approach, www.affymetrix.com) as well as the Robust Multichip Analysis (RMA) approach. Several statistical methods for the determination of differential expression or classification are available in the GeneTraffic package or other software packages (GeneSpring, Bioconductor, Array Analyzer). Genes identified as significantly differentially expressed are annotated with pathway, chromosomal and gene ontology information, providing a functional and organizational view of the data to potentially identify biologically relevant patterns.

APPENDIX A

Li, C., Zienkiewicz, J., Hawiger, J. 2005.

Interactive Sites in the MyD88 Toll/Interleukin (IL) 1 Receptor Domain Responsible for Coupling to the IL1β Signaling Pathway.

J. Biol. Chem., 280: 26152-26159

THE JOURNAL OF BIOLOGICAL CHEMISTRY
Vol. 280, No. 28, Issue of July 15, pp. 26152–26159, 2005
Printed in U.S.A.

Interactive Sites in the MyD88 Toll/Interleukin (IL) 1 Receptor Domain Responsible for Coupling to the IL1β Signaling Pathway*

Received for publication, March 24, 2005
Published, JBC Papers in Press, April 22, 2005, DOI 10.1074/jbc.M503262200

Chunsheng Li‡, Jozef Zienkiewicz, and Jacek Hawiger§

From the Department of Microbiology and Immunology, Vanderbilt University School of Medicine, Vanderbilt University Medical Center, Nashville, Tennessee 37232

Myeloid differentiation factor MyD88 is the essential adaptor protein that integrates and transduces intracellular signals generated by multiple Toll-like receptors including receptor complex for interleukin (IL) 1β, a key inflammatory cytokine. IL1β receptor complex interacts with MyD88 via the Toll/IL1 receptor (TIR) domain. Here we report structure-function studies that help define the MyD88 TIR domain binding sites involved in IL1β-induced protein-protein interactions. The MyD88 TIR domain, employed as a dominant negative inhibitor of IL1β signaling to screen MyD88 TIR mutants, lost its suppressing activity upon truncation of its Box 3. Accordingly, mutations of Box 3 residues 285–286 reversed the dominant negative effect of the MyD88 TIR domain on IL1β-induced and NFκB-dependent reporter gene activity and IL6 production. Moreover, mutations of residues 171 in helix αA, 195–197 in Box 2, and 275 in βE-strand had similar functional effects. Strikingly, only mutations of residues 195–197 eliminated the TIR-TIR interaction of MyD88 and IL1 receptor accessory protein (IL1RAcP), whereas substitution of neighboring canonical Pro^{200} by His was without effect. Mutations in Box 2 and 3 prevented homotypic MyD88 oligomerization via TIR domain. Based on this structure-function analysis, a three-dimensional docking model of TIR-TIR interaction between MyD88 and IL1RAcP was developed.

The importance of the Toll-like receptor (TLR)[1] family in innate immune response to microbial surfaces and nucleic acids is well established. Surprisingly, two members of this family recognize key inflammatory cytokines interleukin (IL) 1 and IL18. These cytokines induce genes that encode other mediators of inflammation such as pleiotropic inflammatory cytokine IL6 and interferon γ, respectively (1–5).

Consistent with these studies, IL1β is one of the most potent inflammatory cytokines responsible for fever, leukocytosis, thrombocytosis, and production of IL6 and other cytokines (1–3). The signals generated by IL1β binding to its cognate receptor complex, formed by two type I transmembrane proteins, IL1 receptor I (IL1RI) and IL1 receptor accessory protein (IL1RAcP), are transduced by their cytoplasmic segments denoted as the Toll/IL1 receptor (TIR) domain. TIR domain is shared with *Drosophila* Toll, mammalian TLRs, and cytoplasmic adaptors exemplified by MyD88 (6).

MyD88 adaptor integrates signals flowing from IL1 receptor/IL1RAcP and from an array of other TLRs (6, 7). This initial IL1 receptor-MyD88 adaptor interaction evoked by IL1β is a critical step in its signaling to the nucleus and, therefore, represents a potential target for new anti-inflammatory agents. MyD88 has a bipartite structure composed of an amino-terminal Death domain and a carboxyl-terminal TIR domain with a short intervening linker segment (6). Upon IL1β stimulation, IL1RI·IL1RAcP complex recruits MyD88 via its TIR domain (8). In addition, IL1RI-associated kinases are recruited to an IL1RI·IL1RAcP complex including IRAK (9, 10), IRAK-2 (11), IRAK-4 (12) and IRAK-M (13). Our current understanding of IL1 receptor complex-MyD88 adaptor interaction is limited. Here we report studies that help to establish the molecular determinants of MyD88 TIR domain interactions in IL1β signaling pathway.

In terms of its structural features, the MyD88 TIR domain contains three highly conserved motifs denoted Box 1, 2, and 3 (Figs. 1 and 2). Box 2 forms a loop denoted the BB loop that contains an invariant proline residue at position 200, which, in other receptors and adaptors (namely, TLR2, TLR4, IL1RAcP, and MAL/TIRAP), is essential for their signaling function (6, 7). For example, mutating this residue to histidine in TLR4 renders C3H/HeJ mice hyporesponsive to lipopolysaccharide (LPS) (14). This canonical example indicates that conserved structural motifs in TIR domain of TLRs and their adaptors play a highly significant role in proinflammatory ligand- initiated intracellular interactions between TLRs and their adaptors. Depending on the recognition of distinct ligands by TLRs, the preferential usage of its adaptors may require different interacting sites in TIR domain of the same adaptor or an alternative adaptor. The latter applies to TLR3, which requires its adaptor, TRIF, rather than MyD88 for signaling by viral double-stranded RNA. Conversely, TRIF mediates signaling induced by interaction of LPS with TLR4 in the absence of MyD88 (7). We hypothesized that signaling evoked by IL1β through its cognate receptor complex may depend on different interactive sites on TIR domain of MyD88 than the recently reported sites involved in MyD88 interaction with TIR domains of TLR2 and TLR4 (15).

To test this hypothesis, we undertook our studies focused on the potential role of Box 1, 2, and 3 of MyD88 TIR domain in

* This work was supported in part by United States Public Health Service National Institutes of Health Grants HL69542, HL62356, and HL68744. The use of core facilities in this study was supported by National Institutes of Health Grants 2P30CA68485 to the Vanderbilt Ingram Cancer Center and 5P30DK058404-03 to the Vanderbilt Digestive Disease Research Center. The costs of publication of this article were defrayed in part by the payment of page charges. This article must therefore be hereby marked "*advertisement*" in accordance with 18 U.S.C. Section 1734 solely to indicate this fact.

‡ Submitted as partial fulfillment of the requirements for the degree of Doctor of Philosophy, Vanderbilt University School of Medicine.

§ To whom correspondence should be addressed: Dept. of Microbiology and Immunology, Vanderbilt University School of Medicine, 1161 21st Ave. South, A-5321 MCN, Nashville, TN 37232-2363. Tel.: 615-343-8280; Fax: 615-343-8278; E-mail: jacek.hawiger@vanderbilt.edu.

[1] The abbreviations used are: TLR, toll-like receptor; TIR, Toll/interleukin 1 receptor; IL, interleukin; MAL, MyD88 adaptor-like protein, IL1RAcP, IL1 receptor accessory protein; NFκB, nuclear factor κB; IL1RI, IL1 receptor I; IRAK, interleukin 1 receptor-associated kinase; HEK, human embryonic kidney; LPS, lipopolysaccharide.

IL1β signaling. Within these three boxes, we focused on residues representing AA loop, BB loop, and EE loop that were reported to participate in interactions of MyD88 with TLR2 and TLR4 (15). The functional consequences of this mutational analysis were monitored by NFκB-dependent reporter gene activity and by IL1β-induced expression of the endogenous gene that encodes inflammatory cytokine IL6. Our structure-function studies of MyD88 TIR domain led to the development of a three-dimensional docking model of MyD88 and IL1RAcP interaction mediated by their respective TIR domains.

EXPERIMENTAL PROCEDURES

Maintenance and Treatment of Cell Lines—Human embryonic kidney (HEK) 293T cells and human fibroblast MRC-5 cells were obtained from the American Type Culture Collection (Manassas, VA). HEK 293T cells were cultured in Dulbecco's modified Eagle's medium (Cellgro) supplemented with 10% heat-inactivated fetal bovine serum containing no detectable LPS (<6 pg/ml) as determined by the manufacturer (Atlanta Biological, Norcross, GA), L-glutamine (2 mM), penicillin (100 units/ml), and streptomycin (100 μg/ml). MRC-5 cells were maintained in minimum Eagle's medium supplemented with 10% heat-inactivated fetal bovine serum, L-glutamine (2 mM), penicillin (100 units/ml), and streptomycin (100 μg/ml). All cells were maintained at 37 °C in a humidified atmosphere of 5% CO_2.

Plasmids and Reagents—The NFκB-luciferase reporter construct (NFκB-luc) containing five κB elements was provided by Dean Ballard (Vanderbilt University, Nashville, TN). The *Renilla* thymidine kinase luciferase reporter construct (RL-TK luc) was purchased from Promega. The AU1-tagged MyD88-expressing plasmid was a gift from Marta Muzio (Mario Negri Institute, Milan, Italy) (16). All MyD88-TIR constructs were cloned into pcDNA3.1. An AU1 tag or a Myc tag was introduced at the amino terminus of MyD88 or MyD88-TIR by PCR. IL1RAcP with a Myc tag at the amino terminus was cloned by reverse transcription-PCR into pcDNA3.1. All constructs were verified by sequencing.

Mutagenesis—The mutated MyD88 and MyD88 TIR domain sequences were generated using an *in vitro* site-directed PCR mutagenesis method and subcloned into plasmid pcDNA3.1 (Invitrogen) as described previously (17). Briefly, PCR was utilized with a supercoiled double-stranded DNA template and two synthetic complementary oligonucleotides containing the desired mutation and followed by removal of methylated parental DNA template with DpnI. The nicked DNA containing the desired mutations was transformed into the DH5α strain of competent *Escherichia coli*. All the mutants were confirmed by DNA sequencing and subsequently tested in transiently transfected HEK 293T cells.

Transient Transfection of HEK 293T Cells and NFκB Reporter Gene Activity—The cDNAs for all MyD88 and MyD88 TIR domain mutants were inserted into the pcDNA3.1 vector that drives transcription from a cytomegalovirus promoter enhancer and contains an AU1 epitope tag for immunodetection of transiently expressed mutants in HEK 293T cells. Transfection of HEK 293T cells was performed with the indicated cDNAs by a conventional calcium phosphate method. One day before transfection, cells were seeded at a density of 2.5×10^5 ml^{-1}/100-mm plate. After 18 h, the culture medium was replaced with fresh medium, and after 24 h, the cells were treated as indicated, harvested, and submitted to subsequent analysis. When the cells were stimulated with IL1β, the culture medium was replaced by fresh medium containing IL1β (CellSciences, Canton, MA) at 10 ng/ml or as indicated otherwise and either further cultured for 6 h or left untreated for the indicated period of time. For NFκB reporter gene activity assay, HEK 293T cells co-transfected with NFκB-luc and RL-TK luc plasmids were harvested and submitted to subsequent dual-luciferase assay according to manufacturer's protocol (Promega).

Western Blotting and Indirect Immunofluorescence—To check the protein expression after transient transfection, HEK 293T cells were seeded (2.5×10^5 ml^{-1}) onto 100-mm dishes 24 h prior to transfection with combinations of plasmids (20 μg, total) or as indicated, using calcium phosphate method. Thirty-six hours after transfection, cells were washed by the addition of 5 ml of ice-cold phosphate-buffered saline. Cells were lysed on ice for 10 min in lysis buffer containing 150 mM NaCl, 2 mM EDTA, 10% glycerol, 0.1% Nonidet P-40, 0.2 mM phenylmethylsulfonyl fluoride, 0.2 mM Na_3VO_4, and 1 $\mu g/ml^{-1}$ leupeptin. Cell lysate proteins (50 μg) were separated by SDS-PAGE and then analyzed by Western blotting. Monoclonal antibodies against the epitope tags c-Myc and AU1 were obtained from Covance Company (Princeton, NJ). For indirect immunofluorescence, 10^6 transfected HEK 293T cells were cytocentrifuged onto a glass slide and fixed with 3.5% paraformaldehyde. After washing with phosphate-buffered saline, cells were permeabilized with 0.25% Triton X-100 for 10 min and then probed with anti-AU1 antibody followed by Rhodamine Red-X-labeled goat anti-mouse IgG antibody (Jackson ImmunoResearch Lab, West Grove, PA) as described previously (18). Slides with stained cells were mounted in Poly/Mount (Polysciences, Warrington, PA) and analyzed in an Olympus fluorescence microscope using a ×100 oil immersion lens.

Measurement of IL6 Expression Using Cytometric Bead Array Assay—One million MRC-5 cells were transfected with Cell Line Nucleofector Kit R (Amaxa, Gaithersburg, MD) program U23, following the manufacturer's protocol. After 8 h, cells were washed with Hanks' balanced salt solution, and fresh media were added. Cells were stimulated with IL1β for 6 h, and culture medium was collected and analyzed for production of cytokine IL6. Analysis of IL1β-induced expression of cytokine IL6 in human fibroblast MRC-5 cells was performed using the Human Inflammation Kit (BD Biosciences) according to the manufacturer's protocol.

Immunoprecipitation—HEK 293T cells were plated at the density of 5×10^6 cells/100-mm plate. Twenty-four hours later, cells were transfected with either (*a*) 10 μg of Myc-IL1RAcP and 10 μg of AU1-MyD88 or MyD88 mutants or (*b*) 10 μg of Myc-MyD88 and 10 μg of AU1-TIR or TIR mutants using calcium phosphate method. Fresh medium was added 18 h later, and cells were incubated for 24 h. In co-immunoprecipitation of IL1RAcP and MyD88, the cells were treated with 100 ng/ml IL1β for 5 min. The cells were washed with phosphate-buffered saline and resuspended in 400 μl of hypotonic gentle lysis buffer (10 mM Tris-HCl, pH 7.5, 10 mM NaCl, 10 mM EDTA, 0.5% Triton X-100, 1 mM phenylmethylsulfonyl fluoride, 1 μM aprotinin, and 1 μM leupeptin). Lysates were initially precleared with normal mouse serum in combination with protein A-Sepharose 4 fast flow beads (Amersham Biosciences), and then 200 μg of lysate was incubated with 10 μg of anti-Myc at 4 °C overnight. Protein A-Sepharose 4 fast flow slurry (10 μl) was added and incubated for 3 h at 4 °C. Beads were washed eight times with 0.5 ml of wash buffer (10 mM Tris-HCl, pH 7.5, 150 mM NaCl, 10 mM EDTA, 0.5% Triton X-100, 1 mM phenylmethylsulfonyl fluoride, 1 μM aprotinin, and 1 μM leupeptin). Beads were resuspended in 20 μl of 2× Laemmli buffer. The samples were fractionated on 15% SDS-PAGE, transferred to a polyvinylidene difluoride membrane, and subjected to immunoblotting analysis with anti-AU1 antibody. As a control, 50 μg of total cell lysate was applied to Western blot with both anti-c-Myc and anti-AU1 antibodies.

Modeling Studies—The three-dimensional models of MyD88 TIR and IL1RAcP TIR domains were established by a comparative (homology) computation modeling method using Swiss-Model: An Automated Comparative Protein Modeling Server (swissmodel.expasy.org//SWISS-MODEL.html) (19, 20). At least six Protein Data Bank records are available within known three-dimensional structure of TIR domain from highly homologous members of human TLR family. TIR domain of TLR2 with 31% alignment identity and >50% similarity (21) was used for comparative modeling of MyD88 TIR domain (Protein Data Bank code 1O77). TIR domain of TLR1 with 33% identity and 66% similarity (22) was used to generate the three-dimensional model of IL1RAcP (Protein Data Bank code 1FYV). All modeling processes were done in four steps: template selection (BLASTP2), target-template alignment (SIM), model building (ProModII), and energy minimization (GROMOS96). Templates, selected by sequence identity with the target sequence, were then prepared to create the core of the model by averaging of the backbone atom positions. Atoms with significantly deviating position were excluded from modeling process. The Constraint Space Programming (CSP) protocol was used for generation of insertion coordinates. The best loop was selected using a score scheme including force field energy, steric hindrance, and specific or nonspecific interaction, *i.e.* hydrogen bond formation or dipole-dipole interaction. Side chains were reconstructed by weighting positions of corresponding residues in the template structure and their iso-steric replacement. The final model was optimized by steepest descent energy minimization with GROMOS96. The visualizations of the three-dimensional model were performed with the DeepView (Swiss-PdbViewer) freeware program, available for download from the Swiss-Model webpage.

The Three-dimensional Docking Model of MD88 TIR and IL1RAcP TIR Interaction—Many aspects, such as molecular surface, geometry, surface topology, charge distribution, electrostatic field, and residue localization, were considered before an arrangement was constructed. First, a possible position of two interacting TIR domains was prepared manually in stereoviewed mode with the PSSHOW program (SYBYL-Tripos package). When the proper position was chosen, computation was conducted by merging receptor (IL1RAcP-TIR) into adaptor (MyD88-TIR), coordinates of the backbone atoms were then frozen, and

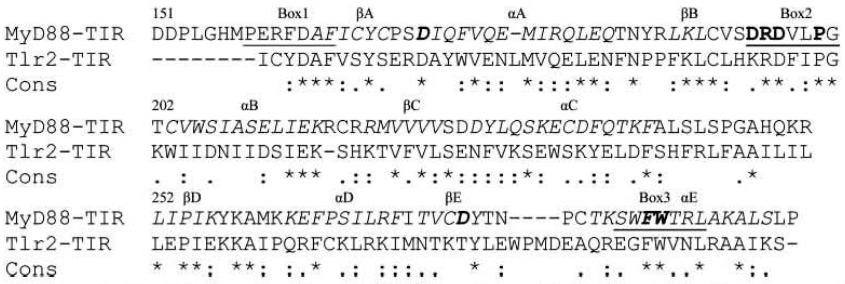

FIG. 1. **Sequence alignment of the TIR domains of human MyD88 and human TLR2 as the basis of homology modeling performed with T-COFFEE.** Boxes 1–3 are *underlined*. Residues substituted with alanine (Asp^{171}, Asp^{195}, Arg^{196}, Asp^{197}, Asp^{275}, Phe^{285}, and Trp^{286}) or histidine (Pro^{200}) are shown in *bold*. α helices and β strands are italic.

the heavy atom aggregate was created and optimized. In the next step, hydrogen atoms were added, and the final model was optimized by energy minimization followed by molecular dynamics. Both steps were performed with the SANDER program (AMBER software package) using integral Newtonian equation of motion with 2000 cycles each. Once the computation process was completed, the coordinates were transformed into a Protein Data Bank file. The three-dimensional docking models of dot-surface and contact surface were obtained with PSSHOW software. The ribbon structure of docking model was prepared with DeepView (Swiss-PdbViewer).

Statistical Analysis—Statistical differences between mean values were analyzed using the two-sided Student's *t* test.

RESULTS AND DISCUSSION

The IL1β signaling pathway depends on an orchestrated interplay of intracellular protein-protein interactions (1–3). MyD88 plays a pivotal role in these interactions by directing the flow of signals from IL1β-occupied cognate receptor complex to downstream signal transducers (2, 3). Within MyD88, the TIR domain provides an interacting surface for heterotypic interaction with the TIR domain of IL1RAcP (3). Therefore, we embarked on structure-function analysis of MyD88 TIR domain that is essential for the transduction of IL1β signaling to downstream effector(s). Our stepwise strategy consisted of analysis of the secondary and tertiary structure of MyD88 TIR domain. These data were obtained on the basis of the available crystal structure of TLR2 TIR domain (21). Drawing from these modeling studies, two series of mutagenesis experiments were carried out. In the first set of experiments, construct containing only TIR domain of MyD88, as its dominant negative inhibitor, was mutated, and the expressed mutants were screened for their inhibitory effect on IL1β-induced signaling to the nucleus. In the second set of experiments, selected TIR residues were mutated in full-length MyD88 to assess the impact of specific replacements on heterotypic interaction of MyD88 with IL1RAcP and homotypic MyD88 oligomerization mediated by its TIR domain. The results of this structure-function analysis led us to the development of the three-dimensional docking model of MyD88 interaction with IL1RAcP mediated by their respective TIR domains.

Structural Characterization of MyD88 TIR Domain—MyD88 TIR domain is modeled on the basis of the crystal structure solved for TLR2 (21). It has an α-β-fold similar to that of the bacterial chemotaxis protein CheY and contains three highly conserved motifs termed Boxes 1, 2, and 3 (3). On the basis of primary structure alignment obtained with the program T-COFFEE, presented in Fig. 1, the crystal structure of human TLR2 TIR domain (Protein Data Bank code 1O77) was selected as the best template for MyD88 TIR domain with 31% identity and >50% similarity. Results obtained from the server were visualized using the DeepView program (Swiss-PdbViewer). As shown in Fig. 2, the secondary structure of TIR domain consists of five β-strands (βA, βB, βC, βD, and βE) forming the core of molecule that is surrounded by five α-helices (αA, αB, αC, αD, and αE). The five loops (AA, BB, CC, DD, and FF) form specific links between β-strand and corresponding α-helix.

In terms of its tertiary structure, as depicted in Fig. 2, MyD88 TIR domain has a globular shape. Among three highly conserved motifs, Box 1, located at the amino terminus of TIR domain, forms a part of βA-strand. Box 2 makes the second part of the BB loop, whereas Box 3 creates the first part of the αE-helix, which is located at the carboxyl terminus of MyD88 TIR domain. As shown in Fig. 2*B*, distribution of charged residues indicates that the molecular surface of MyD88 TIR domain is mostly positively charged (*blue*), with a few distinct negatively charged knobs (*red*). They surround a larger swatch of negatively charged surface (*red*), formed by three loops (AA, BB, and part of DD) and αC-helix. Moreover, the BB loop projects from the globular TIR domain, forming a quasi-plane on its surface.

NFκB Reporter Gene Activity Assay Indicates that Box 3 of MyD88 TIR Domain Is Involved in IL1β-induced Signaling—NFκB reporter gene activity assay was used to test MyD88 TIR domain as a dominant negative inhibitor of IL1β-induced signaling to the nucleus. As documented in Fig. 3, HEK 293T cells transfected with plasmid containing NFκB-dependent luciferase gene responded to sub-nanogram doses of IL1β. This activation reached the maximum at 1 ng/ml IL1β, attesting to the high sensitivity of transfected HEK 293T cells to this inflammatory cytokine. Consistent with prior studies (23, 24), the MyD88 TIR domain, used as a dominant negative inhibitor of IL1β signaling, almost completely suppressed its activating effect on NFκB reporter gene over a wide range of IL1β concentrations (Fig. 3). We engineered a deletion mutant of MyD88 TIR domain to establish the utility of the NFκB reporter gene activity assay for screening MyD88 TIR domain mutants for their inhibitory effect on IL1β-induced signaling. The deleted segment encompassed Box 3 (^{282}KSWFWTRLAK^{291}) located at the carboxyl terminus of MyD88 TIR domain. This deletion caused the loss of the dominant negative inhibitory function of MyD88 TIR (Fig. 3*B*), suggesting that Box 3 was essential for IL1β-induced signaling. The carboxyl-terminal deletion mutant was expressed in transfected cells at a level comparable with that of the intact MyD88 TIR domain (see Fig. 3*B*, *inset*).

Mutagenesis of MyD88 TIR Domain: Loss of Its Dominant Negative Inhibitory Activity toward IL1β-induced Signaling—The involvement of Box 3, as compared with Boxes 1 and 2, in signaling induced by IL1β and mediated by the MyD88 TIR domain was analyzed in the first series of mutagenesis experiments. Mutations of TIR domain (residues 152–296) included two bulky hydrophobic residues (Phe^{285} and Trp^{286}) in a highly conserved short motif in Box 3 (SWFWTRL) and proline at position 200. The canonical P712H mutation in TLR4 renders

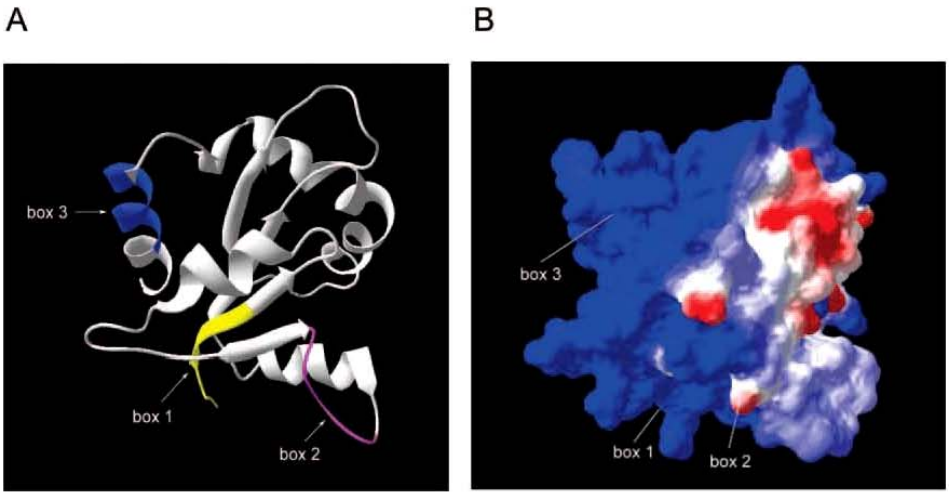

FIG. 2. **Structural model of TIR domain with conserved Boxes 1–3.** Comparative modeling of MyD88-TIR was performed with Swiss-Model (19, 20) by alignment to the crystal structure of hTLR2 (21, 22) optimized by GROMOS96 and visualized by DeepView/Swiss-PdbViewer. *A*, structural features representing the conserved boxes of the MyD88 TIR domain are shown in *yellow* (Box 1), *purple* (Box 2), and *blue* (Box 3). *B*, electrostatic potential of MyD88 TIR with the indicated position of structural features (Boxes 1–3) corresponding to the same features in *A*. The color scale is as follows: *red*, most negative; and *blue*, most positive.

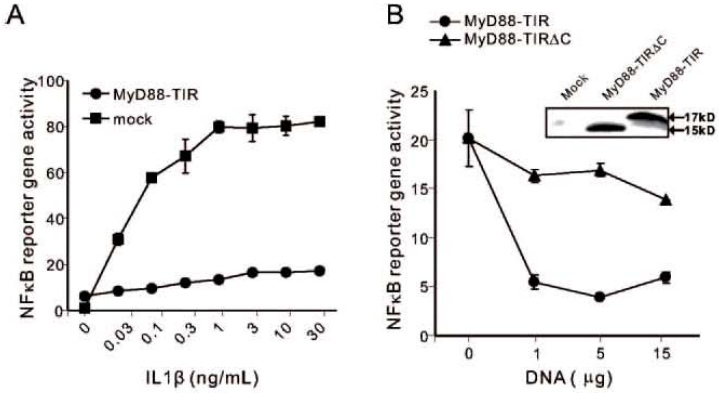

FIG. 3. Inhibition of IL1β-induced NFκB reporter gene activity by MyD88-TIR domain is reversed upon truncation of its Box 3. *A*, IL1β-induced NFκB reporter gene activation was inhibited in HEK 293T cells transfected with MyD88-TIR-(152–296). The HEK 293T cells were transfected with MyD88-TIR together with NFκB-luc (5 μg) and RL-TK (2.5 μg). After 24 h, IL1β was added at the indicated concentrations for 6 h. NFκB reporter gene activity was determined and normalized on the basis of RL-TK activity. *B*, MyD88-TIRΔC-(152–283) construct was cloned into pcDNA3.1 using PCR at BamHI and EcoRI sites. HEK 293T cells were transfected with MyD88-TIR or MyD88-TIRΔC-(152–283) constructs together with NFκB-luc (5 μg) and RL-TK (2.5 μg). After 24 h, IL1β was added at a concentration of 10 ng/ml for 6 h. NFκB reporter gene activity was measured and normalized on the basis of RL-TK activity. *Inset*, expression levels of MyD88-TIR and MyD88-TIRΔC-(152–283) in transfected 293T cells determined by Western blotting with anti-AU1 antibody. Data show a representative experiment from a series of three experiments performed in triplicates. *Error bars* indicate the S.E. of the mean value of triplicate.

C3H/HeJ mice hyporesponsive to LPS (14). This highly conserved proline residue is located at position 200 in the MyD88 TIR domain (15). It was mutated to histidine in MyD88-TIR domain (residues 152–296 (P200H)). Furthermore, alignment of members of the TLR family reveals two short motifs in Box 1 (PERFDAF) and Box 2 (DRDVLPG) that are conserved along with Box 3 motif in MyD88 TIR domain. Alanine substitutions were primarily based on selection of charged residues either in the conserved region or predicted to be on the surface. In addition, two mutations, Val^{204} and Gln^{229}, were in the region predicted to interact with MAL (15). The expression of mutants varied as compared with that of wild-type MyD88 TIR domain (data not shown). Five mutants listed in Table I were expressed at a level comparable with that of wild-type MyD88 TIR domain (see Fig. 4*B*, *inset*). The expression of other mutants was

TABLE I
Information about the MyD88 TIR mutants analyzed in this study

All the TIR mutations were generated as indicated under "Experimental Procedures." MyD88 TIR mutants that did not inhibit NFκB reporter gene activity by >2.5-fold were considered loss of inhibition phenotype as compared with the dominant negative inhibitory effect of wild-type MyD88 TIR domain.

Mutant	Mutation(s)	Location	Loss of inhibition
T1	D171A	AA loop[a]	Yes
T2	D195A/R196A/D197A	Box 2	Yes
T3	P200H	BB loop[b]	No
T4	D275A	βE-strand	Yes
T5	F285A/W286A	Box 3	Yes

[a] Predicted interactive site of TLR4 (see Ref. 15).
[b] Similar to TLR4 P712H mutation in C3H/HeJ mice *Lps*^{d} allele (see Ref. 14).

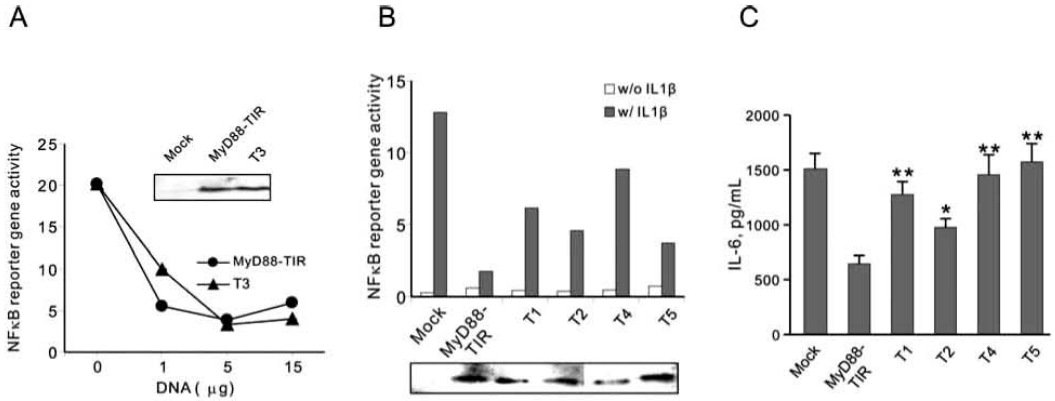

FIG. 4. **Functional analysis of MyD88-TIR domain mutants tested in NFκB reporter gene activity (*A* and *B*) and cytokine IL6 production (*C*) assays.** *A*, concentration-dependent inhibition of NFκB reporter gene activity by wild-type and T3 mutant (P200H). *B*, inhibition of NFκB reporter gene activity by mutants T1, T2, T4, and T5. HEK 293T cells were transfected with MyD88-TIR or its mutant constructs (1–15 μg in *A* and 12.5 μg in *B*) together with NFκB-luc and RL-TK. After 24 h, IL1β was added at concentration of 10 ng/ml for 6 h. Cells were harvested and split for both reporter assay and Western blotting. NFκB reporter gene activity was analyzed and normalized on the basis of RL-TK activity. The figure shown was a representative of three experiments. *Insets* in *A* and *B*, expression levels of TIR and TIR mutants as determined by Western blotting. *C*, inhibition of IL6 production by T1, T2, T4, and T5 mutants. MRC-5 cells were transiently transfected with TIR mutants and stimulated with 10 ng/ml IL1β for 6 h. IL6 production was analyzed with cytometric bead array as described under "Experimental Procedures." Data represent combined results from three independent experiments done in triplicate. *Error bars* indicate the S.E. **, $p < 0.01$; *, $p < 0.05$, by two-sided Student's *t* test.

reduced or undetectable, presumably due to misfolding and/or degradation. The mutants listed in Table I were screened for potential inhibitory effect on NFκB reporter gene activation following stimulation with IL1β.

Of particular significance is the result with the P200H mutant (T3), analogous to the Pro/His mutation in TLR4, which is responsible for the LPS hyporesponsiveness of C3H/HeJ mice (14). Similar loss of signaling in other TIR-containing molecules such as MAL/TIRAP (25) and IL1RAcP (26, 27) has been reported, indicating that the invariant proline in the BB loop of Box 2 in these molecules is one of the interactive sites for other TIR domain-containing proteins. In striking contrast, a similar mutation (P200H) in MyD88 TIR domain, tested within a range of input concentrations, did not change the dominant negative effect of MyD88 TIR on IL1β-induced NFκB reporter gene activation in 293T cells (Fig. 4*A*). These cells showed a similar level of expression of wild-type and mutant proteins (Fig. 4*B*, *inset*). This result is consistent with recent modeling studies of the interaction of MyD88 with TLR2 and TLR4 (15), which suggested that the highly conserved proline residue may not participate in the protein-protein interactions of MyD88 with TLRs.

In contrast to the canonical P200H mutation, the following mutants displayed >2.5-fold loss of the dominant negative effect on IL1β-stimulated NFκB reporter gene activation as compared with the wild-type MyD88 TIR domain (Fig. 4*B*): D171A in helix αA (T1), triple mutant D195A/R196A/D197A (T2) in Box 2, D275A in βE-strand (T4), and double mutant F285A/W286A (T5) in Box 3. The result with the F285A/W286A mutant is consistent with the loss of inhibition displayed by Box 3-deleted MyD88 TIR domain (Fig. 3*B*). All these mutants and the wild-type MyD88 TIR domain were expressed at a comparable level in HEK 293T cells (Fig. 4*B*, *inset*).

These mutants were chosen for further validation of the functional significance of mutated MyD88 TIR domain residues. We selected IL1β-induced expression of an endogenous gene that encodes inflammatory cytokine, IL6, in human fibroblast MRC-5 cells for testing MyD88 TIR domain mutants. The expression of the IL6 gene is regulated by NFκB, and its mobilization by IL1β is dependent on MyD88 (1–3). Upon stimulation of MRC-5 cells with IL1β, an inflammatory cytokine, IL6, was expressed. This expression of endogenous IL6 gene was suppressed 2.5-fold by the dominant negative TIR domain of MyD88 (Fig. 4*C*). The observed degree of inhibition of endogenous IL6 gene expression is smaller than suppression of NFκB reporter gene activity by the MyD88 TIR domain in HEK 293T cells, most likely due to the lower transfection efficiency of MRC-5 cells, which minimizes the impact of potential inhibitors on IL6 expression. Nevertheless, inhibition of IL1β-induced IL6 production was dependent on residues Asp^{171}, Asp^{275}, $Asp^{196}/Arg^{196}/Asp^{197}$ and Phe^{285}/Trp^{286} because alanine substitutions reduced the dominant negative effect of wild-type MyD88 TIR domain. These functional studies of IL1β-induced IL6 production are consistent with NFκB-dependent reporter gene activation (Fig. 4*B*). Thus, our first series of mutagenesis experiments identified interactive sites within the MyD88 TIR domain responsible for coupling IL1β signaling to NFκB translocation to the nucleus and induction of endogenous IL6 gene.

Mutagenesis of Full-length MyD88 Reveals an Interactive Site for Direct Contact with IL1RAcP—It is still unknown which of the interactive sites identified in the MyD88 TIR domain are responsible for direct contact of MyD88 with the IL1 receptor complex subunit, IL1RAcP, which is indispensable for IL1β signaling (26). Alternatively, these interactive sites within MyD88 could participate in IL1β-induced oligomerization of MyD88 through homotypic interactions mediated by its TIR domain.

To sort out these possibilities, a second series of mutagenesis experiments was conducted. Five selected mutations were engineered in full-length MyD88 to allow a comparative analysis of its direct interaction with IL1RAcP (Table II). HEK 293T cells were co-transfected with Myc-IL1RAcP and AU1-MyD88 or its mutant constructs. We used immunoprecipitation followed by Western blotting to assess the effect of mutated residues on the receptor TIR- adaptor TIR interaction. As demonstrated in Fig. 5, only MyD88 D195A/R196A/D197A mutant showed loss of binding to IL1RAcP, whereas other mutants, including MyD88 P200H, retained their ability to bind IL1RAcP. This selective loss of receptor binding function by the MyD88 D195A/R196A/D197A mutant led us to develop the

TABLE II
Information about the MyD88 mutants analyzed in this study
All the MyD88 mutants in this study were generated as indicated under "Experimental Procedures."

Mutant	Mutation(s)
M1	MyD88-D171A
M2	MyD88-P200H
M3	MyD88-D195A/R196A/D197A
M4	MyD88-D275A
M5	MyD88-F285A/W286A

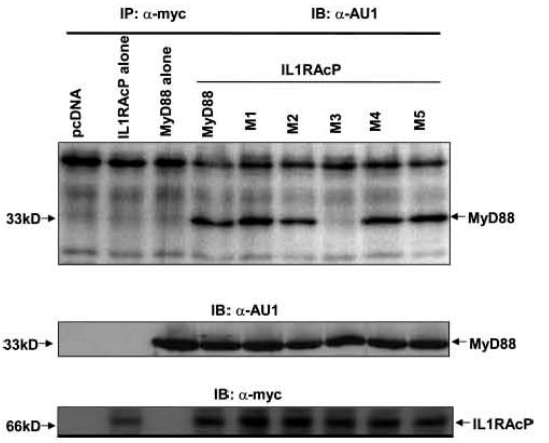

FIG. 5. **Interaction of MyD88 mutants with IL1RAcP.** HEK 293T cells were transiently transfected with Myc-IL1RAcP (10 μg) and full-length MyD88 or its mutants (10 μg). After 24 h, the cells were stimulated with 100 ng/ml IL1β for 5 min, harvested, and immunoprecipitated as described under "Experimental Procedures." Protein samples bound to anti-Myc antibody protein A beads were subjected to SDS-PAGE, and the immunoprecipitated MyD88 or its mutants were monitored by immunoblotting with anti-AU1 antibody (*top panel*). Expression of MyD88 and its mutants (*middle panel*) and IL1RAcP (*bottom panel*) was analyzed by immunoblotting.

three-dimensional docking model of MyD88 and IL1RAcP and verify the strategic position of these three residues as a main interactive site on the surface of the MyD88 TIR domain for its binding to the TIR domain of IL1RAcP.

The Development of the Three-dimensional Docking Model of MyD88-IL1RAcP Interaction—The three-dimensional docking model (Fig. 6) was developed by optimized superposition of two mutually interacting TIR domains of MyD88 and IL1RAcP. The negatively charged side of MyD88 TIR (see Fig. 2*B*) was selected as a possible interface of the molecule. This side contains $Asp^{195}/Arg^{196}/Asp^{197}$ residues that are essential, on the basis of mutagenesis studies (Fig. 5), for MyD88-TIR heterotypic interaction with IL1RAcP-TIR. Then, a suitable positively charged site of IL1RAcP was selected to conduct the modeling computation process. This modeling was based on geometry optimization by energy minimization followed by molecular dynamic computation using the program SANDER (AMBER software package). Ribbon structure was developed with the DeepView program, whereas the molecular surface of associated proteins was determined by PSSHOW (SYBIL-Tripos software package). Separation surface indicates that there is no crossing of molecular surfaces, and the distance between them is within the range of 0.4–4.7 Å, whereas their topology is diverse and contains several deep pockets.

Development of this three-dimensional model allowed us to verify the contribution of the triplet of functionally important residues $Asp^{195}/Arg^{196}/Asp^{197}$ to the binding reaction with IL1RAcP TIR domain. An analysis of the tertiary structure of two TIR domains that participate in the docking model indicates that three mutated residues ($Asp^{195}/Arg^{196}/Asp^{197}$), which are responsible for a loss of MyD88 binding to IL1RAcP, are involved in the interaction with residues 527–534 of IL1RAcP previously identified to play a key role in the IL1β signaling pathway (26, 27). Thus, our study identified a complementary site on the MyD88 TIR domain that contributes to its interaction with the IL1RAcP TIR domain. We therefore postulate that the negatively charged "knob," partially composed of BB loop on the surface of the MyD88 TIR domain (Fig. 2*B*), fits into the positively charged lysine patch formed by residues 527, 530, and 532 of the IL1RAcP TIR domain previously identified by Radons *et al.* (26, 27) as essential for IL1β signaling.

Interactive Sites Involved in Oligomerization of MyD88 through Homotypic Interaction of Its TIR Domain—Following IL1β-induced interaction of IL1RAcP with MyD88, this adaptor oligomerizes and interacts with downstream signal transducers (2, 3, 7). Homotypic oligomerization of MyD88 due to its forced expression resulted in robust activation of NFκB reporter gene activity observed in the absence of IL1β stimulation. This receptor-independent effect of ectopically expressed MyD88 oligomers was abolished by co-transfected MyD88-TIR domain (data not shown). Therefore, we examined the direct interaction of full-length MyD88 co-expressed with MyD88 TIR domain or its mutants. We co-transfected HEK 293T cells with full-length MyD88 that contained c-Myc epitope tag along with the wild-type or mutated TIR domain that contained AU1 epitope tag. As demonstrated in Fig. 7, P200H mutant bound to full-length MyD88 to a similar extent as wild-type MyD88 TIR domain. However, mutations in Box 2 (D195A/R196A/D197A) and Box 3 (βE-strand D275A and F285A/W286A) caused a loss of binding to MyD88, suggesting that these mutated residues constitute the interactive sites for homotypic oligomerization of the MyD88 TIR domain. Thus, the interacting site in Box 2 composed of residues $Asp^{195}/Arg^{196}/Asp^{197}$ potentially has an additional function that may encroach on the ability of MyD88 to interact with IL1RAcP. However, in a cascade of signaling steps induced by IL1β, heterotypic interaction of IL1RAcP TIR domain with MyD88 TIR domain precedes oligomerization of MyD88. The latter depends on homotypic binding mediated by its TIR domain. Therefore, the interactive site in Box 3 is not likely to be involved in binding of MyD88 to IL1RAcP. Rather, this site participates in homotypic MyD88 oligomerization and possibly other transactions involving downstream signal transducers. This interpretation is consistent with the loss of inhibition of IL1β-induced signaling by the MyD88 TIR domain upon truncation of its carboxyl-terminal segment that contains Box 3.

Taken together, our results identify key residues in the MyD88 TIR domain that are responsible for its heterotypic interaction with IL1RAcP. In addition, we identified interactive sites for homotypic oligomerization of MyD88. These protein-protein interactions evoked by IL1β are essential for its signaling to the nucleus mediated by NFκB and other proinflammatory stress-responsive transcription factors. Mutations identified on the interacting surface of the MyD88 TIR domain are functionally important because they interfere with the induction of endogenous gene that encodes IL6. This inflammatory cytokine, along with IL1β, is responsible for cardinal signs of systemic inflammation: fever, leukocytosis, thrombocytosis, acute phase protein response, and tissue injury (1, 5). The development of the docking three-dimensional model of MyD88-IL1RAcP binding, in which a cluster of highly charged residues in Box 2 plays a key role, reaffirms their strategic role in contacting complementary site on IL1RAcP TIR domain. This site is composed of several positively

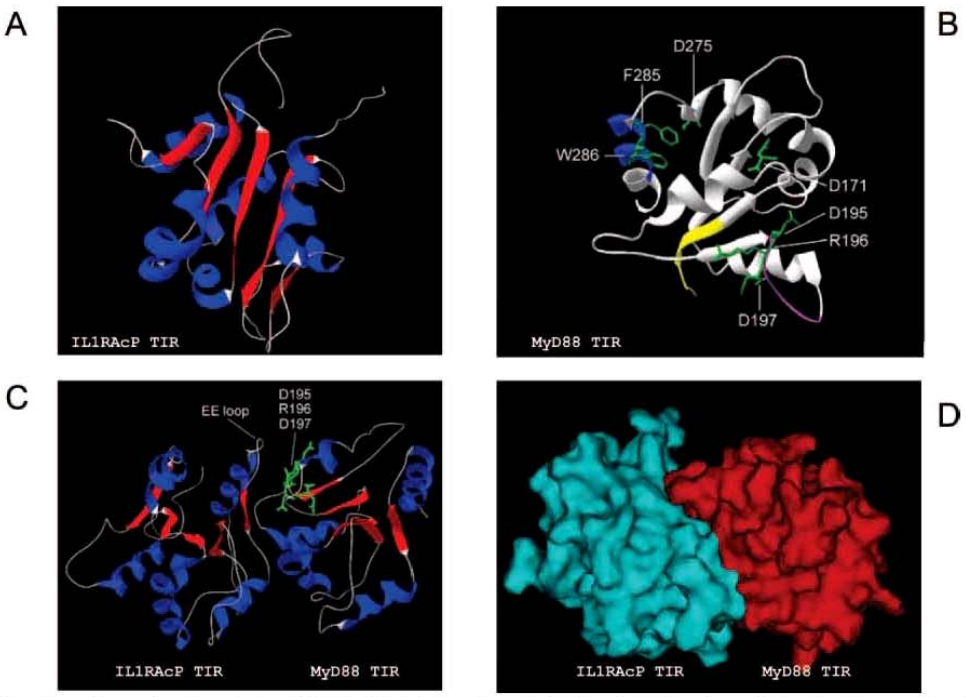

FIG. 6. **The three-dimensional models of IL1RAcP TIR domain and MyD88 TIR domain and the docking model of TIR-TIR interaction of MyD88 and IL1RAcP.** *A* and *B*, ribbon structure of IL1RAcP TIR domain and MyD88 TIR domain, respectively, obtained from homology computation performed using Swiss-Model and visualized using DeepView (Swiss-PdbViewer). Structural features representing the conserved boxes of the MyD88 TIR domain are shown in *B* in *yellow* (Box 1), *purple* (Box 2), and *blue* (Box 3). The selected side chains of mutated residues in *B* and *C* are marked in *green*. *C*, ribbon representation of TIR-TIR interaction optimized with SANDER energy minimization software (AMBER package). The side chains of identified residues (Asp^{195}, Arg^{196}, and Asp^{197}) required for direct binding of MyD88 TIR to IL1RAcP TIR are shown in *green*. The structural motifs in *A* and *C* are colored as follows: *blue*, α-helices; *red*, β-strands; and *white*, loops. *D*, top view of docking superposition presented in molecular surface mode.

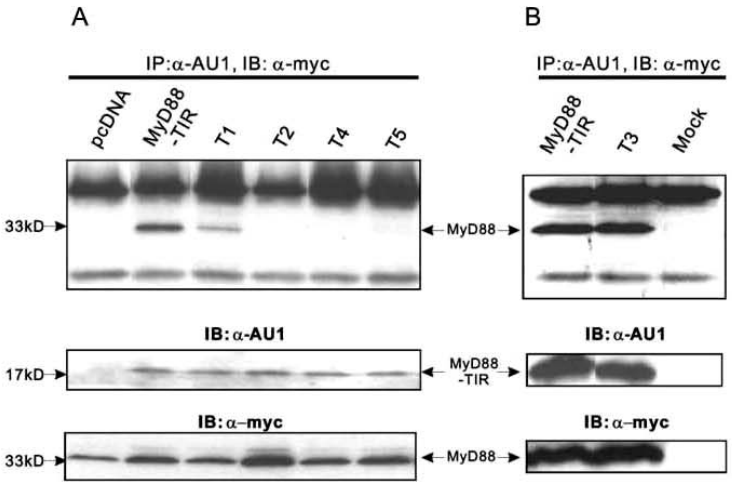

FIG. 7. **Homotypic interaction of the TIR domain of MyD88 with full-length MyD88.** The HEK 293T cells were transiently transfected with c-Myc-tagged full-length MyD88 (5 μg) and AU1-tagged MyD88-TIR (5 μg) or AU1-tagged MyD88-TIR mutants (5 μg). After 24 h, the cells were harvested and immunoprecipitated as described under "Experimental Procedures." Protein samples bound to anti-AU1 antibody protein A beads were subjected to SDS-PAGE and immunoprecipitated. MyD88-TIR or MyD88-TIR mutants were detected with anti-c-Myc antibody (*top panel*). Expression of MyD88-TIR and MyD88-TIR mutants (*middle panel*) or MyD88 (*bottom panel*) was analyzed by immunoblotting.

charged residues identified previously in EE loop residues 527–534 (26, 27). Thus, it is not surprising that the invariant Pro^{200} is inconsequential for MyD88-ILRAcP interaction. However, canonical mutation of the invariant proline to histidine in TLR4, which abolishes its signaling by LPS (14), indicates that different ligands and their cognate TLRs utilize MyD88 in a structurally distinct way. In addition to TLR4, a proline to histidine mutation attenuated signaling mediated by TLR2, MAL, and IL1RAcP (14, 25, 26). We interpret the latter result as indicative of invariant proline playing a significant role in reshaping the EE loop in IL1RAcP or in interactions with the TIR domain of IL1RI or with signaling molecules other than MyD88.

In summary, our data indicate that following stimulation with IL1β, the MyD88 TIR domain binds to the IL1RAcP TIR domain via a highly charged interactive site composed of residues 195–197 within the BB loop of Box 2. We postulate, on the

basis of the three-dimensional docking model developed herein, that this interactive site is complementary to the previously identified site composed of residues 527–534 within the EE loop of the IL1RAcP TIR domain (26, 27). Despite its proximity to the interactive site, invariant Pro^{200} of the MyD88 TIR domain does not play a role in IL1β-induced signaling. However, residues located in Box 3 are essential for subsequent homotypic interaction of MyD88 TIR domain. In a broader context, the results suggest that the IL1β signaling pathway differs from other ligand-initiated TLR intracellular signaling by usage of distinct structural motifs within the MyD88 TIR domain. Further mapping of the MyD88 surface will expand our understanding of its role in integrating signals derived from a variety of Toll-like receptors.

Acknowledgments—We thank Dean Ballard for critical reading of the manuscript, Jarrod Smith for experimental advice, and Ana Maria Hernandez for assistance in the preparation of the manuscript.

REFERENCES

1. Dinarello, C. A. (2002) *Clin. Exp. Rheumatol.* **20,** Suppl. 27, S1–S13
2. Yamamoto, M., Takeda, K., and Akira, S. (2004) *Mol. Immunol.* **40,** 861–868
3. Akira, S., and Sato, S. (2003) *Scand. J. Infect. Dis.* **35,** 555–562
4. Vannier, E., and Dinarello, C. A. (1994) *J. Biol. Chem.* **269,** 9952–9956
5. Dinarello, C. A. (1996) *Blood* **87,** 2095–2147
6. McGettrick, A. F., and O'Neill, L. A. (2004) *Mol. Immunol.* **41,** 577–582
7. Akira, S. (2003) *J. Biol. Chem.* **278,** 38105–38108
8. Wesche, H., Henzel, W. J., Shillinglaw, W., Li, S., and Cao, Z. (1997) *Immunity* **7,** 837–847
9. Wesche, H., Korherr, C., Kracht, M., Falk, W., Resch, K., and Martin, M. U. (1997) *J. Biol. Chem.* **272,** 7727–7731
10. Huang, J., Gao, X., Li, S., and Cao, Z. (1997) *Proc. Natl. Acad. Sci. U. S. A.* **94,** 12829–12832
11. Volpe, F., Clatworthy, J., Kaptein, A., Maschera, B., Griffin, A. M., and Ray, K. (1997) *FEBS Lett.* **419,** 41–44
12. Li, S., Strelow, A., Fontana, E. J., and Wesche, H. (2002) *Proc. Natl. Acad. Sci. U. S. A.* **99,** 5567–5572
13. Kobayashi, K., Hernandez, L. D., Galan, J. E., Janeway, C. A., Jr., Medzhitov, R., and Flavell, R. A. (2002) *Cell* **110,** 191–202
14. Poltorak, A., He, X., Smirnova, I., Liu, M. Y., Van Huffel, C., Du, X., Birdwell, D., Alejos, E., Silva, M., Galanos, C., Freudenberg, M., Ricciardi-Castagnoli, P., Layton, B., and Beutler, B. (1998) *Science* **282,** 2085–2088
15. Dunne, A., Ejdeback, M., Ludidi, P. L., O'Neill, L. A., and Gay, N. J. (2003) *J. Biol. Chem.* **278,** 41443–41451
16. Muzio, M., Ni, J., Feng, P., and Dixit, V. M. (1997) *Science* **278,** 1612–1615
17. Kunkel, T. A. (1985) *Proc. Natl. Acad. Sci. U. S. A.* **82,** 488–492
18. Lin, Y. Z., Yao, S. Y., Veach, R. A., Torgerson, T. R., and Hawiger, J. (1995) *J. Biol. Chem.* **270,** 14255–14258
19. Schwede, T., Kopp, J., Guex, N., and Peitsch, M. C. (2003) *Nucleic Acids Res.* **31,** 3381–3385
20. Guex, N., and Peitsch, M. C. (1997) *Electrophoresis* **18,** 2714–2723
21. Xu, Y., Tao, X., Shen, B., Horng, T., Medzhitov, R., Manley, J. L., and Tong, L. (2000) *Nature* **408,** 111–115
22. Tao, X., Xu, Y., Zheng, Y., Beg, A. A., and Tong, L. (2002) *Biochem. Biophys. Res. Commun.* **299,** 216–221
23. Burns, K., Martinon, F., Esslinger, C., Pahl, H., Schneider, P., Bodmer, J. L., Di Marco, F., French, L., and Tschopp, J. (1998) *J. Biol. Chem.* **273,** 12203–12209
24. Dupraz, P., Cottet, S., Hamburger, F., Dolci, W., Felley-Bosco, E., and Thorens, B. (2000) *J. Biol. Chem.* **275,** 37672–37678
25. Horng, T., Barton, G. M., and Medzhitov, R. (2001) *Nat. Immunol.* **2,** 835–841
26. Radons, J., Gabler, S., Wesche, H., Korherr, C., Hofmeister, R., and Falk, W. (2002) *J. Biol. Chem.* **277,** 16456–16463
27. Radons, J., Dove, S., Neumann, D., Altmann, R., Botzki, A., Martin, M. U., and Falk, W. (2003) *J. Biol. Chem.* **278,** 49145–49153

APPENDIX B

Liu, D., Li, C., Chen, Y., Burnett, C., Liu, XY., Downs, S., Collins, R.D., Hawiger, J. 2004

Nuclear import of proinflammatory transcription factors is required for massive liver apoptosis induced by bacterial lipopolysaccharide.

J Biol Chem. 279:48434-48442.

THE JOURNAL OF BIOLOGICAL CHEMISTRY
Vol. 279, No. 46, Issue of November 12, pp. 48434–48442, 2004
Printed in U.S.A.

Nuclear Import of Proinflammatory Transcription Factors Is Required for Massive Liver Apoptosis Induced by Bacterial Lipopolysaccharide*

Received for publication, June 28, 2004, and in revised form, August 24, 2004
Published, JBC Papers in Press, September 1, 2004, DOI 10.1074/jbc.M407190200

Danya Liu‡, Chunsheng Li‡, Yiliu Chen‡, Christie Burnett‡, Xue Yan Liu‡, Sheila Downs‡, Robert D. Collins§, and Jacek Hawiger‡¶

From the ‡Departments of Microbiology and Immunology and §Pathology, Vanderbilt University School of Medicine, Vanderbilt University Medical Center, Nashville, Tennessee 37232

Stimulation of macrophages with lipopolysaccharide (LPS) leads to the production of cytokines that elicit massive liver apoptosis. We investigated the *in vivo* role of stress-responsive transcription factors (SRTFs) in this process focusing on the precipitating events that are sensitive to a cell-permeant peptide inhibitor of SRTF nuclear import (cSN50). In the absence of cSN50, mice challenged with LPS displayed very early bursts of inflammatory cytokines/chemokines, tumor necrosis factor α (1 h), interleukin 6 (2 h), interleukin 1 β (2 h), and monocyte chemoattractant protein 1 (2 h). Activation of both initiator caspases 8 and 9 and effector caspase 3 was noted 4 h later when full-blown DNA fragmentation and chromatin condensation were first observed (6 h). At this time an increase of pro-apoptotic Bax gene expression was observed. It was preceded by a decrease of anti-apoptotic Bcl2 and $BclX_L$ gene transcripts. Massive apoptosis was accompanied by microvascular injury manifested by hemorrhagic necrosis and a precipitous drop in blood platelets observed at 6 h. An increase in fibrinogen/fibrin degradation products and a rise in plasminogen activator inhibitor 1 occurred between 4 and 6 h. Inhibition of SRTFs nuclear import with the cSN50 peptide abrogated all these changes and increased survival from 7 to 71%. Thus, the nuclear import of SRTFs induced by LPS is a prerequisite for activation of the genetic program that governs cytokines/chemokines production, liver apoptosis, microvascular injury, and death. These results should facilitate the rational design of drugs that protect the liver from inflammation-driven apoptosis.

Programmed cell death (apoptosis) is the major mechanism of embryonic development and remodeling of tissues and organs, homeostatic control of immune cells that recognize self and non-self antigens, and removal of virally infected cells (1). Apoptosis of hepatocytes may occur in fulminant hepatitis, an inflammatory process that is caused by viral and non-viral agents (2). For example, recent gene therapy approaches to correct an inborn error of metabolism led to fulminant liver failure (3). This inflammation-related complication of gene therapy impedes broader application of viral vectors (4, 5). The sequence of intracellular signaling events that underlie inflammation-driven development of ultimately fatal liver apoptosis remains incompletely understood.

Fulminant liver apoptosis has been studied in several animal models. These studies indicate that activation of T cells with concanavalin A (6) or with agonists that interact with T cell receptor such as staphylococcal enterotoxin B can lead to massive apoptosis (7, 8). Staphylococcal enterotoxin B-induced apoptosis occurs under conditions of metabolic stress imposed by 2-amino-2-deoxy-D-galactosamine (D-Gal).[1] Similarly, activation of macrophages with their Toll-like receptors (TLR) agonists, such as lipopolysaccharide (LPS, endotoxin), induces massive liver apoptosis when animals are treated with ethanol or D-Gal (9, 10). By reversibly depleting hepatic stores of uridine triphosphate (UTP), D-Gal sensitizes hepatocytes to the cytotoxic effects of tumor necrosis factor α (TNFα) (10, 11). Accordingly, massive liver apoptosis induced by a macrophage agonist, LPS, or a T cell agonist, staphylococcal enterotoxin B, in combination with a metabolic inhibitor, D-Gal, was abrogated in animals deficient in TNFα receptor 1 (TNFR-1) (12–14). These *in vivo* models of liver apoptosis offer an excellent way to study fulminant liver injury mediated by inflammatory cytokines because they provide a well defined and reliable end point, which is relevant to human disease states.

The genetic programs for inflammation and apoptosis are regulated by stress-responsive transcription factors (SRTFs) either alone or in various combinations (15). These SRTFs include nuclear factor κB (NFκB), nuclear factor of activated T cells, activator protein 1, and signal transducer and activator of transcription 1. In response to proinflammatory stimuli, SRTFs are translocated to the nucleus via a set of adaptor proteins known as importins/karyopherins α, which in tandem with their β subunit ferry the cargo to the nucleus (15, 16).

* This work was supported in part by United States Public Health Service, National Institutes of Health Grants HL69542, HL62356, HL68744, and DK54072. The use of core facilities in this study was supported by National Institutes of Health Grants 2P30 CA 68485 (to the Vanderbilt Ingram Cancer Center) and 5P30DK058404-03 (to the Vanderbilt Digestive Disease Research Center). The costs of publication of this article were defrayed in part by the payment of page charges. This article must therefore be hereby marked "*advertisement*" in accordance with 18 U.S.C. Section 1734 solely to indicate this fact.

¶ To whom correspondence should be addressed: Dept. of Microbiology and Immunology, Vanderbilt University School of Medicine, 1161 21st Ave. South, A-5321 MCN, Nashville, TN 37232-2363. Tel.: 615-343-8280; Fax: 615-343-8278; E-mail: jacek.hawiger@vanderbilt.edu.

[1] The abbreviations used are: D-Gal, 2-amino-2-deoxy-D-galactosamine; TLR, Toll-like receptors; LPS, lipopolysaccharide; TNFα, tumor necrosis factor α; TNFR-1, tumor necrosis factor α receptor 1; SRTF, stress-responsive transcription factors; NFκB, nuclear factor κB; cSN50, cyclized form of SN50 peptide carrying an NLS derived from NFκB1 (p50); SM, control peptide carrying a non-functional NLS mutation; RAW, murine macrophage cell line RAW 264.7; IL, interleukin; MCP-1, monocyte chemoattractant protein 1; ALT, alanine aminotransferase; AST, aspartate aminotransferase; FDP, fibrin degradation products; PAI-1, plasminogen activator inhibitor-1; TUNEL, TdT-dependent dUTP-biotin nick end labeling; ANOVA, analysis of variance; NLS, nuclear localization sequence.

Importin/karyopherin α2 (Rch1, KPNA2) is the target for a cell-permeant peptide-cyclized form of SN50 (cSN50), which prevents the nuclear import of SRTFs (17, 18). Here we report *in vivo* studies with cSN50 showing that this cell permeant peptide prevents liver apoptosis and death in a murine model of LPS toxicity. These findings demonstrate a key role for SRTFs in the development of fulminant liver injury induced by LPS and mediated by inflammatory cytokines and chemokines.

EXPERIMENTAL PROCEDURES

Peptide Synthesis and Purification—cSN50 and SM were synthesized, purified, filter-sterilized, and analyzed as described elsewhere (7, 18).

Maintenance and Treatment of Cell Line—Murine macrophage cell line RAW 264.7 (RAW) was obtained from the American Type Culture Collection (Manassas, VA; TIB-71). These cells were cultured in Dulbecco's modified Eagle's medium (Cellgro, VA) supplemented with 10% heat-inactivated fetal bovine serum containing no detectable LPS (<0.006 ng/ml as determined by the manufacturer, Atlanta Biological, Norcross, GA), 2 mM L-glutamine, 100 units/ml penicillin, and 100 μg/ml streptomycin. The viability of RAW cells was >80% in all experiments. RAW cells were placed in 96-well plates (200 μl/well at 2 × 10^6/ml) and treated with different concentrations of cSN50 and SM peptides (0, 5, 10, 30, and 50 μM) 30 min before stimulation by 2 ng/ml LPS from *Escherichia coli* 0127:B8 (Sigma). Each experimental sample was run in duplicate or triplicate. Cells were incubated for 6 h at 37 °C in 5% CO_2. Supernatant samples from the medium of RAW cells treated with LPS and/or peptide were collected and frozen at −80 °C until assayed for cytokine levels.

Animal Treatment Protocols—Female C57BL/6 mice (8–12 weeks old, ~20 g) were purchased from The Jackson Laboratory (Bar Harbor, ME). Mice were injected intraperitoneally with 1 μg of LPS (5 μg/ml, Sigma) and 20 mg of D-Gal (100 mg/ml, Sigma), both in pyrogen-free saline. Mice were randomly divided into two groups; diluent control, which received 5% dimethyl sulfoxide in sterile H_2O, or a treatment group that received the cSN50 peptide (0.7 mg in 200 μl of 5% dimethyl sulfoxide in sterile H_2O as diluent). The treatment group received seven intraperitoneal injections before (30 min) and after (30, 90, 150, and 210 min and 6 and 12 h) LPS and D-Gal challenge. However, the control group usually received five intraperitoneal injections of diluent because of the worsening condition of the animals and their rapid death. An additional group of 15 mice received the SM peptide (cell-permeant but functionally inactive analog of cSN50) in a dose of 2 mg given intraperitoneally before (30 min) and after (30, 90, 150, and 210 min). Due to the rapid demise of these mice, two additional injections at 6 and 12 h could not be administered. Animals were observed at hourly intervals for signs of acute toxicity (piloerection, ataxia, and the lack of reaction to cage motion) that herald imminent death. Inactive animals were euthanized. Animals without apparent signs of disease (survivors) were euthanized at 72 h after LPS and D-Gal. Some survivors were observed for an additional 7 days and then were euthanized. The blood samples from the saphenous vein were collected in heparinized tubes for plasma separation and in regular tubes for serum separation before and after LPS and D-Gal challenge at the indicated times. Some experimental animals were sacrificed at 2, 4, and 6 h for collection of organs. The liver was removed, and some pieces were frozen in liquid nitrogen and stored at −80 °C for caspase assay and RNA isolation. Other parts of the liver as well as other organs (spleen, kidney, lung, and heart) were immersed in 10% formalin for histologic analysis. Animal handling and experimental procedures were performed in accordance with the American Association of Accreditation of Laboratory Animal Care guidelines and approved by the Institutional Animal Care and Use Committee.

Cytokine Assays of Plasma and Cultured Cell Supernatants—Supernatant levels of TNFα, interleukin (IL)-1β, and IL-6 in cultured RAW cells and plasma levels of IL-1β were measured by enzyme-linked immunosorbent assay according to the manufacturer's instructions (ELISA, R&D Systems, Minneapolis, MN). TNFα and IL-6 in plasma, monocyte chemoattractant protein 1 (MCP-1) in plasma, and in cultured RAW cell supernatant were measured by a Cytometric Bead Array (BD Biosciences) according to the manufacturer's instructions (7, 19).

Measurement of Liver Enzymes—Activities of the liver enzymes alanine aminotransferase (ALT) and aspartate aminotransferase (AST) were measured in serum according to the modified manufacturer's instructions (Catachem Inc., Bridgeport, CT). Briefly, ALT or AST-working reagent and serum samples on ice were mixed at 12:1 ratio in cuvettes and then incubated in a 37 °C water bath for 5 min. After incubation, the decrease in absorbance at 340 nm was monitored at 1-min intervals for at least 5 min, and the decrease in absorbance per minute was calculated (ΔA). ALT or AST concentration (unit/liter) in samples was calculated using the formula, unit/liter = $\Delta A \times 1929$.

Caspase Assays—Caspase 3, 8, and 9 activities in liver tissue were measured using a Caspase-Glo assay kit (Promega) and modified protocol. Briefly, the proluminescent substrate containing the DEVD, LETD, or LEHD (sequences are in a single-letter amino acid code) is cleaved by caspase-3, caspase-8, and caspase-9, respectively. After caspase cleavage, a substrate for luciferase (aminoluciferin) is released; this results in the luciferase reaction and the production of luminescent signal. Cytosolic extracts from liver tissue were prepared by Dounce homogenization in hypotonic extraction buffer (25 mM HEPES, pH 7.5, 5 mM $MgCl_2$, 1 mM EGTA, 1 mM Pefablock, and 1 μg/ml each pepstatin, leupeptin, and aprotinin) and subsequently centrifuged (15 min, 13,000 rpm, 4 °C) (19). The protein concentration of supernatant was adjusted to 1 mg/ml with extraction buffer and stored at −80 °C. An equal volume of reagents and 10 μg/ml cytosolic protein were added to a white-walled 96-well plate and incubated at room temperature for 1 h. The luminescence of each sample was measured in a plate-reading luminometer.

RNA Preparation and cDNA Synthesis—Total RNA was extracted from frozen liver tissue with Versagene RNA tissue kit (Gentra Systems, Inc., Minneapolis, MN) and treated with DNase (Versagene DNase treatment kit, Gentra Systems, Inc.) following the manufacturer's instructions. The integrity of RNA preparations was assessed using a NanoDrop® ND-1000 spectrophotometer and agarose gel electrophoresis. First-strand cDNA was synthesized with a High Capacity cDNA Archive kit (Applied Biosystems, Foster City, CA). Briefly, 1 μg of total RNA was used as the template for synthesis of cDNA in a 50-μl reaction and incubated at 25 °C for 10 min followed by 37 °C for 120 min.

RNA Quantification with Specific Probes by Real-time PCR—Detection of mRNA expression levels by real-time PCR with a reporter probe has been established in amplification kinetics studies using reverse-transcribed transcripts as template (20, 21). RNA quantification of specific genes was performed using a TaqMan assay (Applied Biosystems). A probe for eukaryotic 18 S rRNA endogenous control (product 4319413E) was VIC/minor groove binder-labeled. The primers and FAM/minor groove binder-labeled probes for the following genes were purchased from ABI (TaqMan Assay-on-Demand): Bcl2 (assay ID Mm00477631_m1), $BclX_L$ (assay ID Mm00437783_m1), and Bax (assay ID Mm00432050_m1). Eukaryotic 18 S rRNA was used as an endogenous control in a multiplex PCR reaction with a primer/probe of the gene of interest. For each reaction, 2× TaqMan universal PCR master mix (Applied Biosystems), 900 nM primers, and 250 nM probes in 10 μl were added to 384-well plate. Real-time PCR and subsequent analysis were performed with the ABI Prism 7900HT sequence detection system (SDS v2.1) (Applied Biosystems) using the following conditions: 50 °C for 2 min, 95 °C for 10 min, and then 40 cycles of amplification (95 °C denaturation for 15 s, 60 °C annealing/extension for 1 min). All PCR reactions were performed in triplicate for each sample and were repeated three times.

Platelet Count, Detection of Fibrin Degradation Products (FDPs), and Plasminogen Activator Inhibitor 1 (PAI-1) Total Antigen—Heparinized fresh blood was diluted 1:60 in 1% ammonium oxalate (EM Science) and rocked for 20 min. The sample was added to hemacytometer, and after 20 min, platelets were counted. FDPs in serum were detected by staphylococcal clumping test as described elsewhere (22). Briefly, staphylococci (*Staphylococcus aureus* sp. *aureus* ATCC 25904) that express clumping factor were grown and processed to prepare a standardized smooth bacterial suspension for determining a clumping titer in serum samples. The clumping titer was expressed as a reciprocal of the highest dilution of tested serum giving a positive clumping reaction. PAI-1 total antigen in plasma was measured by an ELISA kit according to the manufacturer's instructions (Molecular Innovations, Inc., Southfield, MI).

Histology Analyses—Organ samples (liver, spleen, kidney, lung, and heart) were collected from mice showing typical signs of acute toxicity shortly before death or from surviving mice that were euthanized after 72 h or at the indicated times. Formalin-fixed, paraffin-embedded sections were stained with hematoxylin and eosin or periodic acid-Schiff and hematoxylin to assess injury and hemorrhage. Apoptosis of the liver was evaluated by characteristic cytologic changes and by TdT-dependent dUTP-biotin nick end-labeling (TUNEL) assay using the Apop Tag reagent (Intergen) according to the manufacturer's instructions.

Statistical Analysis—All experimental data except survival were expressed as the mean ± S.E. A one-way analysis of variance, a two-way

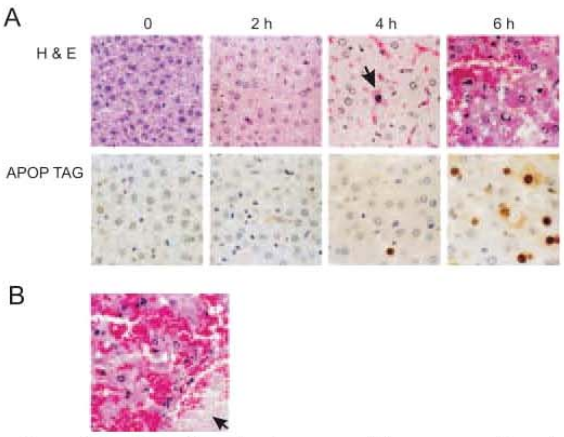

FIG. 1. **Time-dependent development of liver apoptosis and hemorrhagic necrosis.** *A*, liver sections from C57BL/6 mice injected with LPS and D-Gal and sacrificed at indicated times were stained with hematoxylin and eosin (*H & E*) or with Apop Tag (TUNEL assay). A single dying cell is seen at 4 h (*arrow*), whereas there is massive necrosis, hemorrhage, and apoptosis at 6 h. *B*, liver section at 6 h stained with hematoxylin and eosin shows aggregates of platelets within a blood vessel (*arrow*).

repeated measure analysis of variance, and Student's *t* test were used to determine the significance of the difference. A log rank test was used for analysis of survival.

RESULTS

In Vivo System for Studying Apoptosis in the Liver—Mice challenged with a high dose of LPS (40 mg/kg) do not manifest hepatocyte apoptosis despite excessive production of TNFα (18). This tolerance of hepatocytes to TNFα can be dramatically lowered by administering LPS (50 μg/kg) in combination with D-Gal (10, 23, 24), which leads to massive liver apoptosis. This striking shift in LPS toxicity led us to explore the mechanism of LPS action on the apoptotic process in sensitized mice. As shown in Fig. 1*A*, sequential analysis of liver apoptosis, manifest by DNA fragmentation detected by TUNEL assay and chromatin condensation, indicates the lack of major changes until 4 to 6 h after the administration of LPS and D-Gal. Concomitant with massive apoptosis, the livers displayed hemorrhagic necrosis at 6 h, an apparent consequence of a breakdown of endothelial integrity. This form of microvascular injury is presumably responsible for platelet thrombi as shown in Fig. 1*B*. Thus, the development of massive apoptosis of the liver is accompanied by hemorrhagic necrosis, a consequence of microvascular injury. The lack of DNA fragmentation and a paucity of other detectable changes in liver architecture during the first 4 h raise a series of questions about the dynamics of liver apoptosis induced by LPS. First, is this process regulated by nuclear import of SRTFs? Second, would blockade of nuclear import result in (*a*) cytoprotection against the leakage of liver enzymes, (*b*) suppression of initiator and effector caspases, (*c*) maintenance of the balance between the expression of anti-apoptotic and pro-apoptotic genes, and (*d*) prevention of hemorrhagic necrosis? To address these mechanistic questions, we performed time course studies and monitored markers of inflammation, hepatocyte dysfunction, apoptosis, and microvascular injury.

LPS-induced Expression of Inflammatory Cytokines and Chemokines in Murine Macrophages Depends on Nuclear Import of SRTFs—Macrophages comprise an estimated 20–40% of the liver cells in rats and mice and display TLR4, a receptor for LPS (23, 25, 26). In response to TLR4-generated signals, NFκB and other SRTFs are deployed to the nucleus, where they regulate a myriad of genes encoding mediators of inflammation and apoptosis (15). A cell-permeant nuclear import inhibitor, cSN50 peptide, was developed by us to suppress the deployment of SRTFs in the nucleus (18). This bipartite inhibitor contains a membrane-translocating motif, which allows rapid penetration of cell membrane, and a "cargo" comprised of a cyclized nuclear localization sequence (NLS) that enables this peptide to competitively inhibit cytoplasmic/nuclear import of NLS-containing SRTFs. To validate the dependence of LPS-induced inflammatory cytokines/chemokines production on nuclear import of SRTFs, we evaluated the potency of cSN50 peptide as compared with its mutated analog, SM peptide, in cultured murine macrophage RAW cells stimulated with LPS. As shown in Fig. 2, the cSN50 peptide in a range of concentrations from 5 to 50 μM significantly inhibited LPS-induced expression of inflammatory cytokines TNFα ($p < 0.0001$), IL-6 ($p < 0.0001$), IL-1β ($p < 0.0001$), and chemokine MCP-1 ($p < 0.0001$). In contrast, the cell-permeant SM peptide that contains mutated NLS as cargo was without effect on LPS-induced inflammatory cytokine/chemokine expression, attesting to the specificity of a nuclear import inhibitory sequence. Importantly, these two peptides, cSN50 and SM, did not affect the viability of LPS-stimulated RAW macrophages (>80% under these experimental conditions). These results extend our previous findings of inhibition of SRTF nuclear import in LPS-stimulated macrophages (18) to the concentration-dependent inhibition of inflammatory cytokine/chemokine expression.

Time Course of Inflammatory Cytokines and Chemokine Expression—We serially monitored the levels of inflammatory cytokines/chemokines in blood to investigate the sequence of events preceding massive apoptosis of the liver, which was not fully apparent until 6 h after administration of LPS and D-Gal (Fig. 1). As shown in Fig. 3, TNFα levels rose very rapidly in the circulation, reaching a peak in plasma at 1 h. Bursts of IL-6 and chemokine MCP-1 at 2 h followed a very early rise in TNFα. On the other hand IL-1β showed a more progressive rise in systemic levels. Administration of LPS alone induced similar response of inflammatory cytokines and chemokine, but D-Gal alone did not have a detectable effect on inflammatory cytokines and chemokine production *in vivo* (data not shown), thereby confirming the requirement for LPS to induce an inflammatory cytokine/chemokine response. This response was suppressed significantly by the cSN50 peptide, affirming the dependence of the *in vivo* production of inflammatory mediators on the nuclear import of SRTFs.

Time-dependent Induction of Enzyme Markers for Hepatocyte Injury—ALT and AST measured in serum provide an index of hepatocyte integrity. Leakage of ALT/AST into the extracellular compartment and a subsequent rise in serum reflect hepatocyte damage. These enzymes are significantly elevated in a number of conditions that cause liver injury including viral and bacterial infections, alcohol, and drug toxicity (27). As shown in Fig. 4, the serum ALT and AST activity increased rapidly during the first 4 h after administration of LPS and D-Gal and then dropped precipitously at 6 h. This drop most likely reflects liver failure (see Fig. 1). Significantly, the cSN50 peptide prevented the rise in liver enzymes ALT and AST. Thus, by suppressing expression of inflammatory mediators, a nuclear import inhibitor exerts a cytoprotective effect on liver cells in this model. Solo administration of LPS or D-Gal to the control groups of mice produced a moderate increase in serum ALT and AST levels with delayed peaks of activity at 8 and 24 h, respectively, and without massive apoptosis or reduced survival (data not shown).

Activation Kinetics of Initiator and Effector Caspases—Although the peak of TNFα required for activation of its cognate

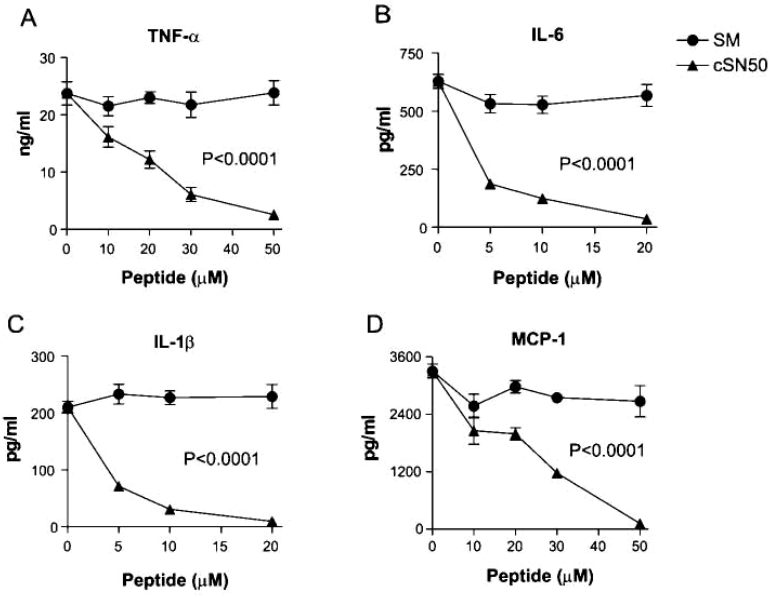

FIG. 2. **Nuclear import inhibitor, the cSN50 peptide, suppresses in a concentration-dependent manner inflammatory cytokine and chemokine expression in murine macrophage RAW cells induced by LPS.** cSN50 peptide (*triangles*) and mutant peptide SM (*circles*) were added to cells at different concentrations 30 min before the addition of LPS (2 ng/ml). Supernatant samples from the medium were collected after 6 h of culture and analyzed by ELISA for levels of cytokines TNFα (*A*), IL-6 (*B*), and IL-1β (*C*) or by Cytometric Bead Array for chemokine MCP-1 (*D*). *Error bars* in *panels A–D* indicate the ± S.E. of the mean value from three independent experiments. *p* values represent the significance of difference between the SM peptide and cSN50 peptide-treated groups (two-way ANOVA) as well as the cytokine level with or without cSN50 peptide (one-way ANOVA).

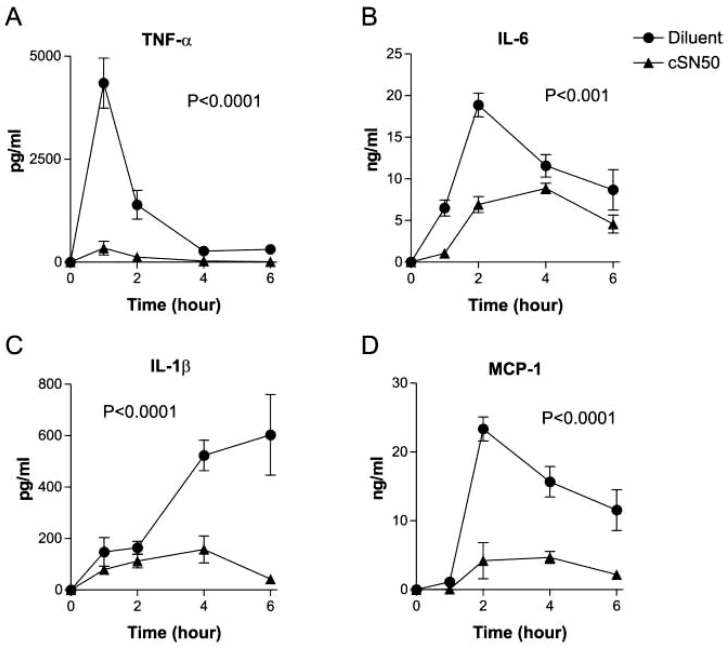

FIG. 3. **Time-dependent expression of inflammatory cytokines and a chemokine in control and cSN50 peptide-treated mice.** Wild-type C57BL/6 mice were treated with cSN50 peptide (0.7 mg in 200 μl of 5% dimethyl sulfoxide) or diluent (200 μl) in 7 intraperitoneal injections before (30 min) and after (30, 90, 150, and 210 min and 6 and 12 h) intraperitoneal administration of LPS with D-Gal. Blood plasma levels of cytokines TNFα (*A*), IL-6 (*B*), IL-1β (*C*), and chemokine MCP-1 (*D*) were measured in diluent controls (*circles*) and cSN50 peptide-treated animals (*triangles*) over the 6-h time period after LPS/D-Gal challenge. *Error bars* in *panels A–D* indicate the ± S.E. of the mean value in five mice that are represented by each data point. *p* values represent the significance of the difference between the control and the cSN50 peptide-treated groups (two-way ANOVA).

death receptor TNFR-1 occurs at 1 h, activation of initiator and effector caspases is observed much later. This family of intracellular aspartate-specific cysteine proteases exists as inactive proenzymes ("zymogens"). Caspase activation can be measured using specific substrates. Caspase 8 mediates TNFR-1-proximal events in cell death signaling. Caspase 9 is activated by cytochrome *c* released from mitochondria. Caspase 3 is dubbed DEVDase because it cleaves a DXXD motif, a substrate shared with caspase 7; it is an "executioner caspase," which can be activated directly by caspase 8 or by caspase 9 (28–32). Thus, a cascade of proteolytic events initiated by TNFα and mediated by caspases leads to nucleosomal DNA fragmentation and chromatin condensation as documented in Fig. 1. Despite a very early burst in TNFα production (see Fig. 3), the caspase cascade was considerably delayed. As shown in Fig. 5, the initiator caspases 8 and 9 were activated between 4 to 6 h in mice given LPS and D-Gal. Consistent with these findings, "effector" caspase 3 was not activated during the first 4 h. Caspase 3 (and caspase 7) showed a burst of proteolytic activity at 6 h. Thus, anti-apoptotic mechanisms significantly slowed death receptor signaling initiated by TNFα. Moreover, caspase activation was almost totally suppressed in the livers of mice treated with the cSN50 peptide. Thus, nuclear import of SRTFs is a rate-limiting step for initiation of pro-apoptotic signaling by TNFα and

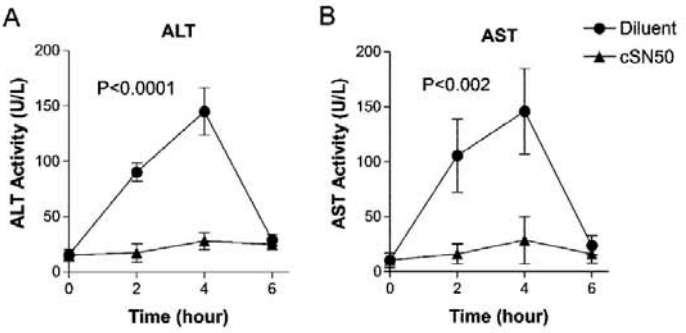

FIG. 4. **Time-dependent liver enzyme induction by LPS and D-Gal in control and cSN50 peptide-treated mice.** Wild-type C57BL/6 mice were treated with cSN50 peptide (0.7 mg) or diluent as indicated in Fig. 3 before and after intraperitoneal administration of LPS with D-Gal. Blood serum levels of ALT (*A*) and AST (*B*) were measured in diluent controls (*circles*) and cSN50 peptide-treated animals (*triangles*) over the 6-h time period after LPS/D-Gal challenge. *Error bars* indicate the ± S.E. of the mean value in five mice that are represented by each data point. *p* values represent the significance of the difference between the control and the cSN50 peptide-treated groups (two-way ANOVA). *U/L*, unit/liter.

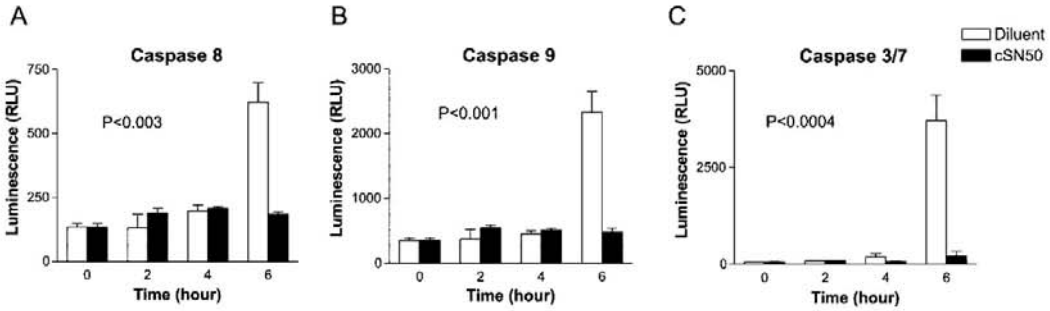

FIG. 5. **Time-dependent activation of initiator and effector caspases in control and cSN50 peptide-treated mice.** Wild-type C57BL/6 mice were treated with cSN50 peptide (0.7 mg in 200 μl of 5% dimethyl sulfoxide) or diluent before and after intraperitoneal administration of LPS with D-Gal according to the protocol described under "Experimental Procedures." Caspase activities in liver were measured in diluent controls (*open bar*) and cSN50 peptide-treated animals (*solid bar*). *Error bars* indicate the ± S.E. of the mean value in four mice that are represented by each data point. *p* values represent the significance of the difference between the control and the cSN50 peptide-treated groups (two-way ANOVA). *RLU*, relative light units.

other inflammatory cytokines in the LPS-induced model of liver apoptosis (10, 11, 24).

Alteration in the Balance between Gene Expression of Anti-apoptotic and Pro-apoptotic Proteins Induced by LPS and D-Gal—The observed delay in caspase activation could be due to the initial balance between anti-apoptotic Bcl2 family proteins *e.g.* Bcl2, $BclX_L$, and pro-apoptotic proteins, *e.g.* Bax, Bid. Such a balance is important for maintaining cell homeostasis (33, 34). Quantitative analysis of the liver transcripts of the pro-apoptotic gene *bax* indicated that its expression was significantly increased at 6 h after challenge with LPS and D-Gal (Fig. 6*A*). Conversely, expression of Bcl2 and $BclX_L$ was significantly decreased at 2 h (Fig. 6, *B* and *C*). Treatment with the cSN50 peptide suppressed the transcriptional activation of Bax gene and prevented the subsequent shift in balance of these transcripts that favors apoptosis.

Time-dependent Changes in Markers for Microvascular Injury—In this model of LPS-induced liver apoptosis the DNA fragmentation is demonstrated by 6 h along with extensive hemorrhagic necrosis of the liver (see Fig. 1*A*). Hemorrhage reflects a break in the integrity of microvascular endothelium associated with the formation of intravascular platelet thrombi (Fig. 1*B*). The mechanism of microvascular injury remains unexplained.

To sequentially analyze this process, we monitored circulating platelets. The platelet count demonstrated that its normal range is maintained during the first 4 h after administration of LPS and D-Gal (Fig. 7). However, a precipitous drop in circulating platelets occurred between 4 and 6 h. In tandem with platelet count, we measured FDP in murine serum by the staphylococcal clumping test that detects this marker of intravascular coagulation (22). FDP level was significantly increased at 4 and 6 h. For comparison, PAI-1, which promotes vascular thrombosis in mice (35), was significantly increased at 6 h. The mice injected with LPS alone ($n = 4$) or D-Gal alone ($n = 4$) did not show alterations in platelet count. In contrast, PAI-1 levels were elevated in LPS-challenged mice but not in those that received D-Gal alone (data not shown). Thus, these markers of microvascular injury peak at 6 h when there is histologic evidence of massive apoptosis of the liver and widespread hemorrhagic necrosis in response to LPS and D-Gal (Fig. 1, *A* and *B*). More importantly, these markers of microvascular injury were significantly suppressed when mice were treated with the cSN50 peptide, further indicating the overall dependence of this process on the nuclear import of proinflammatory SRTFs.

Massive Apoptosis of the Liver and Survival of the Mice Are Dependent on Nuclear Import of SRTFs—A combination of LPS and D-Gal in this model leads to death with massive apoptosis and hemorrhagic necrosis of the liver. As documented in Fig. 8, control mice treated with diluent showed characteristic progressive signs of sickness resulting in the early death of 26 of the 28 mice within 6–12 h. In contrast, the administration of the cSN50 peptide produced a dramatically protective effect. Twenty of 28 mice recovered fully from LPS/D-Gal challenge and survived at least 72 h. Thus, the cSN50 peptide increased survival from 7 to 71%. Based on the log rank test, the difference in the survival rate between cSN50 peptide-treated mice and the control mice was statistically significant ($p < 0.0001$). Another group of 15 mice, which were treated with the SM peptide (twice the cumulative dose level of cSN50), showed rapid signs of LPS/D-Gal toxicity and died within 6–12 h (results not shown). These control experiments with the SM peptide containing a mutated NLS confirm the essential role of

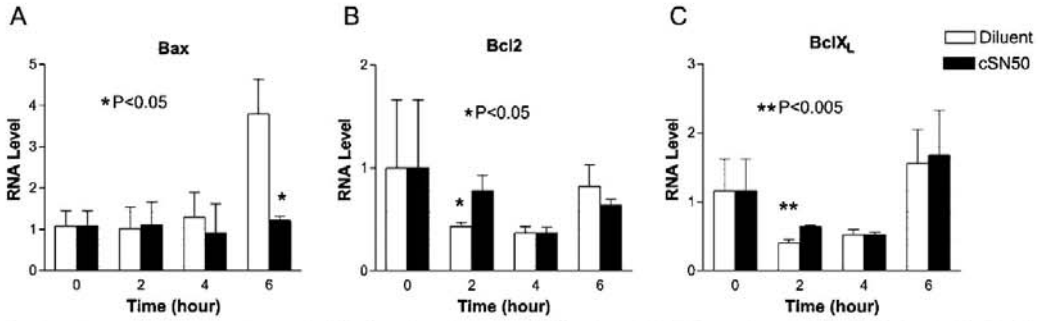

FIG. 6. **Gene expression of pro-apoptotic (*Bax*) and anti-apoptotic (*Bcl2* and *BclX$_L$*) members of the Bcl2 family in the livers of control and cSN50 peptide treated mice.** Wild-type C57BL/6 mice were treated with cSN50 peptide (0.7 mg in 200 μl of 5% dimethyl sulfoxide) or diluent before and after intraperitoneal administration of LPS with D-Gal according to the protocol described under "Experimental Procedures." Bax (*A*), Bcl2 (*B*) and BclX$_L$ (*C*) mRNA levels in liver were measured using real-time PCR. The relative expression of each mRNA compared with 18 S rRNA was calculated according to the equation ($\Delta Ct = Ct_{target} - Ct_{18\,S\,rRNA}$. The relative amount of target mRNA in control (*open bar*) and cSN50 peptide-treated animals (*solid bar*) was expressed as $2^{-(\Delta\Delta Ct)}$, where $\Delta\Delta Ct_{treatment} = \Delta Ct_{treatment} - \Delta Ct_{control}$. *Error bars* indicate the ± S.E. of the mean value in four mice that are represented by each data point. *p* values represent the significance of the difference between the control and the cSN50 peptide-treated groups (Student's *t* test).

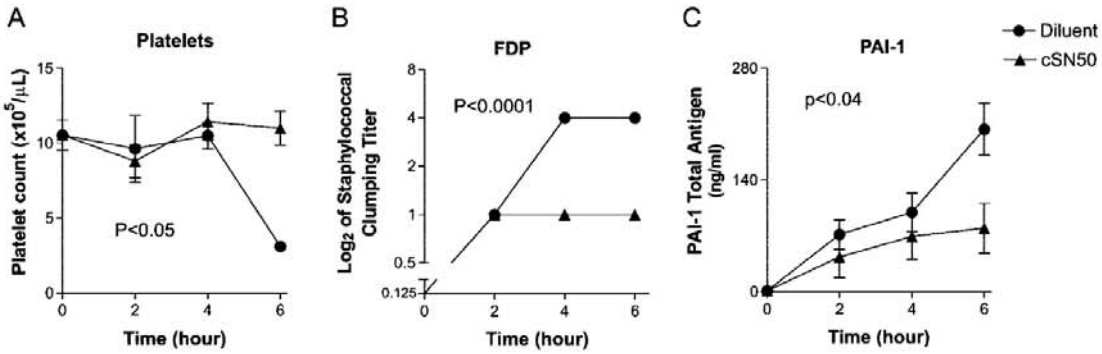

FIG. 7. **Time-dependent changes in the markers of microvascular injury in control and cSN50 peptide-treated mice.** Wild-type C57BL/6 mice were treated with diluent (*circles*) or cSN50 peptide (*triangles*) as indicated in Fig. 3 before and after intraperitoneal administration of LPS with D-Gal. Platelet count (*A*) was performed manually, and FDP levels in serum were measured by the staphylococcal clumping test in which the clumping titer was expressed as a reciprocal of the highest dilution of tested serum giving a positive clumping reaction (*B*). PAI-1 total antigen (*C*) in plasma was measured by ELISA. *Error bars* indicate the ± S.E. of the mean value in four mice/group (*A* and *B*) or 9 mice/group (*C*) that are represented by each data point. *p* values represent the significance of the difference between the control and the cSN50 peptide-treated groups (two-way ANOVA).

this sequence in nuclear import blockade achieved with cSN50. Mice that received either LPS (1 μg) alone (n = 5) or D-Gal (20 mg) alone (n = 10) did not show signs of sickness and survived (data not shown). These survival data correlated with suppression of apoptotic injury and hemorrhagic necrosis of the liver (Fig. 8*B*). Non-survivors exhibited severe liver injury characterized by extensive apoptosis and hemorrhagic necrosis. In contrast, the mice that were treated with the cSN50 peptide and survived showed normal tissue architecture with normal content of periodic acid-Schiff-positive material (*e.g.* glycogen) and without signs of apoptosis. Thus, a nuclear import inhibitor in this model prevents the entire process of massive liver apoptosis and microvascular injury induced by LPS.

DISCUSSION

This study demonstrated that blocking nuclear import of proinflammatory SRTFs counteracts a full-blown apoptosis and necrosis of the liver and has a death-sparing effect in this LPS-induced and macrophage-mediated model of fulminant liver failure. The SRTFs signaling network is an attractive target for therapeutic intervention in this context because a nuclear import inhibitor administered parenterally significantly offsets the hepatotoxicity of LPS. These new results expand the previous findings obtained in a different model of staphylococcal enterotoxin B-induced and T cell-based fatal liver injury (7). We have now demonstrated the beneficial effects of SRTF nuclear import blockade in two diverse models of liver injury. These highly reproducible models allow experimental study of an important biologic process. inflammation-associated apoptosis. Moreover, these models broaden our understanding of inflammation-driven liver apoptosis, which constitutes a life-threatening disease mechanism of increasing incidence. Among an estimated 2 billion cases of viral hepatitis worldwide, ~20 million will develop fulminant liver failure associated with apoptosis (6). Similarly, scores of alcoholic liver disease cases can be complicated by concomitant infection/inflammation-driven and TNFα-mediated apoptotic liver injury (36–38). The need for new therapeutic approaches to protect the liver from these devastating complications is apparent. Targeting nuclear import of proinflammatory SRTFs comprises one of the potential approaches to the control of inflammation-driven liver apoptosis.

The following lines of evidence establish the essential role of nuclear import of SRTFs in development of massive apoptosis and microvascular injury of the liver. (i) TNFα, a key inflammatory cytokine responsible for development of liver apoptosis (11, 24) was suppressed by our inhibitor of nuclear import of

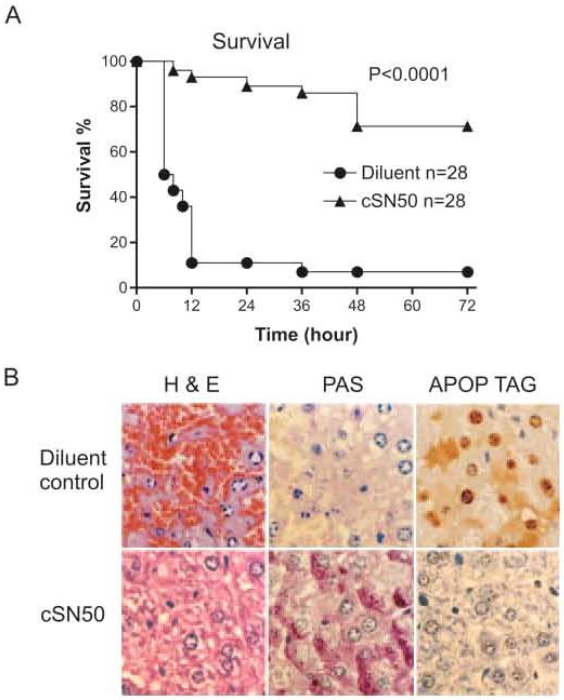

FIG. 8. **Survival and liver apoptosis accompanied by hemorrhagic necrosis in control mice as compared with the cSN50 peptide-treated mice.** *A*, survival of wild-type C57BL/6 mice challenged with LPS and D-Gal that were treated with cSN50 peptide (*triangles*) or diluent (*circles*) as indicated in Fig. 3. *p* values represent the significance of the difference between the control and the cSN50 peptide-treated groups. *B*, liver sections stained with hematoxylin and eosin (*H & E*), periodic acid-Schiff (*PAS*), or with Apop Tag (TUNEL assay). Note the hallmarks of acute liver injury (apoptosis, hepatocyte necrosis, and erythrocyte extravasation) in diluent controls and preserved liver architecture without apoptosis and hemorrhagic necrosis in cSN50 peptide-treated mice. Histologic examination of survivors observed for 10 days showed no lesions (not shown). Mice receiving either D-Gal alone (n = 10) or LPS alone (n = 5) survived and after 3 days of observation showed no evidence of liver injury (not shown).

SRTFs, (ii) other inflammatory cytokines (IL-6 and IL-1β) and the chemokine MCP-1 were also suppressed, indicating a broad spectrum of inhibition of these inflammatory mediators by cSN50 peptide in contrast to the inactive SM peptide containing mutated NLS, (iii) suppression of inflammatory mediators was accompanied by a cytoprotective effect on hepatocytes reflected by normal level of ALT and AST in serum of animals treated with cSN50, (iv) initiator and effector caspases were suppressed, and a balance between anti-apoptotic and pro-apoptotic gene transcripts was maintained, (v) DNA fragmentation in the liver cells was averted, (vi) microvascular injury was prevented, and (vii) survival of mice that were treated with cSN50, an inhibitor of SRTFs nuclear import, was significantly improved. In contrast to non-survivors that usually died within the first 12 h after administration of LPS and D-Gal, the surviving animals lived at least 3 days and did not display histologic evidence of liver injury. The lack of signs of liver and other organ injury in mice that received a nuclear import inhibitor persisted for at least a week when observation was extended. Thus, inhibition of nuclear import of SRTFs affords a lasting protection from highly deleterious effects of LPS and D-Gal that induce fulminant liver injury. The cSN50 peptide is rapidly (~20 min) distributed within mouse blood cells and organs after an intraperitoneal injection (18). However, further studies will be required to determine the pharmacokinetics, long-term toxicity, and therapeutic efficacy of this new class of nuclear import peptide inhibitors.

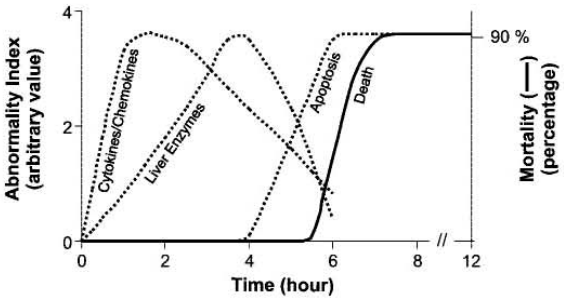

FIG. 9. **Schematic depiction of time course of cytokine/chemokine activation, hepatocyte injury as indicated by release of liver enzymes, apoptosis, and death in this model of LPS-induced liver injury.** *Abnormality index* represents the -fold increase in parameter studied.

As depicted in Fig. 9, sequential analysis of the events leading to death due to LPS-induced fulminant liver injury indicates a lag phase of at least 4 h before activation of initiator and effector caspases was detected in the liver. During this lag phase the production and action of TNFα and other mediators of inflammation depend on signaling to the nucleus in LPS-responsive cells that encompass liver macrophages (Kupffer cells) (25). This LPS-induced signaling depends on expression of TLR4 because TLR4-deficient C3H/HeJ mice escape massive apoptosis (24). Moreover, there is a requirement for metabolic changes; without the depleting action of D-Gal on UTP in hepatocytes, LPS is unable to induce massive apoptosis despite a robust burst in TNFα (18). When administered alone, LPS is responsible for a rise in TNFα and other cytokines. Neither LPS nor D-Gal administered alone induces massive apoptosis of the liver and death (10). Thus, development of fulminant apoptosis requires a combination of transient hepatocyte metabolic dysfunction and the burst of inflammatory cytokines to overcome anti-apoptotic defenses of the liver.

The experimental model employed in this study depends upon cross-talk between macrophages and hepatocytes as schematically depicted in Fig. 10. Macrophages respond to LPS via TLR-4 and produce TNFα along with other mediators of inflammation in a SRTFs nuclear import-dependent manner. Apparently, TNFα via its "death" receptor (TNFR-1) evokes a different pro-apoptotic signaling in a hepatocyte that is metabolically altered by D-Gal. The primary effect of D-Gal is its capacity to lower the level of UTP in hepatocytes (10, 24). A cascade of initiator and effector caspases is activated in hepatocytes and ultimately leads to the execution of a program of DNA fragmentation and chromatin condensation. Sequential analysis of pro-apoptotic and anti-apoptotic genes expression in the liver indicates that in this model of fulminant liver injury there is an early block in transcription of anti-apoptotic genes, Bcl2 and $BclX_L$, before pro-apoptotic gene Bax is transcriptionally activated (Fig. 6). The Bax expression between 4 and 6 h coincided with activation of initiator caspases 8 and 9 (Fig. 7). Activation of caspase 8 reflects signaling by death receptors represented by TNFR-1. Activation of caspase 9 indicates that changes in mitochondrial integrity have occurred. Such changes are usually due to a rise in intracellular Ca^{2+}, generation of reactive oxygen species, ceramide, and pro-apoptotic protein Bax (39, 40). These changes destabilize mitochondria and lead to the release of cytochrome *c*. Although we detected occasional DNA fragmentation in the liver using a TUNEL assay at 4 h, the most dramatic changes were observed at 6 h

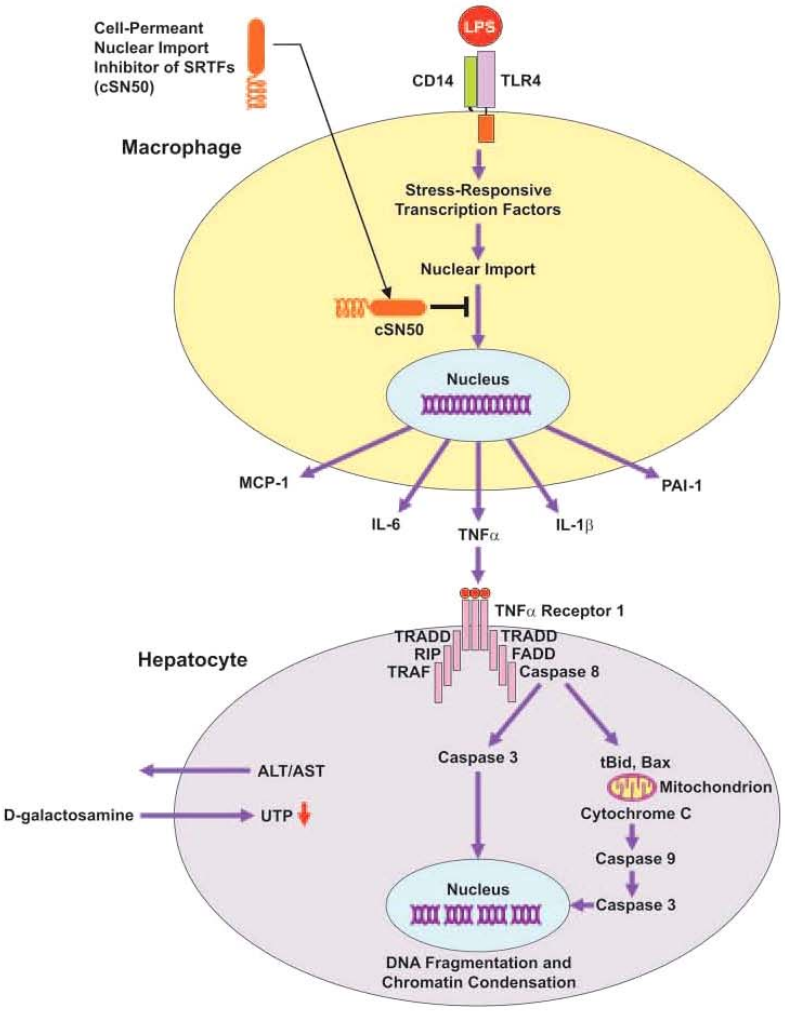

FIG. 10. **Diagrammatic representation of the cross talk of macrophages and hepatocytes during LPS-induced liver apoptosis.** LPS interaction with Toll-like receptor 4 (*TLR-4*), which is associated with CD14, evokes in macrophages a cascade of signaling events leading to nuclear import of SRTF. As a consequence, genes that encode inflammatory cytokines and chemokine are activated (Figs. 2 and 3). Expressed TNFα interacts with its cognate death receptor TNFR-1, which triggers a cascade of initiator and executioner caspases in D-Gal-sensitized hepatocytes, which have a depleted supply of UTP (Fig. 5). The DNA fragmentation ensues. The cSN50 peptide blocks the nuclear import of SRTFs and prevents the activation of genes that encode inflammatory cytokines/chemokines and PAI-1. See "Discussion" for details. *FADD*, FAS (TNFRSF6)-associated death domain protein. *TRADD*, TNFRSF1A-associated via death domain. *TRAF*, TNF receptor-associated factor. *tBid*, truncated BH3-interacting domain death agonist. *RIP*, receptor (TNFRSF)-interacting serine-threonine kinase 1.

(Fig. 1*A*). Thus, pro-apoptotic signaling induced by TNFα in D-Gal-sensitized liver cells requires at least 4 h to overcome anti-apoptotic mechanisms as documented in Fig. 1. Subsequently, sometime between the fourth and sixth hour, the consequences of the "life or death" decision made by hepatocytes become apparent. Thus, this 2-h time span is decisive for development of a full-blown apoptosis. Importantly, overexpression of Bcl2 prevents cells from undergoing apoptosis by blocking cytochrome *c* release from mitochondria induced by a variety of stimuli (41). Moreover, inhibition of caspase-3 activity with YVAD-chloromethyl ketone protected mice from liver apoptosis and death caused by LPS and D-Gal (42).

The association of massive apoptosis of the liver with hemorrhagic necrosis reflects a concomitant microvascular injury due to a loss of endothelial integrity with attendant extravasation of erythrocytes and intravascular formation of platelet aggregates (Fig. 1*B*). This is accompanied by a precipitous decrease in circulating platelets and generation of FDP. In view of the fulminant nature of liver failure in this model, our inability to detect fibrin in histologic sections is not surprising. Nevertheless, combination of acute platelet consumption and generation of FDP strongly suggests a process of microvascular injury with thrombosis (43). Consistent with this process, increased expression of PAI-1 was detected. The cSN50 peptide prevented all of these abnormal changes. Thus, three interwoven mechanisms, inflammation, apoptosis, and microvascular dysfunction, depend on induction of a genetic program regulated by SRTFs and controlled by their nuclear import.

Broad inhibition of inducible SRTFs nuclear import prevents massive apoptosis of the adult liver, whereas disruption of physiologic signaling mediated by NFκB led to TNFα-dependent apoptosis of fetal liver (44–46). Although the cSN50 peptide inhibits nuclear import of NFκB, it also blocks nuclear translocation of activator protein 1, nuclear factor of activated T cells, and signal transducer and activator of transcription 1 (17, 18). Apparently, the coordinated regulation of genes that encode mediators of inflammation and apoptosis by multiple SRTFs exceeds the unique role of NFκB in protecting fetal liver from TNFα-mediated developmental injury.

Taken together, our experiments identify a key rate-limiting step in the development of LPS-induced apoptosis of the liver that may be amenable to therapeutic intervention with nuclear import inhibitors. TNFα production and subsequent hepatocyte apoptosis may contribute to the development of a number of inflammatory liver diseases, including viral hepatitis, alcoholic liver disease, Wilson disease, drug-induced liver failure, and

ischemia/reperfusion liver damage (34, 47, 48). Moreover, our results may have therapeutic applications for other disease conditions, such as secondary organ injury after ischemia/reperfusion, due to the excessive production of inflammatory cytokines and subsequent neutrophil involvement (49). Thus, targeting nuclear import of proinflammatory SRTFs offers a new approach to suppress expression of inflammatory and apoptotic mediators in the liver and interrupt the underlying disease mechanisms.

Acknowledgments—We thank Dean Ballard for critical reading of the manuscript, Ruth Ann Veach for experimental advice, and Hui Cai for help with statistical analyses. We also thank Ana Maria Hernandez for assistance in the preparation of the manuscript.

REFERENCES

1. Danial, N. N., and Korsmeyer, S. J. (2004) *Cell* **116,** 205–219
2. Jaeschke, H., Gujral, J. S., and Bajt, M. L. (2004) *Liver Int.* **24,** 85–89
3. Raper, S. E., Yudkoff, M., Chirmule, N., Gao, G. P., Nunes, F., Haskal, Z. J., Furth, E. E., Propert, K. J., Robinson, M. B., Magosin, S., Simoes, H., Speicher, L., Hughes, J., Tazelaar, J., Wivel, N. A., Wilson, J. M., and Batshaw, M. L. (2002) *Hum. Gene Ther.* **13,** 163–175
4. Doerschug, K., Sanlioglu, S., Flaherty, D. M., Wilson, R. L., Yarovinsky, T., Monick, M. M., Engelhardt, J. F., and Hunninghake, G. W. (2002) *J. Immunol.* **169,** 6539–6545
5. Shayakhmetov, D. M., Li, Z. Y., Ni, S., and Lieber, A. (2004) *J. Virol.* **78,** 5368–5381
6. Matsumoto, G., Tsunematsu, S., Tsukinoki, K., Ohmi, Y., Iwamiya, M., Oliveira-dos-Santos, A., Tone, D., Shindo, J., and Penninger, J. M. (2002) *J. Immunol.* **169,** 7087–7096
7. Liu, D., Liu, X. Y., Robinson, D., Burnett, C., Jackson, C., Seele, L., Veach, R. A., Downs, S., Collins, R. D., Ballard, D. W., and Hawiger, J. (2004) *J. Biol. Chem.* **279,** 19239–19246
8. Miethke, T., Wahl, C., Heeg, K., Echtenacher, B., Krammer, P. H., and Wagner, H. (1992) *J. Exp. Med.* **175,** 91–98
9. Deaciuc, I. V., Nikolova-Karakashian, M., Fortunato, F., Lee, E. Y., Hill, D. B., and McClain, C. J. (2000) *Alcohol Clin. Exp. Res.* **24,** 1557–1565
10. Galanos, C., Freudenberg, M. A., and Reutter, W. (1979) *Proc. Natl. Acad. Sci. U. S. A.* **76,** 5939–5943
11. Morikawa, A., Sugiyama, T., Kato, Y., Koide, N., Jiang, G. Z., Takahashi, K., Tamada, Y., and Yokochi, T. (1996) *Infect. Immun.* **64,** 734–738
12. Car, B. D., Eng, V. M., Schnyder, B., Ozmen, L., Huang, S., Gallay, P., Heumann, D., Aguet, M., and Ryffel, B. (1994) *J. Exp. Med.* **179,** 1437–1444
13. Rothe, J., Lesslauer, W., Lotscher, H., Lang, Y., Koebel, P., Kontgen, F., Althage, A., Zinkernagel, R., Steinmetz, M., and Bluethmann, H. (1993) *Nature* **364,** 798–802
14. Pfeffer, K., Matsuyama, T., Kundig, T. M., Wakeham, A., Kishihara, K., Shahinian, A., Wiegmann, K., Ohashi, P. S., Kronke, M., and Mak, T. W. (1993) *Cell* **73,** 457–467
15. Hawiger, J. (2001) *Immunol. Res.* **23,** 99–109
16. Weis, K. (2003) *Cell* **112,** 441–451
17. Torgerson, T. R., Colosia, A. D., Donahue, J. P., Lin, Y. Z., and Hawiger, J. (1998) *J. Immunol.* **161,** 6084–6092
18. Liu, X. Y., Robinson, D., Veach, R. A., Liu, D., Timmons, S., Collins, R. D., and Hawiger, J. (2000) *J. Biol. Chem.* **275,** 16774–16778
19. Chen, R., Lowe, L., Wilson, J. D., Crowther, E., Tzeggai, K., Bishop, J. E., and Varro, R. (1999) *Clin. Chem.* **45,** 1693–1694
20. Gibson, U. E., Heid, C. A., and Williams, P. M. (1996) *Genome Res.* **6,** 995–1001
21. Yajima, T., Yagihashi, A., Kameshima, H., Kobayashi, D., Furuya, D., Hirata, K., and Watanabe, N. (1998) *Clin. Chem.* **44,** 2441–2445
22. Hawiger, J., Niewiarowski, S., Gurewich, V., and Thomas, D. P. (1970) *J. Lab. Clin. Med.* **75,** 93–108
23. Freudenberg, M. A., Keppler, D., and Galanos, C. (1986) *Infect. Immun.* **51,** 891–895
24. Lehmann, V., Freudenberg, M. A., and Galanos, C. (1987) *J. Exp. Med.* **165,** 657–663
25. Song, Y., Shi, Y., Ao, L. H., Harken, A. H., and Meng, X. Z. (2003) *World J. Gastroenterol.* **9,** 1799–1803
26. Feng, J. M., Shi, J. Q., and Liu, Y. S. (2003) *Hepatobiliary Pancreat. Dis. Int.* **2,** 265–269
27. Dufour, D. R., Lott, J. A., Nolte, F. S., Gretch, D. R., Koff, R. S., and Seeff, L. B. (2000) *Clin. Chem.* **46,** 2027–2049
28. Green, D., and Kroemer, G. (1998) *Trends Cell Biol.* **8,** 267–271
29. Wang, X. (2001) *Genes Dev.* **15,** 2922–2933
30. Liu, X., Zou, H., Slaughter, C., and Wang, X. (1997) *Cell* **89,** 175–184
31. Liu, X., Li, P., Widlak, P., Zou, H., Luo, X., Garrard, W. T., and Wang, X. (1998) *Proc. Natl. Acad. Sci. U. S. A.* **95,** 8461–8466
32. Enari, M., Sakahira, H., Yokoyama, H., Okawa, K., Iwamatsu, A., and Nagata, S. (1998) *Nature* **391,** 43–50
33. Adams, J. M., and Cory, S. (1998) *Science* **281,** 1322–1326
34. Yin, X. M., and Ding, W. X. (2003) *Curr. Mol. Med.* **3,** 491–508
35. Eitzman, D. T., Westrick, R. J., Nabel, E. G., and Ginsburg, D. (2000) *Blood* **95,** 577–580
36. Zhou, Z., Wang, L., Song, Z., Lambert, J. C., McClain, C. J., and Kang, Y. J. (2003) *Am. J. Pathol.* **163,** 1137–1146
37. McMullen, M. R., Cocuzzi, E., Hatzoglou, M., and Nagy, L. E. (2003) *J. Biol. Chem.* **278,** 38333–38341
38. Lieber, C. S. (1988) *N. Engl. J. Med.* **319,** 1639–1650
39. Kadenbach, B., Arnold, S., Lee, I., and Huttemann, M. (2004) *Biochim. Biophys. Acta* **1655,** 400–408
40. Osawa, Y., Banno, Y., Nagaki, M., Nozawa, Y., Moriwaki, H., and Nakashima, S. (2001) *Liver* **21,** 309–319
41. Yang, J., Liu, X., Bhalla, K., Kim, C. N., Ibrado, A. M., Cai, J., Peng, T. I., Jones, D. P., and Wang, X. (1997) *Science* **275,** 1129–1132
42. Mignon, A., Rouquet, N., Fabre, M., Martin, S., Pages, J. C., Dhainaut, J. F., Kahn, A., Briand, P., and Joulin, V. (1999) *Am. J. Respir. Crit. Care Med.* **159,** 1308–1315
43. Wada, H., Gabazza, E. C., Asakura, H., Koike, K., Okamoto, K., Maruyama, I., Shiku, H., and Nobori, T. (2003) *Am. J. Hematol.* **74,** 17–22
44. Beg, A. A., Sha, W. C., Bronson, R. T., Ghosh, S., and Baltimore, D. (1995) *Nature* **376,** 167–170
45. Doi, T. S., Marino, M. W., Takahashi, T., Yoshida, T., Sakakura, T., Old, L. J., and Obata, Y. (1999) *Proc. Natl. Acad. Sci. U. S. A.* **96,** 2994–2999
46. Rosenfeld, M. E., Prichard, L., Shiojiri, N., and Fausto, N. (2000) *Am. J. Pathol.* **156,** 997–1007
47. Oreopoulos, G. D., Wu, H., Szaszi, K., Fan, J., Marshall, J. C., Khadaroo, R. G., He, R., Kapus, A., and Rotstein, O. D. (2004) *Hepatology* **40,** 211–220
48. McCarter, S. D., Akyea, T. G., Lu, X., Bihari, A., Scott, J. R., Badhwar, A., Dungey, A. A., Harris, K. A., Feng, Q., and Potter, R. F. (2004) *Surgery* **136,** 67–75
49. Qiu, F. H., Wada, K., Stahl, G. L., and Serhan, C. N. (2000) *Proc. Natl. Acad. Sci. U. S. A.* **97,** 4267–4272

REFERENCES

Adachi, O., Kawai, T., Takeda, K., Matsumoto, M., Tsutsui, H., Sakagami, M., Nakanishi, K., and Akira, S. (1998). Targeted disruption of the MyD88 gene results in loss of IL-1- and IL-18-mediated function. Immunity *9*, 143-150.

Akira, S. (2003). Toll-like receptor signaling. J Biol Chem *278*, 38105-38108.

Akira, S., and Sato, S. (2003). Toll-like receptors and their signaling mechanisms. Scand J Infect Dis *35*, 555-562.

Aksentijevich, I., Nowak, M., Mallah, M., Chae, J. J., Watford, W. T., Hofmann, S. R., Stein, L., Russo, R., Goldsmith, D., Dent, P.*, et al.* (2002). De novo CIAS1 mutations, cytokine activation, and evidence for genetic heterogeneity in patients with neonatal-onset multisystem inflammatory disease (NOMID): a new member of the expanding family of pyrin-associated autoinflammatory diseases. Arthritis Rheum *46*, 3340-3348.

Anderson, M. R., and Tary-Lehmann, M. (2001). Staphylococcal enterotoxin-B-induced lethal shock in mice is T-cell-dependent, but disease susceptibility is defined by the non-T-cell compartment. Clin Immunol *98*, 85-94.

Andreakos, E., Foxwell, B., and Feldmann, M. (2004). Is targeting Toll-like receptors and their signaling pathway a useful therapeutic approach to modulating cytokine-driven inflammation? Immunol Rev *202*, 250-265.

Aoki, Y., Hiromatsu, K., Arai, T., Usami, J., Makino, M., Ishida, H., and Yoshikai, Y. (1995). Lethal shock is inducible by lipopolysaccharide but not by superantigen in mice with retrovirus-induced immunodeficiency syndrome. J Immunol *155*, 3494-3500.

Arend, W. P., Malyak, M., Guthridge, C. J., and Gabay, C. (1998). Interleukin-1 receptor antagonist: role in biology. Annu Rev Immunol *16*, 27-55.

Auron, P. E., Webb, A. C., Rosenwasser, L. J., Mucci, S. F., Rich, A., Wolff, S. M., and Dinarello, C. A. (1984). Nucleotide sequence of human monocyte interleukin 1 precursor cDNA. Proc Natl Acad Sci U S A *81*, 7907-7911.

Balaban, N., and Rasooly, A. (2000). Staphylococcal enterotoxins. Int J Food Microbiol *61*, 1-10.

Bartfai, T., Behrens, M. M., Gaidarova, S., Pemberton, J., Shivanyuk, A., and Rebek, J., Jr. (2003). A low molecular weight mimic of the Toll/IL-1 receptor/resistance domain inhibits IL-1 receptor-mediated responses. Proc Natl Acad Sci U S A *100*, 7971-7976.

Barton, J. L., Herbst, R., Bosisio, D., Higgins, L., and Nicklin, M. J. (2000). A tissue specific IL-1 receptor antagonist homolog from the IL-1 cluster lacks IL-1, IL-1ra, IL-18 and IL-18 antagonist activities. Eur J Immunol *30*, 3299-3308.

Basu, A., Krady, J. K., and Levison, S. W. (2004). Interleukin-1: a master regulator of neuroinflammation. J Neurosci Res *78*, 151-156.

Basu, A., Lazovic, J., Krady, J. K., Mauger, D. T., Rothstein, R. P., Smith, M. B., and Levison, S. W. (2005). Interleukin-1 and the interleukin-1 type 1 receptor are essential for the progressive neurodegeneration that ensues subsequent to a mild hypoxic/ischemic injury. J Cereb Blood Flow Metab *25*, 17-29.

Bauer, S., Kirschning, C. J., Hacker, H., Redecke, V., Hausmann, S., Akira, S., Wagner, H., and Lipford, G. B. (2001). Human TLR9 confers responsiveness to bacterial DNA via species-specific CpG motif recognition. Proc Natl Acad Sci U S A *98*, 9237-9242.

Baugh, J. A., and Bucala, R. (2001). Mechanisms for modulating TNF alpha in immune and inflammatory disease. Curr Opin Drug Discov Devel *4*, 635-650.

Bazan, J. F., Timans, J. C., and Kastelein, R. A. (1996). A newly defined interleukin-1? Nature *379*, 591.

Bhardwaj, N., Young, J. W., Nisanian, A. J., Baggers, J., and Steinman, R. M. (1993). Small amounts of superantigen, when presented on dendritic cells, are sufficient to initiate T cell responses. J Exp Med *178*, 633-642.

Bin, L. H., Xu, L. G., and Shu, H. B. (2003). TIRP, a novel Toll/interleukin-1 receptor (TIR) domain-containing adapter protein involved in TIR signaling. J Biol Chem *278*, 24526-24532.

Boothby, M. R., Mora, A. L., Scherer, D. C., Brockman, J. A., and Ballard, D. W. (1997). Perturbation of the T lymphocyte lineage in transgenic mice expressing a constitutive repressor of nuclear factor (NF)-kappaB. J Exp Med *185*, 1897-1907.

Born, T. L., Thomassen, E., Bird, T. A., and Sims, J. E. (1998). Cloning of a novel receptor subunit, AcPL, required for interleukin-18 signaling. J Biol Chem *273*, 29445-29450.

Brint, E. K., Fitzgerald, K. A., Smith, P., Coyle, A. J., Gutierrez-Ramos, J. C., Fallon, P. G., and O'Neill, L. A. (2002). Characterization of signaling pathways activated by the interleukin 1 (IL-1) receptor homologue T1/ST2. A role for Jun N-terminal kinase in IL-4 induction. J Biol Chem *277*, 49205-49211.

Burns, K., Clatworthy, J., Martin, L., Martinon, F., Plumpton, C., Maschera, B., Lewis, A., Ray, K., Tschopp, J., and Volpe, F. (2000). Tollip, a new component of the IL-1RI pathway, links IRAK to the IL-1 receptor. Nat Cell Biol *2*, 346-351.

Burns, K., Janssens, S., Brissoni, B., Olivos, N., Beyaert, R., and Tschopp, J. (2003). Inhibition of interleukin 1 receptor/Toll-like receptor signaling through the alternatively spliced, short form of MyD88 is due to its failure to recruit IRAK-4. J Exp Med *197*, 263-268.

Burns, K., Martinon, F., Esslinger, C., Pahl, H., Schneider, P., Bodmer, J. L., Di Marco, F., French, L., and Tschopp, J. (1998). MyD88, an adapter protein involved in interleukin-1 signaling. J Biol Chem *273*, 12203-12209.

Busfield, S. J., Comrack, C. A., Yu, G., Chickering, T. W., Smutko, J. S., Zhou, H., Leiby, K. R., Holmgren, L. M., Gearing, D. P., and Pan, Y. (2000). Identification and gene organization of three novel members of the IL-1 family on human chromosome 2. Genomics *66*, 213-216.

Cao, Z., Henzel, W. J., and Gao, X. (1996). IRAK: a kinase associated with the interleukin-1 receptor. Science *271*, 1128-1131.

Carrie, A., Jun, L., Bienvenu, T., Vinet, M. C., McDonell, N., Couvert, P., Zemni, R., Cardona, A., Van Buggenhout, G., Frints, S.*, et al.* (1999). A new member of the IL-1 receptor family highly expressed in hippocampus and involved in X-linked mental retardation. Nat Genet *23*, 25-31.

Chen, J. Y., Qiao, Y., Komisar, J. L., Baze, W. B., Hsu, I. C., and Tseng, J. (1994). Increased susceptibility to staphylococcal enterotoxin B intoxication in mice primed with actinomycin D. Infect Immun *62*, 4626-4631.

Couillault, C., Pujol, N., Reboul, J., Sabatier, L., Guichou, J. F., Kohara, Y., and Ewbank, J. J. (2004). TLR-independent control of innate immunity in Caenorhabditis elegans by the TIR domain adaptor protein TIR-1, an ortholog of human SARM. Nat Immunol *5*, 488-494.

Dabrowski, M. P., Stankiewicz, W., Plusa, T., Chcialowski, A., and Szmigielski, S. (2001). Competition of IL-1 and IL-1ra determines lymphocyte response to delayed stimulation with PHA. Mediators Inflamm *10*, 101-107.

Dale, M., and Nicklin, M. J. (1999). Interleukin-1 receptor cluster: gene organization of IL1R2, IL1R1, IL1RL2 (IL-1Rrp2), IL1RL1 (T1/ST2), and IL18R1 (IL-1Rrp) on human chromosome 2q. Genomics *57*, 177-179.

Debets, R., Timans, J. C., Homey, B., Zurawski, S., Sana, T. R., Lo, S., Wagner, J., Edwards, G., Clifford, T., Menon, S.*, et al.* (2001). Two novel IL-1 family members, IL-1 delta and IL-1 epsilon, function as an antagonist and agonist of NF-kappa B activation through the orphan IL-1 receptor-related protein 2. J Immunol *167*, 1440-1446.

Deng, L., Wang, C., Spencer, E., Yang, L., Braun, A., You, J., Slaughter, C., Pickart, C., and Chen, Z. J. (2000). Activation of the IkappaB kinase complex by TRAF6 requires a dimeric ubiquitin-conjugating enzyme complex and a unique polyubiquitin chain. Cell *103*, 351-361.

Dinarello, C. A. (1996). Biologic basis for interleukin-1 in disease. Blood *87*, 2095-2147.

Dinarello, C. A. (2000). Proinflammatory cytokines. Chest *118*, 503-508.

Dinarello, C. A. (2002). The IL-1 family and inflammatory diseases. Clin Exp Rheumatol *20*, S1-13.

Dinarello, C. A. (2004). Therapeutic strategies to reduce IL-1 activity in treating local and systemic inflammation. Curr Opin Pharmacol *4*, 378-385.

Dinarello, C. A., and Wolff, S. M. (1993). The role of interleukin-1 in disease. N Engl J Med *328*, 106-113.

Dinges, M. M., Orwin, P. M., and Schlievert, P. M. (2000). Exotoxins of Staphylococcus aureus. Clin Microbiol Rev *13*, 16-34, table of contents.

Dunne, A., Ejdeback, M., Ludidi, P. L., O'Neill, L. A., and Gay, N. J. (2003). Structural complementarity of Toll/interleukin-1 receptor domains in Toll-like receptors and the adaptors Mal and MyD88. J Biol Chem *278*, 41443-41451.

Dunne, A., and O'Neill, L. A. (2003). The interleukin-1 receptor/Toll-like receptor superfamily: signal transduction during inflammation and host defense. Sci STKE *2003*, re3.

Dupraz, P., Cottet, S., Hamburger, F., Dolci, W., Felley-Bosco, E., and Thorens, B. (2000). Dominant negative MyD88 proteins inhibit interleukin-1beta /interferon-gamma -mediated induction of nuclear factor kappa B-dependent nitrite production and apoptosis in beta cells. J Biol Chem *275*, 37672-37678.

Fitzgerald, K. A., Palsson-McDermott, E. M., Bowie, A. G., Jefferies, C. A., Mansell, A. S., Brady, G., Brint, E., Dunne, A., Gray, P., Harte, M. T.*, et al.* (2001). Mal (MyD88-adapter-like) is required for Toll-like receptor-4 signal transduction. Nature *413*, 78-83.

Fitzgerald, K. A., Rowe, D. C., Barnes, B. J., Caffrey, D. R., Visintin, A., Latz, E., Monks, B., Pitha, P. M., and Golenbock, D. T. (2003). LPS-TLR4 signaling to IRF-3/7 and NF-kappaB involves the toll adapters TRAM and TRIF. J Exp Med *198*, 1043-1055.

Ghayur, T., Banerjee, S., Hugunin, M., Butler, D., Herzog, L., Carter, A., Quintal, L., Sekut, L., Talanian, R., Paskind, M.*, et al.* (1997). Caspase-1 processes IFN-gamma-inducing factor and regulates LPS-induced IFN-gamma production. Nature *386*, 619-623.

Goldfeld, A. E., McCaffrey, P. G., Strominger, J. L., and Rao, A. (1993). Identification of a novel cyclosporin-sensitive element in the human tumor necrosis factor alpha gene promoter. J Exp Med *178*, 1365-1379.

Greenfeder, S. A., Nunes, P., Kwee, L., Labow, M., Chizzonite, R. A., and Ju, G. (1995). Molecular cloning and characterization of a second subunit of the interleukin 1 receptor complex. J Biol Chem *270*, 13757-13765.

Gu, Y., Kuida, K., Tsutsui, H., Ku, G., Hsiao, K., Fleming, M. A., Hayashi, N., Higashino, K., Okamura, H., Nakanishi, K.*, et al.* (1997). Activation of interferon-gamma inducing factor mediated by interleukin-1beta converting enzyme. Science *275*, 206-209.

Guex, N., and Peitsch, M. C. (1997). SWISS-MODEL and the Swiss-PdbViewer: an environment for comparative protein modeling. Electrophoresis *18*, 2714-2723.

Hardiman, G., Jenkins, N. A., Copeland, N. G., Gilbert, D. J., Garcia, D. K., Naylor, S. L., Kastelein, R. A., and Bazan, J. F. (1997). Genetic structure and chromosomal mapping of MyD88. Genomics *45*, 332-339.

Hawiger, J. (1976). Disseminated intravascular coagulation in patients with infections: diagnostic and therapeutic approach. Mater Med Pol *8*, 206-212.

Hawiger, J. (1999). Noninvasive intracellular delivery of functional peptides and proteins. Curr Opin Chem Biol *3*, 89-94.

Hawiger, J. (2001). Innate immunity and inflammation: a transcriptional paradigm. Immunol Res *23*, 99-109.

Hawkins, P. N., Lachmann, H. J., Aganna, E., and McDermott, M. F. (2004). Spectrum of clinical features in Muckle-Wells syndrome and response to anakinra. Arthritis Rheum *50*, 607-612.

Hawkins, P. N., Lachmann, H. J., and McDermott, M. F. (2003). Interleukin-1-receptor antagonist in the Muckle-Wells syndrome. N Engl J Med *348*, 2583-2584.

Hirotani, T., Yamamoto, M., Kumagai, Y., Uematsu, S., Kawase, I., Takeuchi, O., and Akira, S. (2005). Regulation of lipopolysaccharide-inducible genes by MyD88 and Toll/IL-1 domain containing adaptor inducing IFN-beta. Biochem Biophys Res Commun *328*, 383-392.

Hoebe, K., Du, X., Georgel, P., Janssen, E., Tabeta, K., Kim, S. O., Goode, J., Lin, P., Mann, N., Mudd, S.*, et al.* (2003). Identification of Lps2 as a key transducer of MyD88-independent TIR signalling. Nature *424*, 743-748.

Hoffman, H. M., Mueller, J. L., Broide, D. H., Wanderer, A. A., and Kolodner, R. D. (2001). Mutation of a new gene encoding a putative pyrin-like protein causes familial cold autoinflammatory syndrome and Muckle-Wells syndrome. Nat Genet *29*, 301-305.

Hoffman, H. M., Rosengren, S., Boyle, D. L., Cho, J. Y., Nayar, J., Mueller, J. L., Anderson, J. P., Wanderer, A. A., and Firestein, G. S. (2004). Prevention of cold-associated acute inflammation in familial cold autoinflammatory syndrome by interleukin-1 receptor antagonist. Lancet *364*, 1779-1785.

Hofmann, K., and Tschopp, J. (1995). The death domain motif found in Fas (Apo-1) and TNF receptor is present in proteins involved in apoptosis and axonal guidance. FEBS Lett *371*, 321-323.

Hofmeister, R., Wiegmann, K., Korherr, C., Bernardo, K., Kronke, M., and Falk, W. (1997). Activation of acid sphingomyelinase by interleukin-1 (IL-1) requires the IL-1 receptor accessory protein. J Biol Chem *272*, 27730-27736.

Horng, T., Barton, G. M., Flavell, R. A., and Medzhitov, R. (2002). The adaptor molecule TIRAP provides signalling specificity for Toll-like receptors. Nature *420*, 329-333.

Horng, T., Barton, G. M., and Medzhitov, R. (2001). TIRAP: an adapter molecule in the Toll signaling pathway. Nat Immunol *2*, 835-841.

Huang, B., Eberstadt, M., Olejniczak, E. T., Meadows, R. P., and Fesik, S. W. (1996). NMR structure and mutagenesis of the Fas (APO-1/CD95) death domain. Nature *384*, 638-641.

Huang, J., Gao, X., Li, S., and Cao, Z. (1997). Recruitment of IRAK to the interleukin 1 receptor complex requires interleukin 1 receptor accessory protein. Proc Natl Acad Sci U S A *94*, 12829-12832.

Imler, J. L., and Zheng, L. (2004). Biology of Toll receptors: lessons from insects and mammals. J Leukoc Biol *75*, 18-26.

Jo, D., Liu, D., Yao, S., Collins, R. D., and Hawiger, J. (2005). Intracellular protein therapy with SOCS3 inhibits inflammation and apoptosis. Nat Med *11*, 892-898.

Jo, D., Nashabi, A., Doxsee, C., Lin, Q., Unutmaz, D., Chen, J., and Ruley, H. E. (2001). Epigenetic regulation of gene structure and function with a cell-permeable Cre recombinase. Nat Biotechnol *19*, 929-933.

Kaiser, W. J., and Offermann, M. K. (2005). Apoptosis induced by the toll-like receptor adaptor TRIF is dependent on its receptor interacting protein homotypic interaction motif. J Immunol *174*, 4942-4952.

Kaisho, T., Takeuchi, O., Kawai, T., Hoshino, K., and Akira, S. (2001). Endotoxin-induced maturation of MyD88-deficient dendritic cells. J Immunol *166*, 5688-5694.

Kawai, T., Adachi, O., Ogawa, T., Takeda, K., and Akira, S. (1999). Unresponsiveness of MyD88-deficient mice to endotoxin. Immunity *11*, 115-122.

Kawai, T., Takeuchi, O., Fujita, T., Inoue, J., Muhlradt, P. F., Sato, S., Hoshino, K., and Akira, S. (2001). Lipopolysaccharide stimulates the MyD88-independent pathway and results in activation of IFN-regulatory factor 3 and the expression of a subset of lipopolysaccharide-inducible genes. J Immunol *167*, 5887-5894.

Khovidhunkit, W., Memon, R. A., Feingold, K. R., and Grunfeld, C. (2000). Infection and inflammation-induced proatherogenic changes of lipoproteins. J Infect Dis *181 Suppl 3*, S462-472.

Kimoto, M., Nagasawa, K., and Miyake, K. (2003). Role of TLR4/MD-2 and RP105/MD-1 in innate recognition of lipopolysaccharide. Scand J Infect Dis *35*, 568-572.

Klemenz, R., Hoffmann, S., and Werenskiold, A. K. (1989). Serum- and oncoprotein-mediated induction of a gene with sequence similarity to the gene encoding carcinoembryonic antigen. Proc Natl Acad Sci U S A *86*, 5708-5712.

Kobayashi, K., Hernandez, L. D., Galan, J. E., Janeway, C. A., Jr., Medzhitov, R., and Flavell, R. A. (2002). IRAK-M is a negative regulator of Toll-like receptor signaling. Cell *110*, 191-202.

Kobayashi, Y., Yamamoto, K., Saido, T., Kawasaki, H., Oppenheim, J. J., and Matsushima, K. (1990). Identification of calcium-activated neutral protease as a processing enzyme of human interleukin 1 alpha. Proc Natl Acad Sci U S A *87*, 5548-5552.

Kojima, H., Takeuchi, M., Ohta, T., Nishida, Y., Arai, N., Ikeda, M., Ikegami, H., and Kurimoto, M. (1998). Interleukin-18 activates the IRAK-TRAF6 pathway in mouse EL-4 cells. Biochem Biophys Res Commun *244*, 183-186.

Korherr, C., Hofmeister, R., Wesche, H., and Falk, W. (1997). A critical role for interleukin-1 receptor accessory protein in interleukin-1 signaling. Eur J Immunol *27*, 262-267.

Kumar, S., McDonnell, P. C., Lehr, R., Tierney, L., Tzimas, M. N., Griswold, D. E., Capper, E. A., Tal-Singer, R., Wells, G. I., Doyle, M. L., and Young, P. R. (2000). Identification and initial characterization of four novel members of the interleukin-1 family. J Biol Chem *275*, 10308-10314.

Kunkel, T. A. (1985). Rapid and efficient site-specific mutagenesis without phenotypic selection. Proc Natl Acad Sci U S A *82*, 488-492.

Kusumoto, Y., and Miyake, K. (2002). [Functional roles of TLR4/MD-2 and RP105/MD-1 in innate recognition of LPS]. Tanpakushitsu Kakusan Koso *47*, 2103-2108.

Lafage, M., Maroc, N., Dubreuil, P., de Waal Malefijt, R., Pebusque, M. J., Carcassonne, Y., and Mannoni, P. (1989). The human interleukin-1 alpha gene is located on the long arm of chromosome 2 at band q13. Blood *73*, 104-107.

Lemaitre, B., Nicolas, E., Michaut, L., Reichhart, J. M., and Hoffmann, J. A. (1996). The dorsoventral regulatory gene cassette spatzle/Toll/cactus controls the potent antifungal response in Drosophila adults. Cell *86*, 973-983.

Li, C., Zienkiewicz, J., and Hawiger, J. (2005). Interactive sites in the MYD88 TIR domain responsible for coupling to the IL1beta signaling pathway. J Biol Chem.

Li, S., Strelow, A., Fontana, E. J., and Wesche, H. (2002). IRAK-4: a novel member of the IRAK family with the properties of an IRAK-kinase. Proc Natl Acad Sci U S A *99*, 5567-5572.

Lin, Y. Z., Yao, S. Y., Veach, R. A., Torgerson, T. R., and Hawiger, J. (1995). Inhibition of nuclear translocation of transcription factor NF-kappa B by a synthetic peptide containing a cell membrane-permeable motif and nuclear localization sequence. J Biol Chem *270*, 14255-14258.

Liu, D., Li, C., Chen, Y., Burnett, C., Liu, X. Y., Downs, S., Collins, R. D., and Hawiger, J. (2004a). Nuclear import of proinflammatory transcription factors is required for massive liver apoptosis induced by bacterial lipopolysaccharide. J Biol Chem *279*, 48434-48442.

Liu, D., Liu, X. Y., Robinson, D., Burnett, C., Jackson, C., Seele, L., Veach, R. A., Downs, S., Collins, R. D., Ballard, D. W., and Hawiger, J. (2004b). Suppression of Staphylococcal Enterotoxin B-induced Toxicity by a Nuclear Import Inhibitor. J Biol Chem *279*, 19239-19246.

Lord, K. A., Hoffman-Liebermann, B., and Liebermann, D. A. (1990). Nucleotide sequence and expression of a cDNA encoding MyD88, a novel myeloid differentiation primary response gene induced by IL6. Oncogene *5*, 1095-1097.

Lovell, D. J., Bowyer, S. L., and Solinger, A. M. (2005). Interleukin-1 blockade by anakinra improves clinical symptoms in patients with neonatal-onset multisystem inflammatory disease. Arthritis Rheum *52*, 1283-1286.

Lovenberg, T. W., Crowe, P. D., Liu, C., Chalmers, D. T., Liu, X. J., Liaw, C., Clevenger, W., Oltersdorf, T., De Souza, E. B., and Maki, R. A. (1996). Cloning of a cDNA encoding a novel interleukin-1 receptor related protein (IL 1R-rp2). J Neuroimmunol *70*, 113-122.

Madsen, J. M. (2001). Toxins as weapons of mass destruction. A comparison and contrast with biological-warfare and chemical-warfare agents. Clin Lab Med *21*, 593-605.

Mariathasan, S., Newton, K., Monack, D. M., Vucic, D., French, D. M., Lee, W. P., Roose-Girma, M., Erickson, S., and Dixit, V. M. (2004). Differential activation of the inflammasome by caspase-1 adaptors ASC and Ipaf. Nature *430*, 213-218.

Marrack, P., Blackman, M., Kushnir, E., and Kappler, J. (1990). The toxicity of staphylococcal enterotoxin B in mice is mediated by T cells. J Exp Med *171*, 455-464.

Martinon, F., Burns, K., and Tschopp, J. (2002). The inflammasome: a molecular platform triggering activation of inflammatory caspases and processing of proIL-beta. Mol Cell *10*, 417-426.

Mattix, M. E., Hunt, R. E., Wilhelmsen, C. L., Johnson, A. J., and Baze, W. B. (1995). Aerosolized staphylococcal enterotoxin B-induced pulmonary lesions in rhesus monkeys (Macaca mulatta). Toxicol Pathol *23*, 262-268.

McGettrick, A. F., and O'Neill, L. A. (2004). The expanding family of MyD88-like adaptors in Toll-like receptor signal transduction. Mol Immunol *41*, 577-582.

Mercurio, F., Zhu, H., Murray, B. W., Shevchenko, A., Bennett, B. L., Li, J., Young, D. B., Barbosa, M., Mann, M., Manning, A., and Rao, A. (1997). IKK-1 and IKK-2: cytokine-activated IkappaB kinases essential for NF-kappaB activation. Science *278*, 860-866.

Mink, M., Fogelgren, B., Olszewski, K., Maroy, P., and Csiszar, K. (2001). A novel human gene (SARM) at chromosome 17q11 encodes a protein with a SAM motif and structural similarity to Armadillo/beta-catenin that is conserved in mouse, Drosophila, and Caenorhabditis elegans. Genomics *74*, 234-244.

Mitcham, J. L., Parnet, P., Bonnert, T. P., Garka, K. E., Gerhart, M. J., Slack, J. L., Gayle, M. A., Dower, S. K., and Sims, J. E. (1996). T1/ST2 signaling establishes it as a member of an expanding interleukin-1 receptor family. J Biol Chem *271*, 5777-5783.

Miyake, K., Ogata, H., Nagai, Y., Akashi, S., and Kimoto, M. (2000). Innate recognition of lipopolysaccharide by Toll-like receptor 4/MD-2 and RP105/MD-1. J Endotoxin Res *6*, 389-391.

Mrak, R. E., and Griffin, W. S. (2001). Interleukin-1, neuroinflammation, and Alzheimer's disease. Neurobiol Aging *22*, 903-908.

Mulero, J. J., Pace, A. M., Nelken, S. T., Loeb, D. B., Correa, T. R., Drmanac, R., and Ford, J. E. (1999). IL1HY1: A novel interleukin-1 receptor antagonist gene. Biochem Biophys Res Commun *263*, 702-706.

Murphy, J. E., Robert, C., and Kupper, T. S. (2000). Interleukin-1 and cutaneous inflammation: a crucial link between innate and acquired immunity. J Invest Dermatol *114*, 602-608.

Muzio, M., Ni, J., Feng, P., and Dixit, V. M. (1997). IRAK (Pelle) family member IRAK-2 and MyD88 as proximal mediators of IL-1 signaling. Science *278*, 1612-1615.

Muzio, M., Polntarutti, N., Bosisio, D., Prahladan, M. K., and Mantovani, A. (2000). Toll like receptor family (TLT) and signalling pathway. Eur Cytokine Netw *11*, 489-490.

O'Neill, L. A., Fitzgerald, K. A., and Bowie, A. G. (2003). The Toll-IL-1 receptor adaptor family grows to five members. Trends Immunol *24*, 286-290.

Ogata, H., Su, I., Miyake, K., Nagai, Y., Akashi, S., Mecklenbrauker, I., Rajewsky, K., Kimoto, M., and Tarakhovsky, A. (2000). The toll-like receptor protein RP105 regulates lipopolysaccharide signaling in B cells. J Exp Med *192*, 23-29.

Oshiumi, H., Sasai, M., Shida, K., Fujita, T., Matsumoto, M., and Seya, T. (2003). TIR-containing adapter molecule (TICAM)-2, a bridging adapter recruiting to toll-like receptor 4 TICAM-1 that induces interferon-beta. J Biol Chem *278*, 49751-49762.

Pan, G., Risser, P., Mao, W., Baldwin, D. T., Zhong, A. W., Filvaroff, E., Yansura, D., Lewis, L., Eigenbrot, C., Henzel, W. J., and Vandlen, R. (2001). IL-1H, an interleukin 1-related protein that binds IL-18 receptor/IL-1Rrp. Cytokine *13*, 1-7.

Parnet, P., Garka, K. E., Bonnert, T. P., Dower, S. K., and Sims, J. E. (1996). IL-1Rrp is a novel receptor-like molecule similar to the type I interleukin-1 receptor and its homologues T1/ST2 and IL-1R AcP. J Biol Chem *271*, 3967-3970.

Patterson, D., Jones, C., Hart, I., Bleskan, J., Berger, R., Geyer, D., Eisenberg, S. P., Smith, M. F., Jr., and Arend, W. P. (1993). The human interleukin-1 receptor antagonist (IL1RN) gene is located in the chromosome 2q14 region. Genomics *15*, 173-176.

Poltorak, A., He, X., Smirnova, I., Liu, M. Y., Van Huffel, C., Du, X., Birdwell, D., Alejos, E., Silva, M., Galanos, C.*, et al.* (1998). Defective LPS signaling in C3H/HeJ and C57BL/10ScCr mice: mutations in Tlr4 gene. Science *282*, 2085-2088.

Radons, J., Dove, S., Neumann, D., Altmann, R., Botzki, A., Martin, M. U., and Falk, W. (2003). The interleukin 1 (IL-1) receptor accessory protein Toll/IL-1 receptor domain: analysis of putative interaction sites in vitro mutagenesis and molecular modeling. J Biol Chem *278*, 49145-49153.

Radons, J., Gabler, S., Wesche, H., Korherr, C., Hofmeister, R., and Falk, W. (2002). Identification of essential regions in the cytoplasmic tail of interleukin-1 receptor accessory protein critical for interleukin-1 signaling. J Biol Chem *277*, 16456-16463.

Rock, F. L., Hardiman, G., Timans, J. C., Kastelein, R. A., and Bazan, J. F. (1998). A family of human receptors structurally related to Drosophila Toll. Proc Natl Acad Sci U S A *95*, 588-593.

Rosenwasser, L. J. (1998). Biologic activities of IL-1 and its role in human disease. J Allergy Clin Immunol *102*, 344-350.

Roubenoff, R., Roubenoff, R. A., Cannon, J. G., Kehayias, J. J., Zhuang, H., Dawson-Hughes, B., Dinarello, C. A., and Rosenberg, I. H. (1994). Rheumatoid cachexia: cytokine-driven hypermetabolism accompanying reduced body cell mass in chronic inflammation. J Clin Invest *93*, 2379-2386.

Sana, T. R., Debets, R., Timans, J. C., Bazan, J. F., and Kastelein, R. A. (2000). Computational identification, cloning, and characterization of IL-1R9, a novel interleukin-1 receptor-like gene encoded over an unusually large interval of human chromosome Xq22.2-q22.3. Genomics *69*, 252-262.

Schiff, M. H. (2000). Role of interleukin 1 and interleukin 1 receptor antagonist in the mediation of rheumatoid arthritis. Ann Rheum Dis *59 Suppl 1*, i103-108.

Schwede, T., Kopp, J., Guex, N., and Peitsch, M. C. (2003). SWISS-MODEL: An automated protein homology-modeling server. Nucleic Acids Res *31*, 3381-3385.

Seth, A., Stern, L. J., Ottenhoff, T. H., Engel, I., Owen, M. J., Lamb, J. R., Klausner, R. D., and Wiley, D. C. (1994). Binary and ternary complexes between T-cell receptor, class II MHC and superantigen in vitro. Nature *369*, 324-327.

Sica, A., Dorman, L., Viggiano, V., Cippitelli, M., Ghosh, P., Rice, N., and Young, H. A. (1997). Interaction of NF-kappaB and NFAT with the interferon-gamma promoter. J Biol Chem *272*, 30412-30420.

Silverman, N., and Maniatis, T. (2001). NF-kappaB signaling pathways in mammalian and insect innate immunity. Genes Dev *15*, 2321-2342.

Sims, J. E., March, C. J., Cosman, D., Widmer, M. B., MacDonald, H. R., McMahan, C. J., Grubin, C. E., Wignall, J. M., Jackson, J. L., Call, S. M., and et al. (1988). cDNA expression cloning of the IL-1 receptor, a member of the immunoglobulin superfamily. Science *241*, 585-589.

Sims, J. E., Painter, S. L., and Gow, I. R. (1995). Genomic organization of the type I and type II IL-1 receptors. Cytokine *7*, 483-490.

Smith, D. E., Renshaw, B. R., Ketchem, R. R., Kubin, M., Garka, K. E., and Sims, J. E. (2000). Four new members expand the interleukin-1 superfamily. J Biol Chem *275*, 1169-1175.

Srinivasula, S. M., Poyet, J. L., Razmara, M., Datta, P., Zhang, Z., and Alnemri, E. S. (2002). The PYRIN-CARD protein ASC is an activating adaptor for caspase-1. J Biol Chem *277*, 21119-21122.

Suzuki, N., Suzuki, S., Duncan, G. S., Millar, D. G., Wada, T., Mirtsos, C., Takada, H., Wakeham, A., Itie, A., Li, S.*, et al.* (2002). Severe impairment of interleukin-1 and Toll-like receptor signalling in mice lacking IRAK-4. Nature *416*, 750-756.

Swantek, J. L., Tsen, M. F., Cobb, M. H., and Thomas, J. A. (2000). IL-1 receptor-associated kinase modulates host responsiveness to endotoxin. J Immunol *164*, 4301-4306.

Tao, X., Xu, Y., Zheng, Y., Beg, A. A., and Tong, L. (2002). An extensively associated dimer in the structure of the C713S mutant of the TIR domain of human TLR2. Biochem Biophys Res Commun *299*, 216-221.

Taub, D. D., Newcomb, J. R., and Rogers, T. J. (1992). Effect of isotypic and allotypic variations of MHC class II molecules on staphylococcal enterotoxin presentation to murine T cells. Cell Immunol *141*, 263-278.

Tauszig-Delamasure, S., Bilak, H., Capovilla, M., Hoffmann, J. A., and Imler, J. L. (2002). Drosophila MyD88 is required for the response to fungal and Gram-positive bacterial infections. Nat Immunol *3*, 91-97.

Teague, T. K., Hildeman, D., Kedl, R. M., Mitchell, T., Rees, W., Schaefer, B. C., Bender, J., Kappler, J., and Marrack, P. (1999). Activation changes the spectrum but not the diversity of genes expressed by T cells. Proc Natl Acad Sci U S A *96*, 12691-12696.

Thornberry, N. A., Bull, H. G., Calaycay, J. R., Chapman, K. T., Howard, A. D., Kostura, M. J., Miller, D. K., Molineaux, S. M., Weidner, J. R., Aunins, J., and et al. (1992). A novel heterodimeric cysteine protease is required for interleukin-1 beta processing in monocytes. Nature *356*, 768-774.

Torgerson, T. R., Colosia, A. D., Donahue, J. P., Lin, Y. Z., and Hawiger, J. (1998). Regulation of NF-kappa B, AP-1, NFAT, and STAT1 nuclear import in T lymphocytes by noninvasive delivery of peptide carrying the nuclear localization sequence of NF-kappa B p50. J Immunol *161*, 6084-6092.

Tsai, E. Y., Yie, J., Thanos, D., and Goldfeld, A. E. (1996). Cell-type-specific regulation of the human tumor necrosis factor alpha gene in B cells and T cells by NFATp and ATF-2/JUN. Mol Cell Biol *16*, 5232-5244.

Tsuji-Takayama, K., Aizawa, Y., Okamoto, I., Kojima, H., Koide, K., Takeuchi, M., Ikegami, H., Ohta, T., and Kurimoto, M. (1999). Interleukin-18 induces interferon-gamma production through NF-kappaB and NFAT activation in murine T helper type 1 cells. Cell Immunol *196*, 41-50.

Vannier, E., and Dinarello, C. A. (1994). Histamine enhances interleukin (IL)-1-induced IL-6 gene expression and protein synthesis via H2 receptors in peripheral blood mononuclear cells. J Biol Chem *269*, 9952-9956.

Veach, R. A., Liu, D., Yao, S., Chen, Y., Liu, X. Y., Downs, S., and Hawiger, J. (2004). Receptor/transporter-independent targeting of functional peptides across the plasma membrane. J Biol Chem *279*, 11425-11431.

Vigers, G. P., Anderson, L. J., Caffes, P., and Brandhuber, B. J. (1997). Crystal structure of the type-I interleukin-1 receptor complexed with interleukin-1beta. Nature *386*, 190-194.

Volpe, F., Clatworthy, J., Kaptein, A., Maschera, B., Griffin, A. M., and Ray, K. (1997). The IL1 receptor accessory protein is responsible for the recruitment of the interleukin-1 receptor associated kinase to the IL1/IL1 receptor I complex. FEBS Lett *419*, 41-44.

Voronov, E., Shouval, D. S., Krelin, Y., Cagnano, E., Benharroch, D., Iwakura, Y., Dinarello, C. A., and Apte, R. N. (2003). IL-1 is required for tumor invasiveness and angiogenesis. Proc Natl Acad Sci U S A *100*, 2645-2650.

Wald, D., Qin, J., Zhao, Z., Qian, Y., Naramura, M., Tian, L., Towne, J., Sims, J. E., Stark, G. R., and Li, X. (2003). SIGIRR, a negative regulator of Toll-like receptor-interleukin 1 receptor signaling. Nat Immunol *4*, 920-927.

Webb, A. C., Collins, K. L., Auron, P. E., Eddy, R. L., Nakai, H., Byers, M. G., Haley, L. L., Henry, W. M., and Shows, T. B. (1986). Interleukin-1 gene (IL1) assigned to long arm of human chromosome 2. Lymphokine Res *5*, 77-85.

Wesche, H., Henzel, W. J., Shillinglaw, W., Li, S., and Cao, Z. (1997a). MyD88: an adapter that recruits IRAK to the IL-1 receptor complex. Immunity *7*, 837-847.

Wesche, H., Korherr, C., Kracht, M., Falk, W., Resch, K., and Martin, M. U. (1997b). The interleukin-1 receptor accessory protein (IL-1RAcP) is essential for IL-1-induced activation of interleukin-1 receptor-associated kinase (IRAK) and stress-activated protein kinases (SAP kinases). J Biol Chem *272*, 7727-7731.

White, J., Herman, A., Pullen, A. M., Kubo, R., Kappler, J. W., and Marrack, P. (1989). The V beta-specific superantigen staphylococcal enterotoxin B: stimulation of mature T cells and clonal deletion in neonatal mice. Cell *56*, 27-35.

Xu, Y., Tao, X., Shen, B., Horng, T., Medzhitov, R., Manley, J. L., and Tong, L. (2000). Structural basis for signal transduction by the Toll/interleukin-1 receptor domains. Nature *408*, 111-115.

Yamamoto, M., Sato, S., Hemmi, H., Hoshino, K., Kaisho, T., Sanjo, H., Takeuchi, O., Sugiyama, M., Okabe, M., Takeda, K., and Akira, S. (2003a). Role of adaptor TRIF in the MyD88-independent toll-like receptor signaling pathway. Science *301*, 640-643.

Yamamoto, M., Sato, S., Hemmi, H., Uematsu, S., Hoshino, K., Kaisho, T., Takeuchi, O., Takeda, K., and Akira, S. (2003b). TRAM is specifically involved in the Toll-like receptor 4-mediated MyD88-independent signaling pathway. Nat Immunol *4*, 1144-1150.

Yamamoto, M., Sato, S., Mori, K., Hoshino, K., Takeuchi, O., Takeda, K., and Akira, S. (2002). Cutting edge: a novel Toll/IL-1 receptor domain-containing adapter that preferentially activates the IFN-beta promoter in the Toll-like receptor signaling. J Immunol *169*, 6668-6672.

Yamamoto, M., Takeda, K., and Akira, S. (2004). TIR domain-containing adaptors define the specificity of TLR signaling. Mol Immunol *40*, 861-868.

Yan Liu, X., Robinson, D., Veach, R. A., Liu, D., Timmons, S., Collins, R. D., and Hawiger, J. (2000). Peptide-directed suppression of a pro-inflammatory cytokine response. J Biol Chem *275*, 16774-16778.

Yeung, R. S., Penninger, J. M., Kundig, T., Khoo, W., Ohashi, P. S., Kroemer, G., and Mak, T. W. (1996). Human CD4 and human major histocompatibility complex class II (DQ6) transgenic mice: supersensitivity to superantigen-induced septic shock. Eur J Immunol *26*, 1074-1082.

Yu, J. W., Wu, J., Zhang, Z., Datta, P., Ibrahimi, I., Taniguchi, S., Sagara, J., Fernandes-Alnemri, T., and Alnemri, E. S. (2005). Cryopyrin and pyrin activate caspase-1, but not NF-kappaB, via ASC oligomerization. Cell Death Differ.